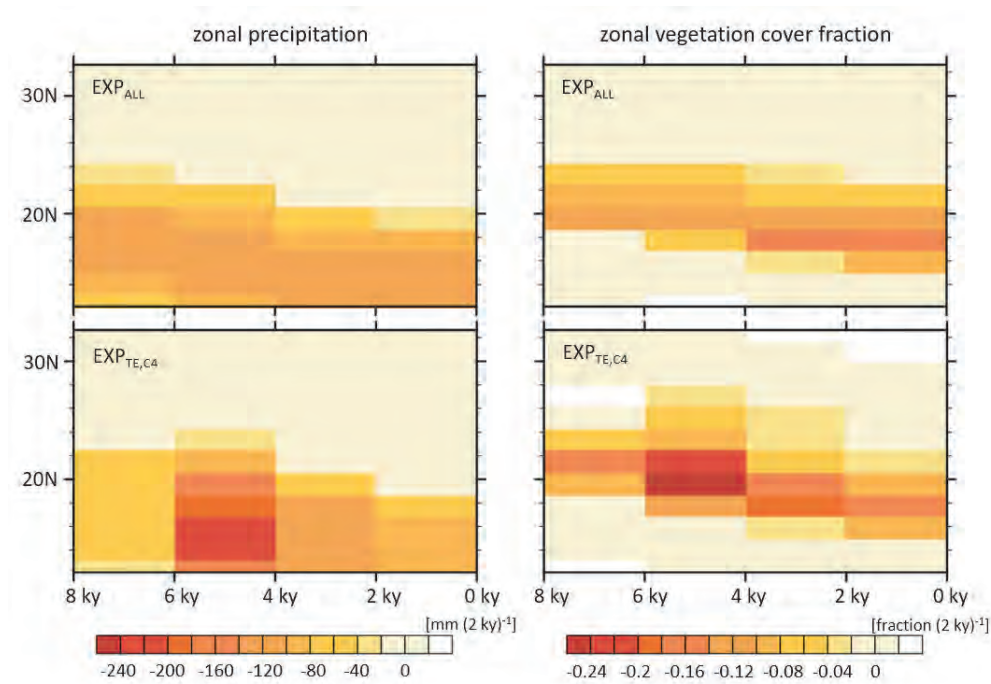


Effects of plant diversity on simulated climate-vegetation interaction towards the end of the African Humid Period



Vivienne Pascale Groner

Hamburg 2017

Hinweis

Die Berichte zur Erdsystemforschung werden vom Max-Planck-Institut für Meteorologie in Hamburg in unregelmäßiger Abfolge herausgegeben.

Sie enthalten wissenschaftliche und technische Beiträge, inklusive Dissertationen.

Die Beiträge geben nicht notwendigerweise die Auffassung des Instituts wieder.

Die "Berichte zur Erdsystemforschung" führen die vorherigen Reihen "Reports" und "Examensarbeiten" weiter.

Anschrift / Address

Max-Planck-Institut für Meteorologie
Bundesstrasse 53
20146 Hamburg
Deutschland

Tel./Phone: +49 (0)40 4 11 73 - 0

Fax: +49 (0)40 4 11 73 - 298

name.surname@mpimet.mpg.de

www.mpimet.mpg.de

Notice

The Reports on Earth System Science are published by the Max Planck Institute for Meteorology in Hamburg. They appear in irregular intervals.

They contain scientific and technical contributions, including Ph. D. theses.

The Reports do not necessarily reflect the opinion of the Institute.

The "Reports on Earth System Science" continue the former "Reports" and "Examensarbeiten" of the Max Planck Institute.

Layout

Bettina Diallo and Norbert P. Noreiks
Communication

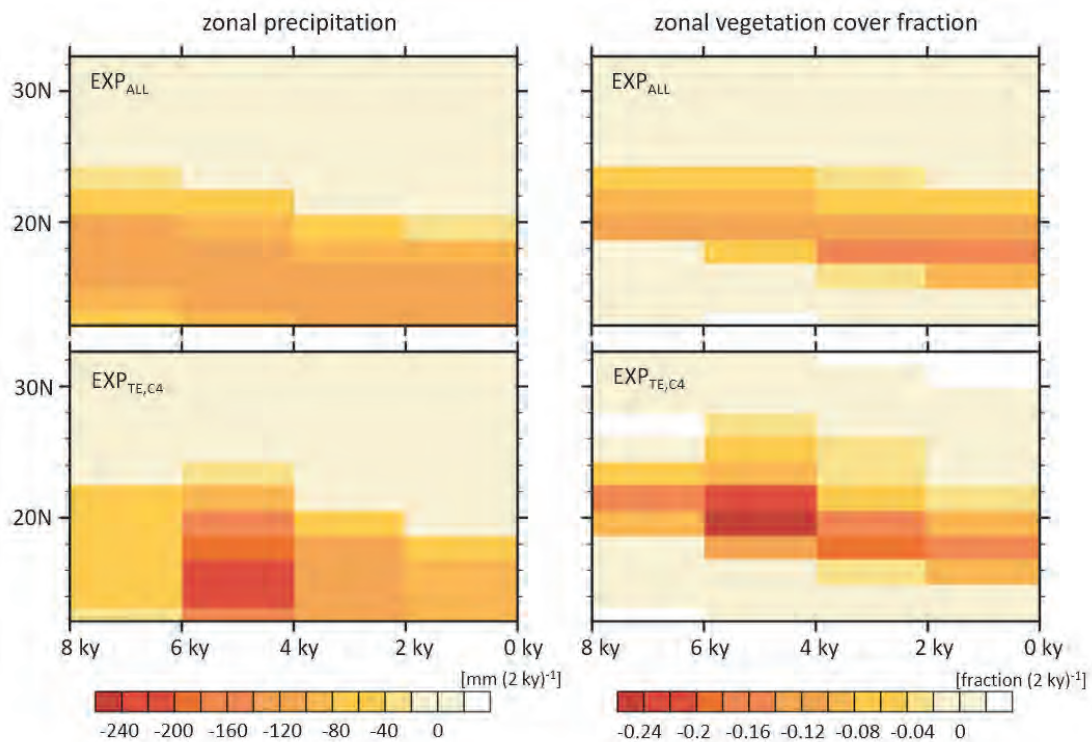
Copyright

Photos below: ©MPI-M

Photos on the back from left to right:
Christian Klepp, Jochem Marotzke,
Christian Klepp, Clotilde Dubois,
Christian Klepp, Katsumasa Tanaka



Effects of plant diversity on simulated climate-vegetation interaction towards the end of the African Humid Period



Dissertation with the aim of achieving a doctoral degree
at the Faculty of Mathematics, Informatics and Natural Sciences
Department of Earth Sciences of Universität Hamburg
submitted by

Vivienne Pascale Groner

Hamburg 2017

Vivienne Pascale Groner

Max-Planck-Institut für Meteorologie
Bundesstrasse 53
20146 Hamburg

Tag der Disputation: 06.07.2017

Folgende Gutachter empfehlen die Annahme der Dissertation:

Prof. Dr. Martin Claußen
Dr. Christian Reick

“Everything has been thought of before but the difficulty is to think of it again.”

Johann Wolfgang von Goethe
German dramatist, novelist, poet, and scientist (1749 - 1832)

Abstract

This thesis explores the role of plant diversity in simulated climate–vegetation interaction towards the end of the “African Humid Period” (AHP) in models of different complexity, from the conceptual model by Claussen et al. (2013) to the Dynamic Global Vegetation Model JSBACH, the land component of the Max Planck Earth System Model MPI-ESM1.

In the light of recently published pollen data and the current state of ecological literature, the conceptual model by Claussen et al. (2013) reproduces the main features of different plant types interacting together with climate, but it does not capture the reconstructed AHP plant diversity. With a new model version adjusted to AHP vegetation, I can simulate a diverse mosaic-like environment as reconstructed from pollen, and I observe a stabilizing effect of high plant diversity on vegetation cover and precipitation. Plant composition ultimately determines the stability of the climate–vegetation system.

The assessment of plant diversity in JSBACH illustrates that the “Plant Functional Type” (PFT) concept is not capable to capture AHP plant diversity and cannot depict mosaic-like environments as reconstructed from pollen. However, offline simulations with different PFT compositions confirm that high PFT diversity can smooth the vegetation response to a – here prescribed linear – precipitation decline. Eventually, the steepness of vegetation decline depends on the composition rather than on the number of PFTs.

In coupled ECHAM6/JSBACH simulations, PFT diversity significantly affects land surface parameters, water cycling, surface energy budget, and atmospheric circulation patterns during the AHP as well as the rate and timing of the transition from a wet “green” state to a dry “desert” state. Higher precipitation is not necessarily associated with a higher vegetation cover fraction and a higher stability of the climate–vegetation system, but determined by the properties of prevailing PFTs, thus PFT composition.

Despite different underlying assumptions, all considered levels of model complexity lead to the same conclusions: high plant diversity could stabilize a climate–vegetation system, but plant composition is the decisive factor for the climate–vegetation feedback strength and consequently for the system response to changes in orbital forcing. This highlights that the choice of plant types/PFTs and their representation in models significantly affect simulated climate–vegetation interaction during the AHP, the extent of the “green” Sahara, and the timing and rate of transition to the “desert” state. From this I conclude that accounting for plant diversity in future studies – not only on palaeoclimates – could significantly improve the understanding of climate–vegetation interaction and the simulation of the vegetation response to changing climate.

Zusammenfassung

Die vorliegende Dissertation untersucht die Rolle von Pflanzendiversität für simulierte Klima–Vegetationsinteraktion gegen Ende der “African Humid Period” (AHP) in Modellen verschiedener Komplexität, vom konzeptionellen Modell nach Claussen et al. (2013) bis zum Dynamischen Globalen Vegetations Modell JSBACH, der Landoberflächenkomponente des Max Planck Erdsystem Modells MPI-ESM1.

Unter Berücksichtigung jüngst veröffentlichter Pollendaten und dem aktuellen Stand ökologischer Literatur reproduziert das konzeptionelle Modell von Claussen et al. (2013) die wesentlichen Aspekte der gemeinsamen Interaktion verschiedener Pflanzentypen mit dem Klima, allerdings kann es rekonstruierte AHP Pflanzendiversität nicht erfassen. Mit einer neuen Modellversion die an AHP Vegetation angepasst ist kann ich eine diverse, mosaikartige Umgebung simulieren wie sie mithilfe von Pollen rekonstruiert wurde, und ich beobachte einen stabilisierenden Effekt hoher Pflanzendiversität auf Vegetationsbedeckung und Niederschlag. Die Pflanzenzusammensetzung bestimmt letztendlich die Stabilität des Klima–Vegetationssystems.

Die Begutachtung der Pflanzendiversität in JSBACH veranschaulicht, dass das “Plant Functional Type” (PFT) Konzept nicht in der Lage ist, AHP Pflanzendiversität zu erfassen und eine mosaikartige Umgebung, wie sie mithilfe von Pollen rekonstruiert wurde, abzubilden. Nichtsdestotrotz bestätigen ungekoppelte Simulationen mit unterschiedlichen PFT Zusammensetzungen, dass hohe Pflanzendiversität die Vegetationsantwort auf einen – hier vorgeschriebenen linearen – Niederschlagsrückgang glätten kann. Letztendlich hängt die Steilheit des Vegetationsrückgangs mehr von der PFT Zusammensetzung ab als von der Anzahl der PFTs.

In gekoppelten ECHAM6/JSBACH Simulationen beeinflusst PFT Diversität signifikant Landoberflächeneigenschaften, Wasserkreislauf, Oberflächenenergiehaushalt und atmosphärische Zirkulationsmuster, ebenso wie die Rate und den Zeitpunkt des Übergangs von der feuchten “grünen” Sahara zum trockenen Wüstenzustand. Höhere Niederschläge sind nicht notwendigerweise mit höherer Vegetationsbedeckung und einer höheren Stabilität des Klima–Vegetationssystems assoziiert, sondern werden von den Eigenschaften der vorherrschenden PFTs bestimmt, somit von der PFT Zusammensetzung.

Trotz großer Unterschiede in den zugrundeliegenden Annahmen führen alle Komplexitätsebenen zu denselben Schlussfolgerungen: hohe Pflanzendiversität könnte ein Klima–Vegetationssystem stabilisieren, die Pflanzenzusammensetzung ist jedoch der ausschlaggebende Faktor für die Stärke der Wechselwirkung zwischen Vegetation und Klima und folglich für die Systemantwort auf Änderungen im orbitale Antrieb. Das unterstreicht,

dass die Auswahl der Pflanzentypen/PFTs und deren Repräsentation in Modellen signifikanten Einfluss auf simulierte Klima–Vegetationsinteraktion während der AHP hat, ebenso wie auf die Ausdehnung der “grünen” Sahara und auf den Zeitpunkt und die Rate des Übergangs zum Wüstenzustand. Daraus schließe ich, dass die Berücksichtigung von Pflanzendiversität in zukünftigen Studien – nicht nur an Paläoklimaten – das Verständnis von Klima–Vegetationsinteraktion und die Simulation der Vegetationsantwort auf sich änderndes Klima signifikant verbessern könnte.

Acknowledgements

Foremost, I would like to express my sincere gratitude to my principal advisor Martin Claussen for giving me the opportunity to accomplish this Ph.D. at the Max Planck Institute for Meteorology in Hamburg, for his time and interest, careful and insightful comments, support and encouragement, and guidance throughout my PhD process.

I am also sincerely grateful to my co-advisor Christian Reick for his time, encouragement, interest and curiosity. Numerous discussions, brainstorming and reviews contributed a great deal of what I can present today.

I extend sincere thanks to my Advisory Panel Chair Eva-Maria Pfeiffer for her time and support as well as for her pleasant energy that made our Panel meetings constructive and cheerful.

Special thanks to Thomas Raddatz for his scientific advice and technical support, for answering all my questions, providing creative suggestions and encouraging me throughout the last years. And for the coffee supply.

I am also very thankful to Sirisha, Sabine, Sylvia, Thomas, Jürgen, and Veit for proof-reading the preliminary manuscript of this work patiently and studiously.

Many many thanks go to Antje Weitz, Wiebke Böhm and Cornelia Kampmann for their continuous support, both administratively and morally. I must also thank the Max Planck Society (and thus, ultimately, the German taxpayers) for making this PhD project possible through their financial support of the International Max Planck Research School on Earth System Modeling.

The last three years would not have been that much fun without the help and company of my fellow PhD students and colleagues, past and present. Thanks for sharing all the ups and downs I have been going through and for patient support and faith in me. Many thanks to Jessica, to my office mates Sabine and Alex for their patience and kindness, to Veit for making sure that I get off by butt at least once per day to get some “fresh air”, to Sirisha, Sylvia, Johannes, Dirk, Leo, Matteo, Ulrike, Daniela, Irina, and all the others.

I'm very grateful for my family and friends who helped shaping me in to the person I am and always encouraged me in all my pursuits, even when it took me far away from home to forge ahead. Words cannot express how thankful I am for Eddy stumbling into my life and making things so much easier, nicer and schärfer.

Finally, many thanks to all who contributed to a good success of this PhD thesis.

Contents

Abstract	iii
Zusammenfassung	iv
Acknowledgements	vi
List of Figures	ix
List of Tables	xv
Abbreviations	xvi
General introduction	1
The African Humid Period	2
Climate–vegetation interaction towards the end of the AHP	12
Plant diversity and climate–vegetation system stability	14
Motivation of this thesis	17
1 Palaeo plant diversity in subtropical Africa – Ecological assessment of a conceptual model of climate–vegetation interaction	19
1.1 Introduction	19
1.2 The conceptual approach by Claussen et al. (2013)	22
1.2.1 The model formulation by Claussen et al. (2013)	22
1.2.2 Assessment of the model set up by Claussen et al. (2013)	24
1.2.3 Assessment of the interpretation of results by Claussen et al. (2013)	25
1.3 Application of the conceptual model by Claussen et al. (2013) to AHP vegetation	27
1.3.1 Does the model by Claussen et al. (2013) capture the diversity of AHP vegetation?	27
1.3.2 Model adjustment	29
1.3.3 Results from the adjusted model	32
1.3.4 Limitations of the adjusted model	37
1.4 Summary and conclusions	38

2	Representation of plant diversity in JSBACH and its impact on the simulated vegetation response to a linear precipitation decline in sub-tropical Africa	42
2.1	Introduction	42
2.2	Plant diversity and vegetation dynamics in JSBACH	44
2.2.1	The concept of Plant Functional Types	44
2.2.2	Natural land cover change and vegetation dynamics in JSBACH	46
2.2.3	General assessment of the PFT concept in JSBACH	50
2.2.4	Analogy between plant diversity in JSBACH and in the conceptual model in Chapter 1	53
2.3	PFT response to a linear precipitation decline	55
2.3.1	Model set up	56
2.3.2	Results	58
2.3.3	Discussion	67
2.3.4	Limitations	69
2.4	Summary and Conclusions	72
3	Effects of plant diversity on simulated climate–vegetation interaction towards the end of the African Humid Period	75
3.1	Introduction	75
3.2	Model set up	79
3.2.1	MPI-ESM1	79
3.2.2	Set up of simulations	80
3.3	Effects of PFT diversity on climate–vegetation interaction during the AHP	82
3.3.1	Results	82
3.3.2	Discussion	91
3.4	Effects of PFT diversity on the transition from the “green” Sahara to the “desert” state	95
3.4.1	Results	95
3.4.2	Discussion	99
3.5	Limitations	102
3.6	Summary and conclusions	104
	Final conclusions	107
	Summary	107
	Future research perspectives	110
	Conclusions and implications	112
	Appendix	113
	Bibliography	124
	Declaration of Authorship	145

List of Figures

1	Savanna types and characteristic life forms in relation to the prevailing climate (modified after Ellenberg (1975); Pfadenhauer & Klötzli (2015)).	3
2	White’s vegetation map of Africa (1983) – Main phytochoria of Africa and Madagascar. Phytochoria considered in this work are highlighted in bold letters. I. Guineo–Congolian regional centre of endemism , II. Zambebian regional centre of endemism , III. Sudanian regional centre of endemism , IV. Somalia-Masai regional centre of endemism , V. Cape regional centre of endemism , VI. Karoo-Namib regional centre of endemism , VII. Mediterranean regional centre of endemism , VIII. Afroalpine archipelago-like regional centre of endemism , including IX. Afroalpine archipelago-like region of extreme floristic impoverishment , X. Guinea-Congolia/ Zambezia regional transition zone , XI. Guinea-Congolia/ Sudania regional transition zone , XII. Lake Victoria regional mosaic , XIII. Zanzibar-Inhambane regional mosaic , XIV. Kalahari-Highveld regional transition zone , XV. Tongaland-Pondoland regional mosaic , XVI. Sahel regional transition zone , XVII. Sahara regional transition zone , XVIII. Mediterranean/Sahara regional transition zone , XIX. East Malagasy regional centre of endemism , XX. West Malagasy regional centre of endemism	7
3	Guineo–Congolian vegetation type: Forest on the banks of the Congo river system (greenpeace.org).	8
4	Sudanian vegetation type: West Sudanian savanna, Burkina Faso (eoeearth.org).	9
5	Sahelian vegetation type: <i>Acacia tortilis</i> wooded grassland, Serengeti (biologie.uni-hamburg.de).	10
6	Saharan vegetation type: Semi-desert, desert-steppe transition, Namibia (geographie.uni-stuttgart.de).	11
7	Stability landscape of “green” Sahara and “desert” state (modified after Bathiany et al. (2016)). The stronger the atmosphere–vegetation feedback, the sharper the transition between the two states.	12
1.1	Vegetation–precipitation stability diagram (V_i^E , P^E) for two hypothetical plant types $i = 1, 2$ after Claussen et al. (2013). Full lines depict the equilibrium curves for vegetation cover $V_i^E(P^E)$ for plant type 1 which is sensitive (red) and for plant type 2 which is resilient (green) to changes in P . Dashed blue lines show hypothetical equilibrium precipitation curves $P^E(V_i^E)$ for different time slices (4500, 4900, 5300, 5700, 6100, and 6500 years BP, from left to right). Intersections between the two types of curves indicate equilibrium coupled states which can be stable or unstable.	22

1.2	Environmental envelopes in terms of moisture requirements of four African Humid Period (AHP) plant types in the adjusted set up. The effective leaf area L_i is plotted as a function of mean annual precipitation P for the Saharan type (red), Sahelian type (green), Sudanian type (blue), and Guineo–Congolian type (light blue).	32
1.3	Transient dynamics of four African Humid Period (AHP) plant types interacting individually (a–c) and together (d–f) with climate. The effective leaf areas L_i and the corresponding precipitation amounts P_i are shown for the Saharan type (red), Sahelian type (green), Sudanian type (blue), and Guineo–Congolian type (light blue). Mean effective leaf area L_S and the corresponding precipitation P are calculated with the niche approach (black) (see Eq. 1.9). Simulations without background noise (a, e) include forward simulations (solid lines) and simulations backward in time (dashed lines). Simulations with background noise are depicted in (b, e) for L_i and L_S , and for precipitation P in (c, f). Thin lines show annual mean values and thick lines show a 100-year running mean.	34
1.4	Transient dynamics of mean effective leaf area L_S illustrate the impact of the removal of plant types. Panels (a–e) show 100-year running means of different simulation set ups. The mean effective leaf area L_S accounting for all plant types ($N = n = 4$ in Eq. 1.10) is shown as a reference (a). In each of the other simulations, one niche is not occupied ($N = 3$ and $n = 4$ in Eq. 1.10): no Saharan type (b), no Sahelian type (c), no Sudanian type (d) or no Guineo–Congolian type (e).	36
2.1	Mean orography (in m) of the simulated study domain in north Africa at 12 to 34° N, -15 to 40° E.	56
2.2	Vegetation cover fraction veg_{max} and precipitation P for simulations with different PFT compositions for one selected grid cell (19.58° N, -3.75° E). Curves depict the transient behaviour of EXP_{C4} (a; orange), $EXP_{TE,C4}$ (a; dark green), $EXP_{SRG,C4}$ (a; red), EXP_{ALL} (b; black), and EXP_{HIDI} (b; magenta). P (blue dashed) is scaled to 100% at the beginning of the simulation period.	58
2.3	Maximum slope of vegetation cover fractions veg_{max} over a 100-years running window for EXP_{ALL} (a), EXP_{C4} (b), $EXP_{TE,C4}$ (c), $EXP_{SRG,C4}$ (d), and EXP_{HIDI} (e). The slope of precipitation P decline is in all simulations 0.03% yr ⁻¹ . Yellowish colors indicate that the slope of veg_{max} is slightly steeper than the slope of P , reddish colors represent grid cells where the slope of veg_{max} is much steeper than the slope of P	59
2.4	Vegetation cover fraction $veg_{max,ALL}$, cover fractions f_i of PFTs i and precipitation P of a simulation with the standard PFT set up (EXP_{ALL}) at 12 to 34° N, -15 to 40° E. P (blue dashed) is scaled to 100% at the beginning of the simulation period for each grid cell individually. f_i are shown for PFTs relevant in the study domain: Tropical Evergreen Tree (TE ; dark blue), Tropical Deciduous Tree (TD ; light blue), Extratropical Evergreen Tree (eTE ; green), Shrub Raingreen (SRG ; red), C3 Grass ($C3$; brown), C4 Grass ($C4$; orange).	61

- 2.5 Vegetation cover fraction veg_{max} and precipitation P for single-PFT and two-PFT simulations at 12 to 34° N, -15 to 40° E. Curves depict the transient behaviour of C4 Grass only in EXP_{C4} (orange), Tropical Evergreen Tree and C4 Grass in $EXP_{TE,C4}$ (dark green), and Raingreen Shrub and C4 Grass in EXP_{SRG} (red). P (blue dashed) is scaled to 100% at the beginning of the simulation period for each grid cell individually. 63
- 2.6 Vegetation cover fraction $veg_{max,HIDI}$, cover fractions f_i of PFTs i and precipitation P of a simulation with the high PFT set up (EXP_{HIDI}) at 12 to 34° N, -15 to 40° E. P (blue dashed) is scaled to 100% at the beginning of the simulation period for each grid cell individually. f_i are shown for modified and standard PFTs relevant in the study domain: Tropical Evergreen Tree (TE, TE_i ; blue), Tropical Deciduous Tree (TD, TD_i ; light blue), Extratropical Evergreen Tree (eTE ; green), Shrub Raingreen (SRG, SRG_i ; red), C3 Grass ($C3, C3_i$; brown), C4 Grass ($C4, C4_i$; orange) with dark colour shade indicating high photosynthetic capacity and light colour shade indicating low photosynthetic capacity. 65
- 2.7 Vegetation cover fraction $veg_{max,HIDI}$, cover fractions f_i of PFTs i and precipitation P (in mm yr^{-1}) of a simulation with the high PFT set up (EXP_{HIDI}) for two example grid cells at 30.77° N, 5.625° E (a) and 17.72° N, -11.25° E (b). P (blue dashed) is scaled to 100% at the beginning of the simulation period for each grid cell individually. f_i are shown for modified and standard PFTs relevant in the grid cells: Tropical Evergreen Tree (TE_i ; blue), Extratropical Evergreen Tree (eTE ; green), Shrub Raingreen (SRG_i ; red), C4 Grass ($C4, C4_i$; orange) with dark (light) colour shade indicating high (low) photosynthetic capacity. 66
- 3.1 Schematic view of the West African Monsoon including some of its key features: the upper-level Tropical Easterly Jet (TEJ), the mid-level African Easterly Jet (AEJ), the InnerTropical Convergence Zone (ITCZ) and the position of the tropical rain belt (adjusted from Nicholson (2009)). 76
- 3.2 Effects of different PFT compositions on precipitation P (left column) and vegetation cover fraction veg_{max} (right column) at 8 ky in Region 1 (18 to 22° N, 5 to 30° E, solid box) and Region 2 (12 to 18° N, -15 to 20° E, dashed box). Panels (a, b) show 100-year averages for the experiment EXP_{ALL} with the standard PFT set up. The following panels illustrate differences in 100-year averages between EXP_{ALL} and EXP_{C4} (c, d), $EXP_{TE,C4}$ (e, f), and $EXP_{SRG,C4}$ (g, h). 84
- 3.3 Mean annual cycle of precipitation P under 8 ky conditions in Region 1 (a; 18 to 22° N, 5 to 30° E) and Region 2 (b; 12 to 18° N, -15 to 20° E). Curves depict monthly averages of 100 simulated years for EXP_{ALL} (black), EXP_{C4} (red), $EXP_{TE,C4}$ (green), and $EXP_{SRG,C4}$ (blue). Stars in the respective colors indicate significant differences to EXP_{ALL} ($\sigma=0.05$). 87

- 3.4 Left: Effects of different PFT compositions on precipitation and horizontal low-level wind fields in the monsoon layer at 8 ky. Right: Vertical cross sections of zonal winds illustrate the strength and position of tropical circulation features associated with the West African Monsoon at 8 ky: low-level equatorial westerlies (LLW, 850 hPa), mid-level African Easterly Jet (AEJ, 600 hPa), upper-level Tropical Easterly Jet (TEJ, 150 hPa). Dotted lines mark the core regions of AEJ and TEJ in EXP_{ALL} . Panels (a, b) show the 100-year average of the monsoon season (JJAS) for the experiment EXP_{ALL} with the standard PFT set up. The following panels illustrate differences between EXP_{ALL} and EXP_{C4} (c, d), $EXP_{TE,C4}$ (e, f), and $EXP_{SRG,C4}$ (g, h). Colored grid cells in panel (c), (e), (g) indicate significant differences to EXP_{ALL} ($\sigma=0.05$). 89
- 3.5 Vegetation–precipitation diagrams ($veg_{max,i}$, P_i) for simulations i with different PFT combinations including all grid cells in the study domain (12 to 34° N, -15 to 40° E). Values are derived from 100-year averages for EXP_{ALL} (a), EXP_{C4} (b), $EXP_{TE,C4}$ (c), and $EXP_{SRG,C4}$ (d). Dots depict relationships at 8 ky, squares represent relationships at 0 ky. . . . 90
- 3.6 Rates of transition from the “green” Sahara to the “desert” state for precipitation P (left column) and vegetation cover fraction veg_{max} (right column) of a simulation with the standard PFT set up (EXP_{ALL}), including Tropical Evergreen Tree (TE), Tropical Deciduous Tree (TD), Extratropical Evergreen Tree (eTE), Extratropical Deciduous Tree (eTD), Shrub Raingreen (SRG), Shrub Deciduous (SD), C3 Grass ($C3$), C4 Grass ($C4$). Plots depict differences between consecutive time slices: 6 ky-8 ky (a, b), 4 ky-6 ky (c, d), 2 ky-4 ky (e, f), and 0 ky-2 ky (g, h). 96
- 3.7 Zonally averaged rates of transition from the “green” Sahara to the “desert” state for precipitation ΔP_i (left column) and vegetation cover fraction $\Delta veg_{max,i}$ (right column) for simulations i : EXP_{ALL} (a, b) includes all standard PFTs (Tropical Evergreen Tree (TE), Tropical Deciduous Tree (TD), Extratropical Evergreen Tree (eTE), Extratropical Deciduous Tree (eTD), Shrub Raingreen (SRG), Shrub Deciduous (SD), C3 Grass ($C3$), C4 Grass ($C4$)), EXP_{C4} (c, d), $EXP_{TE,C4}$ (e, f), and $EXP_{SRG,C4}$ (g, h). 98
- A1 Transient dynamics of four African Humid Period (AHP) plant types interacting individually (a–c) and together (d–f) with climate for $D_B = 0 \text{ mm yr}^{-1}$. The effective leaf areas L_i and the corresponding precipitation amounts P_i are shown for the Saharan type (red), Sahelian type (green), Sudanian type (blue) and Guineo–Congolian type (light blue). Mean effective leaf area L_S and the corresponding precipitation P are calculated with the niche approach (black) (see Eq. 1.9). Simulations without background noise (a, e) include forward simulations (solid lines) and simulations backward in time (dashed lines). Simulations with background noise are depicted in (b, e) for L_i and L_S , and for precipitation P in (c, f). Thin lines show annual mean values and thick lines show a 100-year running mean. 113

- A2 Transient dynamics of four African Humid Period (AHP) plant types interacting individually (a–c) and together (d–f) with climate for $D_B = 50 \text{ mm yr}^{-1}$. The effective leaf areas L_i and the corresponding precipitation amounts P_i are shown for the Saharan type (red), Sahelian type (green), Sudanian type (blue) and Guineo–Congolian type (light blue). Mean effective leaf area L_S and the corresponding precipitation P are calculated with the niche approach (black) (see Eq. 9). Simulations without background noise (a, e) include forward simulations (solid lines) and simulations backward in time (dashed lines). Simulations with background noise are depicted in (b, e) for L_i and L_S , and for precipitation P in (c, f). Thin lines show annual mean values and thick lines show a 100-year running mean. 114
- A3 Transient dynamics of four African Humid Period (AHP) plant types interacting individually (a–c) and together (d–f) with climate for $D_B = 100 \text{ mm yr}^{-1}$. The effective leaf areas L_i and the corresponding precipitation amounts P_i are shown for the Saharan type (red), Sahelian type (green), Sudanian type (blue) and Guineo–Congolian type (light blue). Mean effective leaf area L_S and the corresponding precipitation P are calculated with the niche approach (black) (see Eq. 9). Simulations without background noise (a, e) include forward simulations (solid lines) and simulations backward in time (dashed lines). Simulations with background noise are depicted in (b, e) for L_i and L_S , and for precipitation P in (c, f). Thin lines show annual mean values and thick lines show a 100-year running mean. 115
- A4 Transient dynamics of four African Humid Period (AHP) plant types interacting individually (a–c) and together (d–f) with climate for $D_B = 150 \text{ mm yr}^{-1}$. The effective leaf areas L_i and the corresponding precipitation amounts P_i are shown for the Saharan type (red), Sahelian type (green), Sudanian type (blue) and Guineo–Congolian type (light blue). Mean effective leaf area L_S and the corresponding precipitation P are calculated with the niche approach (black) (see Eq. 9). Simulations without background noise (a, e) include forward simulations (solid lines) and simulations backward in time (dashed lines). Simulations with background noise are depicted in (b, e) for L_i and L_S , and for precipitation P in (c, f). Thin lines show annual mean values and thick lines show a 100-year running mean. 116
- A5 Transient dynamics of mean effective leaf area L_S of four African Humid Period (AHP) plant types interacting together with climate, and the corresponding precipitation P for different feedback sensitivity coefficients D^B . Simulations with background noise are depicted in (a–d) for L_S , and for mean annual precipitation P in (e–h) for $D^B = 0 \text{ mm yr}^{-1}$ (red), $D^B = 50 \text{ mm yr}^{-1}$ (green), $D^B = 100 \text{ mm yr}^{-1}$ (blue), and $D^B = 150 \text{ mm yr}^{-1}$ (black). Without feedback between vegetation and precipitation (a, e), L_S and corresponding P decrease almost linearly. Low feedback coefficients (b, f) result in a non-linear but gradual decline of L_S and corresponding P with small fluctuations. The higher D_B , the stronger the amplitude of fluctuations and the steeper the decline of L_S and corresponding P 117

A6	Mean effective leaf area L_S of four African Humid Period (AHP) plant types i interacting together with climate with different sets of specific climate feedback coefficients D_i^B . 30 simulations with different variations of D_i^B in the range from 0 to 150 mm yr ⁻¹ are shown in gray, the ensemble mean is shown in black.	117
A7	Rates of transition from the “green” Sahara to the “desert” state for precipitation P (left column) and vegetation cover fraction $veg_{max,i}$ (right column) of a simulation with $C4$ grass only (EXP_{C4}).	118
A8	Rates of transition from the “green” Sahara to the “desert” state for precipitation P (left column) and vegetation cover fraction $veg_{max,i}$ (right column) of a simulation with tropical evergreen tree (TE) and $C4$ grass ($EXP_{TE,C4}$).	119
A9	Rates of transition from the “green” Sahara to the “desert” state for precipitation P (left column) and vegetation cover fraction $veg_{max,i}$ (right column) of a simulation with Raingreen shrub (SRG) and $C4$ grass ($EXP_{SRG,C4}$).	120
A10	Effects of the implementation of a tropical tree with modified bioclimatic limits $EXP_{TD,cold}$ (minimum temperature of the coldest month reduced from 15.5 to 10°C) at 8 ky. Plots show the difference between $EXP_{TD,cold}$ and the experiment with the standard PFT set up (EXP_{ALL}) for vegetation cover fraction veg_{max} (a), tree cover fraction (b), shrub cover fraction (c), grass cover fraction (d), precipitation P (e), and horizontal wind fields in the monsoon layer (925 hPa, f). The comparison illustrates that TD_{cold} establishes in the transition zone between desert and savanna at the expense of SRG . As the bioclimatic limit can be overcome, the tropical PFT can establish and outcompete SRG due to its higher productivity. Consequently, $C4$ experiences less competitive pressure on short time scale which favors its expansion. The “greening” of the transition zone results in a northward shift of the ITCZ (f) and enhanced P in the whole study domain (e).	121

List of Tables

1.1	Precipitation thresholds P_i^{C1} to P_i^{C4} (in mm yr^{-1}) and maximum effective leaf area $L_{i,\text{max}}$ (in m^2 per unit niche area) for the African Humid Period (AHP) plant types: Saharan type, Sahelian type, and Sudanian type. . . .	30
2.1	Natural plant functional types in JSBACH, their woodiness type, associated time constants for establishment/mortality τ (in years) (Reick et al., 2013), maximum carboxylation capacities $V_{\text{max},0}$ and electron transport capacities $J_{\text{max},0}$ at 25 °C (in $\mu\text{mol}(\text{CO}_2) \text{m}^{-2} \text{s}^{-1}$) (Kattge et al., 2011), specific leaf area SLA (in $\text{m}^2(\text{leaf}) \text{mol}^{-1}(\text{Carbon})$), and maximum leaf area index LAI_{max} (in $\text{m}^2 \text{m}^{-2}$).	45
2.2	List of performed offline simulations, the number of included PFTs, and the considered dynamics.	57
3.1	CO_2 concentrations (in ppm) and orbital parameters for simulated time slices at 8 ky, 6 ky, 4 ky, 2 ky, and 0 ky. For palaeo simulations, CO_2 concentrations are taken from Joos (2016) and orbital parameters are adjusted according to Berger (1978). The values for 0 ky conform to the standard preindustrial set up of MPI-ESM1.	81
3.2	Effects of different PFT compositions on land surface parameters, surface energy budget, and hydrological cycle in coupled ECHAM6/JSBACH simulations in Region 1 (18 to 22° N, 5 to 30° E) and Region 2 (12 to 18° N, -15 to 20° E). The first two columns contains 100-year averages of the experiment with the standard PFT set EXP_{ALL} , the following show differences between EXP_{ALL} and simulations with modified PFT composition (Tropical Evergreen Tree TE , Raingreen Shrub SRG , C4 Grass $C4$). Bold values are significant ($\sigma = 0.05$) with regard to the time series of 100 years (yearly averages), values in brackets correspond to spatial standard deviations of difference fields.	83
A1	Plant functional types in the high plant diversity set up of JSBACH, their woodiness type, associated time constants for establishment/mortality τ (in years) (Reick et al., 2013), maximum carboxylation capacities $V_{\text{max},0}$ and electron transport capacities $J_{\text{max},0}$ at 25 °C (in $\mu\text{mol}(\text{CO}_2) \text{m}^{-2} \text{s}^{-1}$) (Kattge et al., 2011). Photosynthesis parameter are not available for C4 grasses since their photosynthesis is calculated differently.	122

Abbreviations

a (Chapter 1, Eq. 1.8)	Tuning parameter for conceptual model
a (Chapter 2, Eq. 2.7)	Tuning parameter for desert distribution
A (Chapter 2, Eq. 2.1)	Area
A_C (Chapter 2, Eq. 2.10)	Total rate of carbon fixation
AHP	African Humid Period
AEJ	African Easterly Jet
AEW	African Easterly Waves
AMIP	Atmospheric Model Intercomparison Project
b (Chapter 1, Eq. 1.8)	Tuning parameter for conceptual model
b (Chapter 2, Eq. 2.7)	Tuning parameter for steepness of transition between vegetation and desert in JSBACH
$C3$	Grass with C3 pathway
$C4$	Grass with C4 pathway
c (Chapter 1, Eq. 1.8)	Tuning parameter for conceptual model
CC	Accumulated cloud cover
c_i	Cover fraction of PFT i
C_i	Leaf internal CO ₂ concentration
$C_{G/W,i}^{max}$	Maximum living biomass in PFT i in considered year
d	Inhospitable land
D^B	Climate feedback coefficient
$D_i^{C1,2}$	Slope of $V_i^E(P)$
DGVM	Dynamic Global Vegetation Model
DYNVEG	Dynamic component of JSBACH
ECHAM6	Atmospheric component of MPI-ESM1
E_{PAR}	Photosynthetic photon flux density

<i>ET</i>	Evapotranspiration
<i>eTD</i>	Extratropical deciduous tree
<i>eTE</i>	Extratropical evergreen tree
<i>EXP_{ALL}</i>	Experiment with standard PFTs
<i>EXP_i</i>	Experiment with PFT <i>i</i> only
<i>EXP_j</i>	Experiment with PFT combination <i>j</i>
<i>EXP_{HIDI}</i>	High plant diversity experiment with 58 PFTs
E-space	Ecological space
<i>f</i>	Fraction with substantial vegetation cover
<i>f_i</i>	Fraction of grid cell covered by PFT <i>i</i>
<i>g_i</i>	Grass fraction
GC	Guineo–Congolian
GCM	General Circulation Model
G-space	Geographical space
HIDI	High plant diversity (58 PFTs)
<i>I</i>	Radiation intensity in the photosynthetically active band
ITCZ	InnerTropical Convergence Zone
<i>IWV</i>	Integrated water vapor
<i>J(I)</i>	Radiation dependant carboxylation rate
<i>J_C</i>	Carboxylation rate
<i>J_E</i>	Electron transport rate
<i>J_{max}</i>	Maximum electron transport rate
<i>J_{max,0}</i>	Maximum electron transport rate at 25 °C
JSBACH	Jena Scheme for Biosphere-Atmosphere Interaction in Hamburg, land component of MPI-ESM1
<i>k</i>	PEPCase CO ₂ specificity
<i>K</i>	Number of tiles
<i>K_C, K_O</i>	Michaelis-Menten constants for CO ₂ and O ₂
<i>LAI</i>	Leaf area index
<i>LAI_i^{max}</i>	Maximum leaf area index of PFT <i>i</i> that appeared during considered year
<i>LAI_{max}</i>	Maximum leaf area index of PFT <i>i</i>
<i>LH</i>	Latent heat flux

LLW	Low Level Westerlies
L_i	Effective leaf area of plant type i
L_i^E	Equilibrium effective leaf area of plant type i
$L_{i,max}$	Maximum effective leaf area of plant type i
L_S	Mean effective leaf area
MPI-ESM1	Max Planck Institute Earth System Model
MPIOM	Ocean component of MPI-ESM1
n	Number of existing niches
N	Number of plant types
N^w	Number of woody PFTs
N^g	Number of grass PFTs
NPP	Net primary productivity
O_i	Leaf internal O_2 concentration
P	Mean annual precipitation
P_d	Background precipitation
P_{d0}	Initial precipitation
P^E	Equilibrium precipitation
P_i^{C1-C4}	Precipitation thresholds for plant type i
P_N	White noise forcing added to initial precipitation
PEPCase	Phosphoenolpyruvatcarboxylase
PFT	Plant Functional Type
R_d	Dark respiration
RuBisCO	Ribulose-1,5-bisphosphate-carboxylase/-oxygenase
SD	Deciduous shrub
SH	Sensible heat flux
SHL	Saharan Heat Low
SIC	Sea ice concentration
SLA	Specific leaf area
SRG	Raingreen shrub
SST	Sea surface temperature
$S \downarrow_{net}$	Net incoming solar radiation
t	Time
T	Simulation period

TD	Tropical deciduous tree
TE	Tropical evergreen tree
TEJ	Tropical Easterly Jet
T_{2m}	2 m air temperature
v_i	Area covered by PFT i
veg_{max}	Area hospitable for vegetation, vegetation cover fraction
$veg_{max,i}$	Vegetation cover fraction of PFT i
$veg_{max,j}$	Vegetation cover fraction of PFT combination j
V	Vegetation
V_i	Vegetation cover fraction of plant type i
V_i^E	Equilibrium vegetation cover fraction of plant type i
$V_{i,max}$	Maximum vegetation cover fraction of plant type i
V_{max}	Maximum carboxylation rate of RuBisCO
$V_{max,0}$	Maximum carboxylation rate of RuBisCO at 25 °C
$V_{P,max}$	Maximum carboxylation rate of PEPCase
V_S	Mean vegetation cover fraction
V_{veg}	Area in a grid cell accessible for vegetation
w_i	Woody fraction
WAM	West African Monsoon
y	Year
z_0	Roughness length
α (Chapter 1, Eq. 2.13)	Quantum efficiency of an electron capture
α (Chapter 3)	Albedo
α_i	Integrated C4 quantum specificity
β	Bowen ratio
Γ_*	CO ₂ compensation point
γ_d	Scaling parameter for nitrogen status of a plant
ΔP	Rate of precipitation decline
Δveg_{max}	Rate of vegetation cover fraction decline
θ_S	Curve parameter
τ	Equilibrium timescale for establishment and mortality

General Introduction

Particularly in times of climate change, research on past climates is gaining in importance. Palaeo studies offer insights in the sensitivity of the Earth system's components to internal and external forcings and provide estimates of the potential magnitude and speed of changes in the future. One exceptionally interesting era is the "African Humid Period" (AHP), a wet phase that peaked across north Africa between 9000 and 6000 years before present (BP) and enabled the establishment of the "green" Sahara (Ritchie & Haynes, 1987; Prentice & Jolly, 2000). Scientists agree that the "wetting" and "greening" of the Sahara was triggered by external changes in the Earth's orbit (Kutzbach, 1981; Kutzbach & Guetter, 1986) and amplified by internal feedback mechanisms including ocean (Kutzbach & Liu, 1997; Braconnot et al., 1999), surface water coverage by lakes and wetlands (Coe & Bonan, 1997; Krinner et al., 2012), and vegetation and soil albedo (Claussen & Gayler, 1997; Claussen, 2009; Vamborg et al., 2011). However, the timing and abruptness of the transition from the "green" Sahara to the "desert" state are still under debate. While some studies indicated an abrupt collapse of vegetation implying a strong climate-vegetation feedback (Claussen, 1994; Claussen & Gayler, 1997; Claussen et al., 1998, 1999), others suggested a gradual vegetation decline thereby questioning the existence of a strong climate-vegetation feedback (Kröpelin et al., 2008; Francus et al., 2013; Lézine, 2009; Lézine et al., 2011). Claussen et al. (2013) introduced a new aspect in the discussion illustrating in a conceptual modelling study that plant diversity might increase the stability of the climate-vegetation system in semi-arid regions, buffer the strength of individual plant-precipitation feedback and prevent an abrupt vegetation collapse. A reduction in functional plant diversity may conversely lead to an abrupt collapse of a seemingly stable system. This potential effect of plant diversity on the strength of climate-vegetation feedback has so far been omitted in comprehensive modelling studies on the AHP.

To close this gap, this thesis explores the role of plant diversity in simulated climate–vegetation interaction in models of different complexity, from the conceptual approach by Claussen et al. (2013) to the Dynamic Global Vegetation Model (DGVM) JSBACH, the land component of the Max Planck Earth System Model MPI-ESM1.

The task of the present chapter is to (1) provide a picture of AHP conditions and the prevailing plant types reconstructed from pollen, (2) summarize previous studies on the end of the AHP, and (3) introduce the current state of knowledge and the controversy on the relation between plant diversity and climate–vegetation system stability. The chapter closes with the motivation of this thesis, including the guiding research questions, and gives an overview over the content of the following chapters.

The African Humid Period

During the “African Humid Period” (AHP), large areas of the nowadays hyperarid Sahara and arid Sahel region were vegetated (Ritchie & Haynes, 1987; Prentice & Jolly, 2000), a dense fluvial network was developed (Drake et al., 2011), and open surface water was widespread (Hoelzmann et al., 1998; Kröpelin et al., 2008; Lézine et al., 2011). Fossil pollen records indicate that the Sahel boundary was shifted northwards by 5 to 7° to at least 23° N (Jolly et al., 1998) and tropical plant taxa might have used river banks as migration paths to enter drier environments (Watrin et al., 2009). Consequently, vegetation cover marked a diverse savanna-like mosaic of xeric and tropical species whose ranges do not overlap today (Hély et al., 2014).

Savannas are near-tropical or tropical seasonal ecosystems characterized by the co-dominance of trees and grasses, typically with a continuous herbaceous layer and a discontinuous stratum of shrubs and trees (Frost et al., 1986). The relative representation of these life forms can vary considerably across savanna types as a consequence of numerous interacting factors at various spatial and temporal scales including climate, resource competition, fire and grazing (Scholes & Archer, 1997; Sankaran et al., 2004). Fig. 1 illustrates the range of observed savanna types and characteristic life forms in relation to the prevailing climate. Coughenour & Ellis (1993) suggested a hierarchy of constraints in savannas, in which climatic patterns determine the extent of the biome at the continental scale; rainfall, hydrology and topography influence savanna structure at

the regional to landscape scale; and local scale structure is determined by variations in water availability and disturbance.

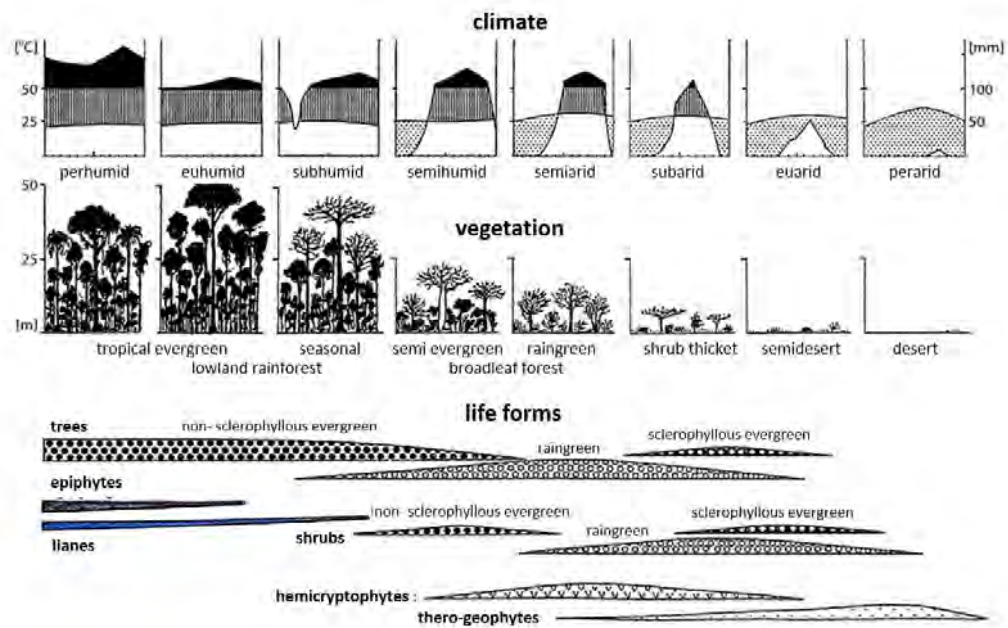


FIGURE 1: Savanna types and characteristic life forms in relation to the prevailing climate (modified after Ellenberg (1975); Pfadenhauer & Klötzli (2015)).

The persistence of tree-grass mixtures without one displacing the other, the determinants of tree-grass ratios, and the involved dynamics remain poorly understood although scientists have worked on the “savanna question” for years (Scholes & Archer, 1997; Jeltsch et al., 2000; Sankaran et al., 2004). Different explanations for the coexistence of trees and grass in savannas invoke different mechanisms: Competition-based approaches explain the coexistence with spatial and/or temporal niche differences between trees and grasses resulting from different resource-acquisition potentials (Peter Chesson, 1997; Amarasekare, 2003; Sankaran et al., 2004); demographic bottleneck approaches propose non-competitive but demographic mechanisms as fundamental processes structuring savannas. It is assumed that “trees and grasses persist in savannas because of climatic variability and/or disturbances such as fire and grazing which limit successful tree seedling germination, establishment and/or transition to mature size classes (Menaut et al., 1990; Hochberg et al., 1994; Jeltsch et al., 1996, 1998, 2000; Higgins et al., 2000; van Wijk & Rodriguez-Iturbe, 2002)” (Sankaran et al., 2004).

Tropical savannas have a high species diversity compared to temperate grasslands and dry tropical woodlands (Solbrig, 1996). Special features increasing the diversity of savannas are so-called “gallery forests”, narrow bands of dense tree cover, sharply separated

from the drier environment (Silva et al., 2008). Gallery forest soils typically have greater nutrient and water availability than the neighboring savanna, and once begin established, positive feedback effects may come into play and stabilize the extent (Silva et al., 2008). Sharp forest savanna boundaries are believed to arise primarily due to fires which are common in savanna but do typically not penetrate into the forest (Azihou et al., 2013).

Plants in semi-arid and arid regions own special adaptations to extreme drought, heat and insolation that allow them to tolerate a certain level of stress/disturbance. Xeromorph plant growth in these regions is realized by either drought resistance or drought tolerance (Wickens, 1998). Drought resistant plants can be poikilohydrous (condition of suspended animation), arido-passive (drought-surviving parts metabolically inactive during dry season, e.g. rainy season annuals and ephemerals (short live cycle), *Synanthus* geophytes, hemicryptophytes), arido-active (metabolically active throughout the year, e.g. bi-seasonal annuals, hysteroanthous geophytes, heterophyllous shrubs, phreatophytes), drought avoiding (escaping or therophytes (seeds only), complete life cycle before onset of extreme drought, tolerant seeds, ephemeral, hygroscopic capsules), drought evading (water spenders ability to obtain large amounts of water during drought, lignotuber, corky layer in xylem, leafs (thickness, veins, more smaller stomata, epidermal or mesophyll cells, thicker walls, cutucula), proline accumulation, moisture from dew or fog, rosette, leaf fall reduction, succulence), and/or drought enduring (ability to reduce water loss to minimum). Drought tolerant plants can be piokilochlorophyllous (loss of chlorophyll on dehydration), poikilohydrous (condition of suspended animation), or they can accumulate sugars.

When plants are exposed to exceptional drought stress, they have different possibilities to minimize water loss. Examples are changes in root/shoot ratio, stomata closure, reduction of stomatal conductance (Susiluoto & Berninger, 2007), reduction of growth in terms of leaf size and leaf number per plant, leaf area index, plant height, stem extension, and root proliferation, optimization of water use efficiency (Anjum et al., 2011), suppression of leaf expansion, early senescence, and rise of leaf temperature (reduced transpiration) (Aroca, 2012). These adaptations lead to a modification of nutrient uptake (carbon, nitrogen, phosphorous), poor water uptake by roots, lesser plant growth, reduction of litter composition, reduction of above ground net primary productivity and finally a higher mortality rate (da Silva et al., 2013). Up to a certain point, plants can react on changing conditions: on long term via evolutionary processes, on shorter

timescales via plasticity (Albert, 2010). A definition of plasticity is given by Bradshaw (1965): “An individual genotype assumes particular given characteristics in a given environment. In a second environment it may remain the same, or it may be different. The amount by which the expressions of individual characteristics of a genotype are changed by different environments is a measure of plasticity of these characters. Plasticity is therefore shown by a genotype when its expression is able to be altered by environmental influences.” Unfortunately, the plasticity of plants is very difficult to predict, since reactions are very individual and depend on various factors. If the conditions become too unfavorable for a plant to maintain its growth, it could either migrate via pollen to regions with better environmental conditions or it would extinct.

Regarding species sensitivities to changing climatic conditions, common ecological understanding provides some general hypothesis : “(1) species with requirements near the mean climate conditions of the studied area should be less sensitive than species with outlying niches (marginal species) (Swihart et al., 2003); (2) species encountering a broader array of climate conditions across their range (generalist species) are expected to have broader tolerances to climate change than climatically restricted species (specialist species) (Brown, 1995); (3) species with restricted ranges are more likely to be sensitive to climate change than widespread species (Johnson, 1998); and (4) species from phytogeographical groups strongly exposed to climate change should be more sensitive” (Thuiller et al., 2005).

The sensitivity and stability of an ecosystem is the sum of all these reactions and adaptations. Higher order features of vegetation/ecosystems emerge from individualistic responses of plant taxa to climate change (Williams et al., 2004). Individualistic shifts in range and abundance for plant taxa scale up to cause compositional shifts within plant communities, appearance/disappearance of novel plant associations, changes in position, area, composition and structure of biomes. Changes in distribution of individual plant taxa therefore scale up to vegetation physiognomy even at continental to global scale.

Biome sensitivity studies suggested that the percentage of rainfall decrease necessary to shift from one biome to another is lowest for deciduous forests, followed by semi-deciduous forest, evergreen forest, grasslands, open woodlands, and finally closed savannas (Hély et al., 2009). It is not clear whether gallery forests are as sensitive to decrease in rainfall as other forest types because gallery forests have abundant access

to ground water and runoff (Silva et al., 2008). Once a gallery forest established in savannas, positive feedback effects may come into play and stabilize the extent of the gallery forest.

In 1983, White classified the vegetation of Africa after physiognomic and phytogeographic characteristics as well as edaphic and hydrological requirements, and proposed “White’s vegetation map of Africa” (Fig. 2). White’s classification provides a framework for the reconstruction of palaeo vegetation distribution and the latitudinal shift of entities over time. For the AHP, palaeo data coverage in subtropical Africa is extremely uneven, particularly in the Sahara and Sahel, and often coming from sedimentary sequences which are discontinuous or poorly dated (Watrín et al., 2009). Hély et al. (2014) applied White’s classification to available palaeo-botanical proxy data from several locations in Africa and from the African Pollen Database to reconstruct the Holocene vegetation distribution in relation to open surface water, derived from palaeo-hydrological proxies. The authors grouped pollen samples into the four main phytogeographical types that prevailed in subtropical Africa during the AHP: Guineo–Congolian type, Sudanian type, Sahelian type, and Saharan type. Reconstructions of these plant types suggest that “three broad latitudinal ecoclimatic entities can be distinguished beyond the omnipresence of Saharan taxa: latitudes north of 25° N were unequivocally dominated by Sahelian and Saharan elements throughout the Holocene. Between 20 and 25° N, the co-occurrence of Sudanian and Sahelian groups defined a typically “Sahelo-Sudanian” vegetational sector (Trochain, 1940). Then, south of 20° N the three phytogeographical groups cohabited, with the clear dominance of the two tropical humid ones” Hély et al. (2014).

The aforementioned four plant types serve as a reference for AHP diversity in this thesis. In the following, I briefly describe their main features and characteristic species. For the presentation of plant types’ individual reconstructed expansion during the AHP, I distinguish between “exclusive” taxa (plant species are exclusively found in a given group) and “non-exclusive” taxa (plant species may encompass several phytogeographical entities), referring to Hély et al. (2014).

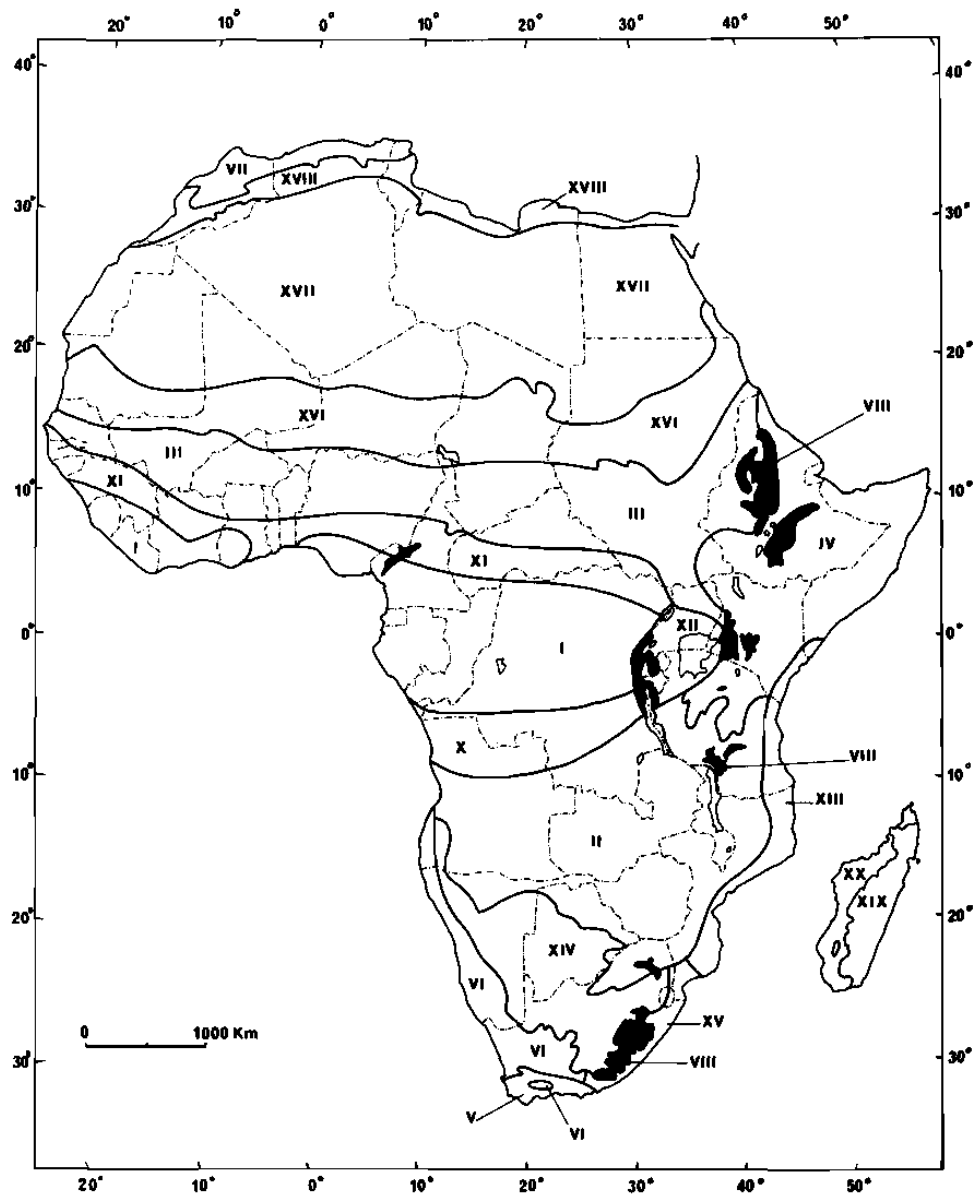


FIGURE 2: White's vegetation map of Africa (1983) – Main phytoria of Africa and Madagascar. Phytoria considered in this work are highlighted in bold letters. **I. Guineo-Congolian regional centre of endemism**, **II. Zambezian regional centre of endemism**, **III. Sudanian regional centre of endemism**, **IV. Somalia-Masai regional centre of endemism**, **V. Cape regional centre of endemism**, **VI. Karoo-Namib regional centre of endemism**, **VII. Mediterranean regional centre of endemism**, **VIII. Afromontane archipelago-like regional centre of endemism**, including **IX. Afroalpine archipelago-like region of extreme floristic impoverishment**, **X. Guinea-Congolia/ Zambezia regional transition zone**, **XI. Guinea-Congolia/ Sudania regional transition zone**, **XII. Lake Victoria regional mosaic**, **XIII. Zanzibar-Inhambane regional mosaic**, **XIV. Kalahari-Highveld regional transition zone**, **XV. Tongaland-Pondoland regional mosaic**, **XVI. Sahel regional transition zone**, **XVII. Sahara regional transition zone**, **XVIII. Mediterranean/Sahara regional transition zone**, **XIX. East Malagasy regional centre of endemism**, **XX. West Malagasy regional centre of endemism**

Guineo–Congolian type

The Guineo–Congolian type consists mainly of tropical humid semi-deciduous or evergreen forest taxa which grow under rainfall conditions with more than 1500 mm yr⁻¹ (Hély et al., 2014). White (1983) defined forest as a continuous stand of trees with a canopy height of 10 to 50 m, interlocking crowns, and several layers and storeys, including epiphytes and lianes. A shrub layer is usually present while the ground layer is of-



FIGURE 3: Guineo–Congolian vegetation type: Forest on the banks of the Congo river system (greenpeace.org).

ten sparse or absent due to low light conditions. Woody plants contribute most to biomass and physiognomy. Nearly all forests in Africa are evergreen or semi-evergreen. The Guineo–Congolian forest shows different forms depending on environmental conditions: rain forest (evergreen), dry forest (dry season several months, shorter, simpler, and floristically poorer than rain forest), semi-evergreen forest (some deciduous species, asynchronous leaf shedding), deciduous forest (mainly deciduous species, simultaneous leaf shedding, bare for several months), locally forests in dry regions, and gallery forests.

Characteristic and abundant Guineo–Congolian woody species in the wetter evergreen forests are nowadays *Caesalpinioideae*, *Soyauxia*, *Berlinia*, *Cynometra*, *Lophira alata*. In drier regions, more deciduous, mixed moist semi-evergreen forests are dominant with large trees such as *Entandrophragma angolense*, *Parinari glabra*, *Nauclea diderrichii*, *Parkia bicolor*. In mosaic formations in dry regions, the grass layer is formed by *Andropogon*, *Hyparrhenia*, *Panicum*, *Schizachyrium*, and fire-resistant trees are dominant such as *Terminalia* and *Combretum*. Some species grow well in gallery forests in the Sudanian region: *Vitex chrysocarpa*, *Syzygium guineense*, *Morelia senegalensis*, *Cola laurifolia*, *Pterocarpus santalinoides*, *Eleis guineensis* (Wittig et al., 2010).

During the AHP, non-exclusive and exclusive Guineo–Congolian taxa reached a maximum potential extension up to 20° N, having a core area around 18° N (Hély et al., 2014).

Sudanian type

The Sudanian type is characterized by tropical dry forest and savanna taxa growing with 500 to 1500 mm yr⁻¹ (Hély et al., 2014). According to White's classification (White, 1983), these species form open to closed woodlands, the most widespread vegetation form in Africa. Nearly all woodlands in Africa are semi-evergreen or deciduous, some evergreen species occur.

Woodlands are defined as open stands of trees, 8 to 20 m high with a surface coverage of < 40%, so crowns are not densely interlocking. Trees are not branched for at least 2 m and perennial or annual surface tussock grasses reach up to 2 m. Undershrub is present but very variable in size and number, mainly regulated by fire intensity and frequency. Most Sudanian trees have very wide geographic ranges and ecological tolerances; the proportion of woody species defines the subcategories: savanna woodlands, tree savannas, shrub savannas, grass savannas (Wittig et al., 2010). Referring to Walter (1971) woodland is the climax vegetation for semi-arid regions with > 500 mm yr⁻¹.

Typical Sudanian species are *Acacia erythrocalix*, *Anogeissus leiocarpa*, *Celtis integrifolia*, *Pterocarpus erinaceus* (Wittig et al., 2010). In the dryer northern woodlands, *Combretaceae* trees and shrubs are very abundant while *Isobertinia* is generally lacking. Characteristic trees are here *Adansonia digitata*, *Lannea microcarpa*, *Parkia biglobosa*, *Tamarindus indica*, *Vitellaria paradoxa*. Annual herbs are dominant such as *Andropogon pseudapricus*, *Loudetia togoensis*, *Schizachyrium exile*; perennials are rare and represented by *Andropogon gayanus*, *Heteropogon contortus*, and *Hyparrhenia subplumosa*. Gallery forests are dominated by Sudanian elements; Sahelian and Guinean species also appear such as *Pterocarpus santalinoides*, *Cola laurifolia*, *Vitex chrysocarpa*, *Syzygium guineense*. Wetter woodlands in the south are dominated by *Isobertinia doka*.

Exclusive Sudanian taxa occupied a similar core area as the Guineo–Congolian taxa (around 18° N) during the AHP. The maximum potential extension of non-exclusive Sudanian taxa reached 25° N (Hély et al., 2014).



FIGURE 4: Sudanian vegetation type: West Sudanian savanna, Burkina Faso (eoeearth.org).

Sahelian type

The Sahelian type is characterized by grassland or wooded grassland taxa growing from 150 to 500 mm yr⁻¹ (Hély et al., 2014). White (1983) located this type in the “Sahelian regional transitional zone” and associated the following vegetation types: (1) grasslands, dominated by grasses and herbs with 0 to 10% canopy-cover of woody species; (2) wooded grass-



FIGURE 5: Sahelian vegetation type: *Acacia tortilis* wooded grassland, Serengeti (biologie.uni-hamburg.de).

lands, dominated by grasses and herbs with woody plants covering 10 to 40% ; (3) shrubland, an open or closed stand of shrubs up to 2 m tall; (4) thicket, a closed stand of bushes and climbers usually between 3 and 7 m tall; (5) bushland, an open stand of bushes usually between 3 and 7 m tall, with a cover of 40% or more; (6) woodland, an open stand of trees at least 8 m tall with a canopy cover of 40% or more, the field layer usually dominated by grasses; (7) gallery forest, a continuous stand of trees along rivers and lakes, at least 10 m tall, with interlocking crowns (Lawesson, 1990). Tree density varies largely with water supply, fire frequency and soil type. Grassland is the climax vegetation in areas with 100 to 250 mm yr⁻¹ where frequent fires and poor soils prevent tree growth. Wooded grassland is the climax vegetation on deep sandy soils with 250 to 500 mm yr⁻¹ (Walter, 1971).

Most frequent woody species are *Acacia tortilis* var. *raddiana*, *A. laeta* and other thorny shrubs like *Commiphora africana*, *Balanites aegyptica*, *Boscia senegalensis*, *Ziziphus mauretania*. In the grass layer, one finds mostly annual grass species such as *Schoenfeldia gracilis* and *Aristida* and weeds such as *Boerhavia coccinea* and *Tribulus terrestris*. Wittig et al. (2010) reports that in the dryer northern sector, characteristic trees are *Acacia ehrenbergiana*, *A. raddiana*, *A. nilotica* var *tomentosa*, *Grewia tenax*, *Salvadora persica*. Abundant herbs are *Aristida* and *Tetrapogon* species. More tropical taxa can be found in gallery forests such as *Anogeissus leiocarpa*, *Mitragyna inermis*, *Acacia ataxacantha*, *A. seyal*. The wetter southern sector is dominated by Sahelian-Saharan woody species such as *Acacia laeta*, *A. nilotica* var *adansonii*, *A. senegal*, *Bauhinia rufescens*, *Boscia*

senegalensis, *Capparis tomentosa*, *Pterocarpus lucens*, *Euphorbia basamifera*. Characteristic herbes are *Brachiaria xantholeuca*, *Aristida hordeacea*, *Cenchrus biflorus*, *Eragrostis elegantissima*. In this region, some characteristic Sudanian species grow such as *Acaria macrostachya*, *Combretum micranthum*, *C. glutinosum*, *C. nigricans*, *Guiera senegalensis*, *Anogeissus leiocarpa*, *Balanites aegyptica*, *Lannea microcarpa*. In the southern wetlands, the vegetation is composed of *Anogeissus leiocarpa*, *Combretum micranthum*, *Celtis integrifolia*, *Mitragyna inermis*, *Daniellia oliveri*, *Vitex doniana*.

Sahelian taxa were always present in the whole Sahara and Sahel during the Holocene. Exclusive taxa had a stable core area centered at 19° N since during the AHP, and the maximum extent of non-exclusive taxa followed the maximum extent of lacustrine area up to 26° N (Hély et al., 2014).

Saharan type

The Saharan type consists of steppe and desert taxa growing with less than 150 mm yr⁻¹ (Hély et al., 2014). Deserts are regions where transpiration exceeds precipitation, leading to a water deficit for vegetation (White, 1983). The sparse vegetation cover in deserts impedes to categorize physiognomically due to highly specialized growth or simply too little individuals. In semi-deserts it is possible to define growth forms such as semi-desert grassland/-shrubland.

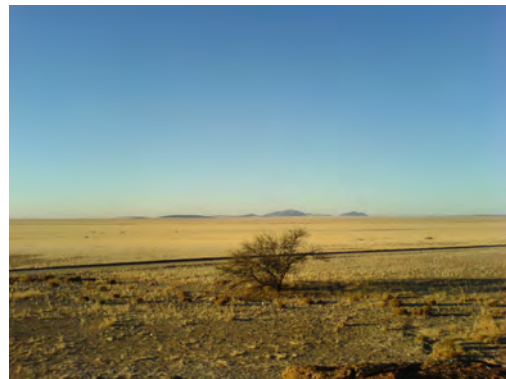


FIGURE 6: Saharan vegetation type: Semi-desert, desert-steppe transition, Namibia (geographie.uni-stuttgart.de).

Woody species occur mainly along watercourses or wadis (Le Houérou, 1980). The most important woody species are *Acacia tortilis* subsp. *raddiana*, *Acacia ehrenbergiana*, *Grewia tenax*, *Boscia senegalensis*, *Capparis decidua*, *Balanites aegyptiaca*, *Ziziphus mauritania*. Important perennial grasses are *Panicum turgidum* and *Aristida* spec.

The Saharan type reached up to 28° N at the peak of the AHP. Together with Sahelian elements, the Saharan taxa dominated latitudes north of 25° N (Hély et al., 2014).

Climate–vegetation interaction towards the end of the AHP

The “greening” of the Sahara during the AHP was triggered by changes in the Earth’s orbit, resulting in a stronger insolation and higher temperatures in the boreal summer than today, accompanied by an intensification of the West African summer Monsoon (WAM) (Kutzbach, 1981; Kutzbach & Guetter, 1986). However, modelling studies showed that the increase in insolation alone is insufficient to explain the vegetation cover reconstructed from palaeo records (see Yu & Harrison, 1996). It has been shown that several feedback mechanisms including ocean (Kutzbach & Liu, 1997; Braconnot et al., 1999), surface water coverage by lakes and wetlands (Coe & Bonan, 1997; Krinner et al., 2012), and vegetation and soil albedo (Claussen & Gayler, 1997; Claussen, 2009; Vamborg et al., 2011) could have amplified the changes due to orbital forcing.

A positive feedback between vegetation and precipitation in the Sahel was first proposed by Charney (1975) to explain the self-stabilization of deserts: the high albedo of bare soils implies a low energy input to the overlying atmosphere which induces a sinking motion of air and thereby suppresses convection and thus precipitation. In contrast, the low albedo of vegetation relative to bare desert soil implies more absorption of solar energy at the surface which heats the lower atmosphere, destabilizes the atmospheric lapse rate of temperature and increases the like-

lihood of convection and precipitation (Warner, 2004). Additionally, vegetation increases evapotranspiration at the expense of drainage and runoff, therewith moistening the atmosphere and further increasing the likelihood of precipitation (Kleidon et al., 2000; Hales et al., 2004). This positive feedback provides a mechanism that might allow for the existence of multiple stable equilibria, first shown in coupled model simulations by Claussen (1994) and Claussen et al. (1998). Depending on climate and environmental conditions, the Sahara could exist in a “green” state with high vegetation cover and

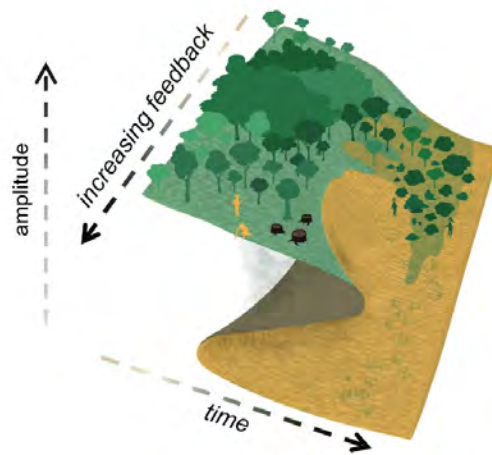


FIGURE 7: Stability landscape of “green” Sahara and “desert” state (modified after Bathiany et al. (2016)). The stronger the atmosphere–vegetation feedback, the sharper the transition between the two states.

a “desert” state without vegetation (Brovkin et al., 1998; Bathiany et al., 2012), illustrated in the lower edge of Fig. 7. The potential non-linearity of this feedback might cause an abrupt transition between these states when the system reaches a “tipping point” (Williams et al., 2011). Several climate model studies reproduced such an abrupt transition from “green” to “desert” state at around 5500 years BP for western Africa (e.g. Claussen et al., 1999; Brovkin & Claussen, 2008) and reconstructions of dust flux in the Atlantic supported an abrupt ending of the AHP at least for the western part of the Sahara (deMenocal et al., 2000).

Later studies highlighted the complexity of desertification history and the variety in timing and rate of regional changes. They challenged the hypothesis of an abrupt vegetation decline and doubted the existence of a strong positive climate–vegetation feedback in subtropical Africa. Pollen and sediment records from Lake Yoa in eastern Africa indicated a more gradual transition from “green” to “desert” Sahara (Kröpelin et al., 2008; Francus et al., 2013), implying that the vegetation–climate feedback was rather weak, illustrated in the upper edge of Fig. 7. Palaeo-hydrologically dated records from fluvial, lacustrine, and palustrine environments supported a gradual transition from wet to dry conditions (Lézine, 2009; Lézine et al., 2011). Observation based estimates of feedback strength in northern Africa showed little direct evidence of a strong positive vegetation effect on large-scale precipitation (Liu et al., 2006). In the framework of the Paleoclimate Modeling Intercomparison Project, Phase II (PMIP2), some models even suggested a negative feedback over northern Africa for the mid-Holocene (Braconnot et al., 2007). Liu et al. (2007) demonstrated an abrupt vegetation collapse in coupled transient simulations, but the authors attributed this to a non-linear vegetation response to a precipitation threshold in the presence of strong climate variability, independent of a climate–vegetation feedback. Rachmayani et al. (2015) recently showed a positive effect of vegetation on precipitation caused by evapotranspiration effects rather than albedo effects.

Plant diversity and climate–vegetation system stability

Claussen et al. (2013) introduced a new aspect in the discussion on the strength of climate–vegetation feedback and its impact on the rate of the transition from the “green” Sahara to the “desert” state, namely plant diversity. The authors stated that plant diversity in terms of moisture requirements could affect the strength of climate–vegetation feedback. In a conceptual model study, with hypothetical discrete plant types, they demonstrated that in coupled interaction with precipitation, sensitive plant types tended to sustain longer with decreasing precipitation, while resilient plant types disappeared earlier than they would have done on their own. The mean vegetation cover decreased more gradually with strong fluctuations under drying conditions, capturing the decline in pollen influx into Lake Yoa between 6000 and 4000 years BP fairly (Kröpelin et al., 2008). From this the authors concluded that plant diversity might increase the stability of the climate–vegetation system in semi-arid regions, buffer the strength of individual plant–precipitation feedback and prevent an abrupt vegetation collapse. Further, the authors suggested that plant composition is of high importance for the rate of transition and a reduction in functional plant diversity may lead to an abrupt regime shift.

Plant diversity is the subcategory of biodiversity that concerns vegetation. The first recorded definition of the broad term biodiversity was proposed by Wilson (1988) as “The variety of life at every hierarchical level and spatial scale of biological organizations: genes within populations, populations within species, species within communities, communities within landscapes, landscapes within biomes, and biomes within the biosphere.” The definition from the “Convention on Biological Diversity” (1992) is nowadays the internationally accepted definition of biodiversity: “Biological diversity means the variability among living organisms from all sources including, *inter alia*, terrestrial, marine and other aquatic ecosystems and the ecological complexes of which they are a part; this includes diversity within species, between species and of ecosystems.” I am hereinafter explicit in the use of terminology following Hooper et al. (2005), referring to “richness” or “abundance” when talking about numbers of plants, “plant diversity” when talking about more general attributes including relative abundances and composition, and “biodiversity” only when the broadest scope of the term is valid.

The spectrum of diversity measures is wide because of the large range of components. Diversity can be described in terms of numbers of entities (how many genotypes, species,

or ecosystems), the evenness of their distribution, the differences in their functional traits, and their interactions (Hooper et al., 2005). Traditionally, recording diversity is based on species diversity and the niche concept, described in detail by Whittaker (1972). The ecological niche of a species describes its position in a multidimensional hyperspace, where the axes correspond to all gradients of an environment. Species differ not only in the position in the hyperspace, but also in the proportion of niche hyperspace they are able to occupy and the share of resource they utilize (= productivity). Species evolve to use different parts of these gradients to minimize competition, but in reality, the extent of a species niche is reduced from the “potential niche” under optimum conditions to the “realized niche” which accounts for actual biotic and abiotic environmental conditions. Through time, additional species can enter the system or leave due changing conditions.

In the last years, the focus changed from species diversity to functional diversity. Functional types are non-phylogenetic groups that include a set of species with similar effects on a specific ecosystem process or similar response to environmental conditions (Hooper et al., 2005; Wilson, 1999). Mason & de Bello (2013) proposed a definition of functional trait diversity as the distribution in functional trait space of the species presence and abundance in a community, including three components: the amount of functional trait space filled by species in the community (functional richness), the evenness of abundance distribution in filled trait space (functional evenness), and the degree to which the distribution of species abundances maximizes divergence in functional traits (functional divergence). In the modelling community, functional plant diversity is nowadays typically reflected in the concept of “Plant Functional Types” (PFTs), discussed in more detail later on in Chapter 2.

The importance of plant diversity for climate–vegetation system stability and ecosystem stability has been debated over several decades, amongst other things because stability has several facets and ecological studies do not always refer to the same aspect. Commonly, there are four properties associated with stability: persistence, the tendency of a system to exist in the same state through time; resistance, the capability of a system to remain unchanged in the face of external pressures such as disturbances; resilience, the ability of a system to return to its original or equilibrium state after it has been displaced from it by external pressure; and temporal variability, used as an inverse measure of resistance (Scherer-Lorenzen, 2005). Before 1970, ecologists assumed a positive

relationship between biodiversity and ecosystem stability based on simplified observations (Elton, 1958; MacArthur, 1955). This intuitive idea was questioned by May (1973), who proposed a destabilizing effect of species richness on ecosystem dynamics based on a statistical model approach with random populations. This statement was supported by other studies, pointing to the relevance of different trophic levels in stability studies (Pimm & Lawton, 1978). Later, longterm field studies on grasslands indicated that biodiversity stabilizes community and ecosystem processes (Tilman, 1996; Tilman et al., 1997). Sankaran & McNaughton (1999) suggested that “across larger ecological scales, extrinsic determinants of biodiversity such as disturbance regimes and site history may be the primary determinants of certain measures of community stability”. The overall opinion is nowadays that biodiversity might on average rise the stability of ecosystems regarding all properties of stability, but it is not the driver (McCann, 2000). Numerous features of ecosystems affect stability, including the number of species, the variety of functional types, effects of dominant species, keystone species, ecological engineers, and interactions among species (e.g., competition, facilitation, mutualism, disease, and predation (Tilman et al., 1997; McCann, 2000; Hooper et al., 2005), the topology of food webs, and the sensitivities of species to different types of environmental perturbations (Ives & Carpenter, 2007). “Some ecosystem properties are initially insensitive to species loss because (a) ecosystems may have multiple species that carry out similar functional roles, (b) some species may contribute relatively little to ecosystem properties, or (c) properties may be primarily controlled by abiotic environmental conditions” (Hooper et al., 2005).

Plant diversity changes on timescales of decades to millennia and on spatial scales from local to regional, driven by “Climate change, habitat fragmentation, resource exploitation and transcontinental species introductions” (Jackson & Overpeck, 2000). Extinction and immigration can be triggered by forcing events of different speed (rapid or gradual) and frequency (singular or sequential). Immigration usually lags the forcing because “Colonization of a suitable site requires sequential successes in the dispersal of propagules, establishment of individuals, survival to reproductive maturity, and growth and persistence of populations via continued reproduction; failure or delay in any of these steps leads to delayed immigration [...] Delayed extinction, similar to delayed immigration, also results from demographic and stochastic processes” (Jackson & Sax, 2010). The delayed response of vegetation allows several potential transient conditions to exist

before plant diversity slowly attains equilibrium (Vellend et al., 2006; Diamond, 1972; Brooks et al., 1999). Plant diversity is thus a result of environment and community history on local and regional scale.

Long-term data sets such as pollen profiles derived from sediments provide a basis for studying processes involved in plant diversity changes on longer timescales. Reconstruction of vegetation from pollen is a common approach to investigate palaeo vegetation and changes in plant diversity. Pollen based biome reconstructions capture main features of vegetation distribution, but downplay the magnitude and variety of vegetation responses to climate change (Williams et al., 2004). One of the main open questions is how pollen diversity from samples actually depicts plant diversity. The relation between pollen diversity and parent plant diversity is not straight forward as “Plants remains indicating their past abundances are disproportionate to the abundance of their parent species” (Reitalu et al., 2014). The occurrence and abundance of pollen in a sample depend on many different factors such as basin size, plants’ distance to the basin, sample size, taxonomical precision, differences in pollen productivity, pollen dispersal ability, and sedimentary rate. Palynologists have produced models such as POLLSCAPE (Sugita, 1994) and HUMPOL (Bunting & Middleton, 2005) to calculate pollen dispersal and deposition in heterogeneous landscapes, and the estimation of pollen assemblages in lakes or bogs of given sizes (Gaillard et al., 2008). If biases due to productivity and dispersal are assumed species specific and constant over time, relative changes in plant diversity could be assessed (Xiao et al., 2008).

Motivation of this thesis

The motivation of this thesis is to explore the role of plant diversity in simulated climate–vegetation interaction in models of different complexity, from the conceptual approach by Claussen et al. (2013) to the Dynamic Global Vegetation Model (DGVM) JSBACH, the land component of the Max Planck Earth System Model MPI-ESM1. Therewith, I aim at contributing to the understanding of the role plant diversity plays in simulated climate–vegetation interaction and at shedding light into the discussion on the importance of climate–vegetation feedback towards the end of the AHP. To accomplish that, I address the following three questions:

- *Is the approach by Claussen et al. (2013) ecologically reasonable and do the conclusions hold if the model was adjusted to AHP vegetation reconstructed from pollen?*
- *How is plant diversity represented in the comprehensive land surface model JSBACH and how do variations in plant diversity affect the vegetation response to a prescribed precipitation decline?*
- *How does plant diversity in JSBACH in turn affect precipitation in coupled ECHAM6/JSBACH simulations and what consequences result for the stability of the “green” Sahara and the transition to the “desert” state?*

The first chapter of this thesis opens with an assessment of the conceptual model by Claussen et al. (2013) from an ecological point of view, and provides an improved version that accounts for the diversity of AHP plant types reconstructed from pollen by Hély et al. (2014). Part of this chapter was published in:

V. P. Groner, M. Claussen, and C. Reick. Palaeo plant diversity in subtropical Africa – Ecological assessment of a conceptual model of climate–vegetation interaction. *Clim. Past*, 11, 1361–1374, 2015.

In the second chapter, I assess the representation of plant diversity in JSBACH and study vegetation performance as a function of “Plant Functional Type” (PFT) diversity along a prescribed precipitation decline. This conceptual use of JSBACH in “offline” simulations serves as an intermediate step between the conceptual model in Chapter 1 and the coupled ECHAM6/JSBACH in Chapter 3.

In the third chapter, I present coupled ECHAM6/JSBACH simulations with different degrees of PFT diversity to address how precipitation is in turn affected by PFT composition and diversity, and how the interaction between vegetation and atmosphere could have affected the stability of the “green” Sahara and the transition to the “desert” state.

Finally, I summarize the findings from this thesis regarding the representation of plant diversity in models of different complexity and the effect of plant diversity on simulated climate–vegetation interaction towards the end of the AHP. As an outlook, I suggest future research perspectives that could improve the representation of plant diversity, vegetation dynamics and climate–vegetation feedback in comprehensive dynamic vegetation models, explicitly JSBACH.

Chapter 1

Palaeo plant diversity in subtropical Africa – Ecological assessment of a conceptual model of climate–vegetation interaction

1.1 Introduction

In spite of the rapid development in General Circulation Models (GCMs) over the last years, conceptual models haven't lost their value for addressing complex scientific questions. Reducing a system to its substantial components can help to identify and understand relevant system processes, roles of involved factors, and their interactions. One prominent system that has been extensively studied with conceptual models is the coupled land–atmosphere system. The fascinating questions are (a) whether the feedbacks between climate and land surface could be strong enough to support multiple stable states of the system on a regional or global level, and (b) whether the potential non-linearity of these feedbacks might cause an abrupt transition between these states when the system reaches a “tipping point”.

Early studies with the “energy balance model” proposed two different stable states resulting from a positive albedo-temperature feedback in the high latitudes: an “ice-free” or an “ice-covered” state (e.g. Budyko, 1969; Sellers, 1969; Ghil, 1976; North et al., 1981).

Li et al. (1997) found two stable equilibria of vertical temperature profiles using the “one-dimensional radiative-equilibrium model”. The conceptual model of atmosphere–vegetation interaction in subtropical deserts by Brovkin et al. (1998) exhibited multiple stable states in the system: a “desert” state with low precipitation and absent vegetation and a “green” Sahara state with moderate precipitation and permanent vegetation cover. The above-mentioned two stable states (Claussen, 1994; Claussen & Gayler, 1997; Claussen et al., 1998; Brovkin et al., 1998; Renssen et al., 2003) as well as abrupt transitions between them (Claussen et al., 1999; Wang & Eltahir, 2000; Bathiany et al., 2012) were also found in comprehensive models for the Sahara/Sahel region, supporting the hypothesis of strong climate–vegetation feedback. The origin of this bistability lies in the biophysical and biochemical differences between bare desert soil and vegetation. The low albedo of vegetation relative to bare desert soil implies more absorption of solar energy at the surface which heats the lower atmosphere, destabilizes the atmospheric lapse rate of temperature and increases the likelihood of convection and precipitation (Warner, 2004). Additionally, vegetation increases evapotranspiration at the expense of drainage and runoff, therewith moistening the atmosphere and further increasing the likelihood of precipitation (Kleidon et al., 2000; Hales et al., 2004). More precipitation in turn favors more vegetation and stabilizes the “green” state. On the other hand, the high albedo of bare soils implies a low energy input to the overlying atmosphere inducing a sinking motion of air which suppresses convection and thus precipitation (Charney, 1975). Less precipitation in turn impedes vegetation establishment and stabilizes the “desert” state.

In this context, it should be noted that the existence, strength and sign of this feedback and associated abrupt regime shifts are still under debate as discussed in the General Introduction. Claussen et al. (2013) introduced a new aspect into the discussion, proposing that different viewpoints are not contradicting if one accounts for plant diversity. The authors extended the conceptual approach by Brovkin et al. (1998) by a number of hypothetical discrete plant types to account for plant diversity in terms of moisture requirements. They demonstrated that high plant diversity could stabilize a climate–vegetation system by buffering strong feedbacks between individual plant types and precipitation, whereas a reduction in plant diversity might allow for an abrupt regime shift under gradually changing environmental conditions. Thereby, climate–vegetation feedback strength would not be a universal property of a certain region but depend on

the vegetation composition. However, it remains unclear if the approach by Claussen et al. (2013) is ecologically reasonable and if the conclusions hold if the model was adjusted to AHP vegetation reconstructed from pollen.

The purpose of this chapter is to address this open question with a critical assessment of the conceptual model by Claussen et al. (2013) from an ecological point of view, and the provision of an improved version that accounts for the diversity of plant types that prevailed during the African Humid Period (AHP).

In the first section, I evaluate the representation of plant–plant interaction and plant–climate feedback in the conceptual approach by Claussen et al. (2013) referring to the previously reviewed current state of knowledge in ecological literature, and further discuss how the suggested conclusions fit in an ecological context.

In the second section, I present a new model version adjusted to AHP vegetation by the modification of four fundamental aspects. First, the growth ranges in terms of moisture requirements are extended by upper limits to represent full environmental envelopes. Second, data-based AHP plant types replace the hypothetical plant types. Third, the tropical gallery forest type, indirectly linked to local precipitation, follows mainly the gradual insolation forcing with a linear approximation. Fourth, I replace the dimensionless vegetation cover fraction with individual effective leaf areas to capture different contributions to climate–vegetation feedback. These changes allow for studies on the roles of different real plant types in an ecosystem and their combined climate–vegetation feedback under changing environmental conditions.

Part of this chapter was published in

V. P. Groner, M. Claussen, and C. Reick. Palaeo plant diversity in subtropical Africa – Ecological assessment of a conceptual model of climate–vegetation interaction. *Clim. Past*, 11, 1361–1374, 2015.

1.2 The conceptual approach by Claussen et al. (2013)

1.2.1 The model formulation by Claussen et al. (2013)

The approach by Claussen et al. (2013) is based on a conceptual description of climate–vegetation feedback in semi-arid regions (Brovkin et al., 1998; Liu et al., 2006). The applicability is restricted to a region that experiences a uniform climate, which approximately corresponds to the grid size of a GCM in the order of 100 km². Within this region, the diversity of coexisting plant types $i = 1, \dots, N$ reflects the heterogeneity of the environment that provides ecological niches for N different plant types.

Diversity is defined here in terms of specific moisture requirements and sensitivities to changes in mean annual precipitation P . The model does not explicitly account for direct plant–plant interactions such as competition or facilitation. Claussen et al. (2013) assumed that each plant type can occupy a share of $1/N$ of the ecological space (E-space). The assumption of niche stability/conservatism – a concept that assumes species maintaining the

parameters of their ecological niche following environmental change (Huntley et al., 1989; Peterson et al., 1999; Peterson, 2011; Stigall, 2012) – prohibits the replacement of disappearing plants by remaining plant types. These assumptions are hereinafter referred to as the “niche approach” (Claussen et al., 2013). The change of relative vegetation cover fraction V_i (non-dimensional between 0 and 1) under external forcing is determined by

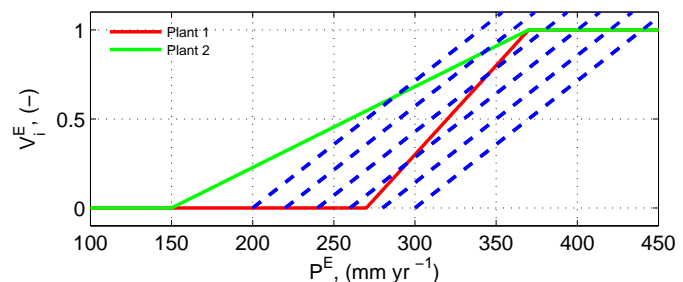


FIGURE 1.1: Vegetation–precipitation stability diagram (V_i^E , P^E) for two hypothetical plant types $i = 1, 2$ after Claussen et al. (2013). Full lines depict the equilibrium curves for vegetation cover $V_i^E(P^E)$ for plant type 1 which is sensitive (red) and for plant type 2 which is resilient (green) to changes in P . Dashed blue lines show hypothetical equilibrium precipitation curves $P^E(V_i^E)$ for different time slices (4500, 4900, 5300, 5700, 6100, and 6500 years BP, from left to right). Intersections between the two types of curves indicate equilibrium coupled states which can be stable or unstable.

$$\frac{dV_i}{dt} = \frac{V_i^E(P) - V_i}{\tau}, \quad (1.1)$$

with the time step t in years, setting $t = 0$ for present day and negative values for the past, and the vegetation equilibrium timescale $\tau = 5$ years (Liu et al., 2006). The equilibrium vegetation cover fraction V_i^E is a function of P , and is shaped by lower and upper precipitation thresholds, P_i^{C1} and P_i^{C2} , respectively. Their difference $D_i^C = P_i^{C2} - P_i^{C1} > 0$ determines the slope of $V_i^E(P)$ in the intermediate precipitation regime

$$V_i^E(P) = \begin{cases} 1 & P \geq P_i^{C2} \\ \frac{(P - P_i^{C1})}{D_i^C} & P_i^{C2} > P > P_i^{C1} \\ 0 & P \leq P_i^{C1} \end{cases} . \quad (1.2)$$

When all plant types interact together with climate, the mean vegetation cover fraction V_S is calculated as the average of all individual plant types:

$$V_S = \frac{1}{N} \sum_{i=1}^N V_i \leq 1 , \quad (1.3)$$

assuming that the atmosphere reacts to the average properties of the whole area. The justification for this assumption is that the difference in crucial surface parameters such as albedo and hydrological properties is smaller between considered plant types than the contrast to desert.

Accounting for climate–vegetation feedback, precipitation is a combination of a background precipitation P_d in absence of vegetation that changes with external gradual insolation forcing, and a precipitation component induced by vegetation feedback. The equilibrium precipitation P^E is defined as

$$P^E(V_S, t) = P_d(t) + D^B \cdot V_S , \quad (1.4)$$

with the climate feedback coefficient D^B that determines the feedback strength. For simplicity, Claussen et al. (2013) assumed the same $D^B = 140 \text{ mm yr}^{-1}$ for all plant types (Liu et al., 2006), implying that the feedback is only sensitive to vegetation cover but not to composition. The background precipitation P_d changes linearly with time, mimicking the weakening of the West African Monsoon due to continuous change in insolation forcing:

$$P_d(t) = P_{d0} (1 - (t + 6500)/T) , \quad (1.5)$$

where $P_{d0} = 300 \text{ mm yr}^{-1}$ is the initial precipitation of the simulation period $T = 6500$ years (Hansen et al., 2007; New & Jones, 1999). The natural variability in precipitation, independent from vegetation, is implemented as additional white noise forcing $P_N(t)$ in the total precipitation

$$P(V_S, t) = \max((P^E(V_S, t) + P_N(t), 0)) . \quad (1.6)$$

The intersections of P and V in a vegetation–precipitation diagram indicate equilibrium-coupled states, see Fig. 1.1. System instability and multiple equilibria only exist for a sufficiently strong positive vegetation feedback with $D^B > D_i^C$ (Liu et al., 2006).

1.2.2 Assessment of the model set up by Claussen et al. (2013)

The basic units in the conceptual model by Claussen et al. (2013) are plant types that reflect the heterogeneity of the environment, occupying different n -dimensional niches. In the actual realization of plant types in the model formulation, plant diversity is only expressed in terms of different precipitation thresholds as a proxy for moisture requirements, which reduces the fundamental multidimensional niche to one portion of its climatic component. The choice of thresholds implicitly defines plants’ sensitivities to changes in precipitation. Moisture requirement is an established measure to characterize plant diversity in recent African ecosystems (White, 1983), and the measure is appropriate in the conceptual model because hydrology is the main determinant of plant growth in the subtropics on the considered scale of the order of 100 km^2 (Coughenour & Ellis, 1993). For a more versatile description of plants’ niches and the explanation of actual vegetation composition and spatial distribution within the considered region, further crucial determinants need to be taken into account. The coexistence of trees and grasses in subtropical regions and the maintenance of their ratios is a complex topic, studied for years in the framework of the “savanna question”, but still not well understood (Sarmiento, 1984; Scholes & Archer, 1997; Jeltsch et al., 2000; Staver et al., 2011). The complexity arises from the many aspects involved such as mean annual precipitation, seasonality, soil type, soil moisture, surface water availability, community structure, competition, community history, and disturbances (fire, herbivory).

With the niche approach, Claussen et al. (2013) designed the effective interaction between vegetation and climate from bottom up. Each plant type has specific requirements

and responds individually to changes in mean annual precipitation, but the combined interaction of all considered plant types with precipitation determines and smooths the evolution of mean vegetation cover on a larger scale. This approach is supported by Williams et al. (2004) who proposed that higher order features of ecosystems emerge from plants' individual responses to changing environmental conditions. Ecosystem features such as composition and physiognomy have a large impact on the exchanges of energy, moisture, aerosols, and trace gases between the land surface and atmosphere and finally on precipitation.

The niche approach also implies that once a specific plant type retreats owing to water scarcity, there may not be any other type that is able to occupy its place in the E-space. From an ecological point of view, existing plants likely benefit from the extinction of others by having less competition and more resources available. It is questionable whether these succeeding species can occupy the niches (E-space) of disappearing species, including their way of using resources, and overtake their ecosystem functions, or if they just occupy the available barren area (geographical space, G-space).

Apart from the diversity in moisture requirements, the variety in feedback strength and climate impact arising from the particular plant properties is not sufficiently reflected in the original model: the dimensionless potential vegetation cover and the homogeneous climate feedback coefficient D^B mainly account for the albedo effect of the total area while inter-plant deviations in colour, reflectance properties, surface roughness, potential leaf area, and evapotranspiration capacities are neglected.

1.2.3 Assessment of the interpretation of results by Claussen et al. (2013)

Based on a number of simulations, Claussen et al. (2013) concluded that plant diversity can have a buffering effect on ecosystem performance and further on the strength of climate–vegetation feedback. They reasoned that in species-rich ecosystems, the likelihood of some species being pre-adapted to changing environmental conditions is higher than in species poor systems. This relationship between high diversity and ecosystem stability has been debated for several decades, among other things due to the inconsistent definition of stability. I follow Pimm (1984) here, who defined stability as a twofold system property: resilience is the speed with which a community returns to a former state having been displaced from it by perturbation, while resistance is the ability to avoid

such displacement. In the light of recent ecological literature, reviewed in the General Introduction, the finding of a positive diversity–stability relationship by Claussen et al. (2013) is reasonable for a region of the order of 100 km². In connection with this relationship, Claussen et al. (2013) concluded that the stability of a climate–vegetation system can determine and arise from individual plant types’ presence over longer timescales. In combined interaction with climate, sensitive plants likely grow longer than they would do on their own as they benefit from additional water and facilitation effects in a more life-sustaining environment. The duration of persistence of resilient plants is likely shortened as they suffer to a certain degree from additional competition (Brooker, 2006). This effect occurs in the model even though interactions are not explicitly modelled.

One of the main conclusions by Claussen et al. (2013) was that strong or weak climate–vegetation feedback was hard to diagnose and disentangle regarding abrupt climate changes on a regional scale. The feedback between climate and a certain plant type could be strong, but this might be capped in combination with other plant types, resulting in a gradual decline of total vegetation. Indeed, vegetation composition can play a crucial role for the ecosystem and the removal or introduction might change the system stability by changes in the ratio of individual influences (Scherer-Lorenzen, 2005). In order to keep ecosystem function stable, a minimum number of functional types is required that occupy a minimum number of niches. The addition of taxa results in a more and more complex network of interactions. While some taxa are redundant, others are irreplaceable. If these so-called “keystone species” disappear, the system might collapse. The appearance of new taxa could also interfere with networks and change energy and matter fluxes in the system, resulting in a destabilization of the ecosystem (McCann, 2000). Hence, Claussen et al. (2013) argued ecologically reasonably that it is difficult to determine the origin of system stability as the overall feedback strength depends on species composition. These difficulties are not inconsistent with previous studies that proposed strong climate–vegetation feedback, resulting in abrupt shifts from a stable “green” state to a stable “desert” state. For example, simulations by Claussen et al. (1999) were performed with the lowest possible number of PFTs, one tree and one grass. The low plant diversity implies a high likelihood for abrupt transitions (Scherer-Lorenzen, 2005; Claussen et al., 2013).

1.3 Application of the conceptual model by Claussen et al. (2013) to AHP vegetation

1.3.1 Does the model by Claussen et al. (2013) capture the diversity of AHP vegetation?

The approach by Claussen et al. (2013) offers a useful tool to deal with the question how plant diversity might affect climate–vegetation interaction in semi-arid regions. However, the model reaches its limits when it comes to the application to AHP vegetation reconstructed from pollen, here referring to Hély et al. (2014). Hély et al. (2014) applied “White’s classification of Africa” (1983) to palaeo-botanical proxy data from several locations in Africa and from the African Pollen Database in order to reconstruct the Holocene vegetation distribution in relation to open surface water, derived from palaeo-hydrological proxies. Pollen samples were grouped into four phytogeographical types, which are mainly characterized by their precipitation requirements and physiognomic structure: (1) Guineo–Congolian type (tropical humid semi-deciduous or evergreen forest taxa, $> 1500 \text{ mm yr}^{-1}$); (2) Sudanian type (tropical dry forest, woodlands, and wooded savanna taxa, $500 \text{ to } 1500 \text{ mm yr}^{-1}$); (3) Sahelian type (grassland or wooded grassland taxa, $150 \text{ to } 500 \text{ mm yr}^{-1}$), and (4) Saharan type (steppe and desert taxa, $< 150 \text{ mm yr}^{-1}$).

Throughout this work, I use the terminology of phytogeographical plant types after Hély et al. (2014) whenever I refer to my work, including the descriptions of the adjusted model and simulations as well as results, discussions, and conclusions. Since literature often refers to the terminology of physiognomic vegetation types, I stick with their terminology in citations and indicate the corresponding phytogeographical plant types after Hély et al. (2014) in brackets to prevent confusions.

When defining the precipitation thresholds for each plant type, a direct relation between precipitation and plant available water was assumed by Claussen et al. (2013). This is not appropriate for all AHP plant types. Tropical Guineo–Congolian taxa (GC type) cannot be captured with this approach using the parameters of Claussen et al. (2013) because the initial precipitation $P(V_S, -6500)$ is too low to reach their minimum threshold P_{GC}^1 . These species grow in gallery forest or ripicolous stripes where a high water availability is more or less constantly provided, and local precipitation is of minor importance. Xeric

species of the Saharan and Sahelian type have special adaptations such as deep tap roots or succulent tissues (e.g. Wickens, 1998) that allow them to grow far below the minimum threshold for a phytogeographic plant type given by literature. Nonetheless, growth ranges of phytogeographic plant types provide a point of reference, and expose the fact that the range of precipitation thresholds assumed by Claussen et al. (2013), between 150 and 370 mm yr⁻¹, is far below the variety of thresholds of AHP vegetation reconstructed from pollen (Hély et al., 2014).

Regarding the calculation of mean vegetation with the niche approach, climate–vegetation interaction provides the expected gradual decline in mean vegetation cover towards the end of the AHP. Niches can only be occupied by specialized plant types, for instance gallery forests (GC) cannot grow beyond a certain distance from surface water while steppe plants (Saharan type) do not survive on moist soils along river banks. However, the niche approach does not account for the evolution of vegetation composition in terms of spatial succession. Pollen data from eastern Africa suggest the decrease in tropical trees and grasses (GC and Sudanian type) starting at around 5500 cal yr BP going hand in hand with the expansion of characteristic desert taxa (Saharan type). The demise of tropical trees (GC and Sudanian type) was temporarily compensated by Sahelian elements (Kröpelin et al., 2008). For the geographically explicit simulation of vegetation change, a model more sophisticated than my conceptual approach is required.

The large diversity of plant properties besides moisture requirements highlights the importance of plant-specific feedback strengths. With a dimensionless vegetation cover fraction, Claussen et al. (2013) mainly account for a homogeneous albedo. Differences in colour and reflectance properties are not implemented. Generally, tropical leaves (GC and Sudanian type) are darker than steppe grasses (Saharan type) (White, 1983) and their albedo-feedback impact should be weighted differently. Structural properties are homogenized, assuming the same feedback coefficient for all plant types. The leaf area of tropical taxa (GC and Sudanian type) might be up to 3 times higher than that of steppe taxa (Saharan type) (Hély et al., 2009), resulting in strong evapotranspiration differences. Evapotranspiration seems to be involved in important feedback mechanisms that influence the strength of the West African Monsoon (Rachmayani et al., 2015).

In summary, the original conceptual model by Claussen et al. (2013) seems to capture the stabilizing effect on ecosystem performance by accounting for differential moisture

requirements and homogeneous feedback for all plant types. Important determinants of vegetation cover, such as fire or competition, and individual feedback strengths due to albedo and evapotranspiration differences are omitted. The diversity of AHP vegetation reconstructed from pollen data cannot be captured; especially tropical gallery forest plant types (GC type) are not represented.

1.3.2 Model adjustment

In order to apply the conceptual model by Claussen et al. (2013) to AHP vegetation, I modify different aspects as described in the following section.

The environmental envelopes in terms of moisture requirements are extended by an upper precipitation threshold. Data-based AHP plant types are implemented, namely the Saharan type, Sahelian type, Sudanian type, and Guineo–Congolian type. Specific tolerance threshold values for these plant types, except for the Guineo–Congolian gallery forest type, are derived from observations on characteristic species (see Tab. 1.1), implicitly accounting for competitive interactions and fire that cannot be separated from water constraints. The optimum growth ranges are based on pollen analysis by Hély et al. (2014). The relative vegetation cover fraction (initially $V_{i,\max} = 1$) is replaced by a weighting factor modelled after the leaf area index. This effective leaf area L_i (in m^2 per unit niche area) of each plant type i changes according to V_i in Eq. 1.1. In equilibrium, L_i^E is specified as a function of total precipitation P :

$$L_i^E(P) = \begin{cases} 0 & P \geq P_i^{C4} \\ L_{i,\max} - \frac{(P - P_i^{C3}) \cdot L_{i,\max}}{D_i^{C2}} & P_i^{C4} > P \geq P_i^{C3} \\ L_{i,\max} & P_i^{C3} > P \geq P_i^{C2} , \\ \frac{(P - P_i^{C1}) \cdot L_{i,\max}}{D_i^{C1}} & P_i^{C2} > P \geq P_i^{C1} \\ 0 & P < P_i^{C1} \end{cases} \quad (1.7)$$

with a maximum potential extension $L_{i,\max}$. $D_i^{C1} = P_i^{C2} - P_i^{C1} > 0$ for the increasing branch and $D_i^{C2} = P_i^{C4} - P_i^{C3} > 0$ for the decreasing branch of the environmental envelope. For simplicity, I aggregate all surface parameters crucial for climate–vegetation feedback – leaf area, albedo, and hydrological properties – in L_i , and keep the climate feedback coefficient D^B constant for all plant types. This is possible because L_G and

TABLE 1.1: Precipitation thresholds P_i^{C1} to P_i^{C4} (in mm yr^{-1}) and maximum effective leaf area $L_{i,\text{max}}$ (in m^2 per unit niche area) for the African Humid Period (AHP) plant types: Saharan type, Sahelian type, and Sudanian type.

	Saharan type	Sahelian type	Sudanian type
P_i^{C1}	0 absolute minimum	20 <i>Acacia tortilis</i> Baumer et al. (1983)	150 <i>Celtis integrifolia</i> Le Hou��rou (1980)
P_i^{C2}	100 Saharan desert boundary 100 mm isohyet Wickens (1998)	150 H��ly et al. (2014)	500 H��ly et al. (2014)
P_i^{C3}	150 H��ly et al. (2014)	500 H��ly et al. (2014)	1500 H��ly et al. (2014)
P_i^{C4}	600 <i>Ziziphus mauritiana</i> Le Hou��rou (1980)	900 <i>Balanites aegyptiaca</i> Baumer et al. (1983)	1800 <i>Pterocarpus erinaceus</i> Le Hou��rou (1980)
$L_{i,\text{max}}$	1	2	3

D^B show up as a product in my model (see Eq. 1.11). Values for $L_{i,\text{max}}$ are chosen to qualitatively represent the variety of these aggregated properties following observation-based classifications (H  ly et al., 2006, 2009). A high L_i also indicates a dark leaf colour, characteristic for tropical taxa (GC and Sudanian type), which is related to a low albedo, a strong climate feedback, and a potentially abrupt collapse. A lower L_i represents dry bright leaves, characteristic for xeric taxa (Saharan and Sahelian type), and is associated with a low albedo feedback potential. The differences between considered plant types might be smaller than the contrast to desert, but investigating individual roles necessitates disentangling the contributions.

The Guineo–Congolian plant type cannot be captured with this approach as the initial precipitation $P(V_S, -6500)$ is too low to reach its minimum threshold P_{GC}^{C1} . This tropical plant type grows in gallery forest or ripicolous stripes where a high water availability is more or less constantly provided. Local precipitation is less important than the large-scale climate which is assumed to be determined by orbital forcing. In order to account for this special relation to water availability, the effective leaf area L_{GC}^E of this plant type is prescribed with a linear approximation, following the gradual insolation forcing and P :

$$L_{GC}^E(t, P) = -a - \frac{1}{b} \cdot t + c \cdot P . \quad (1.8)$$

The parameters a , b and c are tuned such that $L_{GC}^E = 0.5$ for $P = 500 \text{ mm yr}^{-1}$ because gallery forests potentially cover only a small fraction of semi-arid regions and play therefore only a limited role in climate–vegetation feedback, and $L_{GC}^E = 0$ for $t = -3000$ because this is the timing of disappearance reconstructed from pollen (Hély et al., 2014).

The effective leaf area L_S of all plant types together is unconstrained and calculated with the niche approach:

$$L_S = \frac{1}{N} \sum_{i=1}^N L_i . \quad (1.9)$$

For sensitivity studies on the role of plant composition and the effect of introducing or removing single functional plant types, L_S is calculated with a modified version of the niche approach

$$L_S = \frac{1}{n} \sum_{i=1}^N L_i, \quad N \leq n , \quad (1.10)$$

where n is the number of existing niches that can be occupied by N different plant types. This calculation implies the lack of relevant ecosystem functions when a niche is not occupied. I use $n = N + 1$ in our simulations.

The total precipitation is calculated in an analogous manner to Claussen et al. (2013) (see Eq. 1.5) as a combination of a background precipitation P_d in absence of vegetation, and a precipitation component induced by vegetation feedback

$$P^E(L_S, t) = P_d(t) + D^B \cdot L_S , \quad (1.11)$$

with a constant climate feedback coefficient $D^B = 140 \text{ mm yr}^{-1}$ (Liu et al., 2006; Claussen et al., 2013). Results from sensitivity studies on D^B ranging from 0 to 150 mm yr^{-1} are provided in the Appendix. The initial background precipitation is set to $P_{d0} = 500 \text{ mm yr}^{-1}$ which supports an average woody fraction of around 80, based on observational data (Hansen et al., 2007; New & Jones, 1999), the potential maximum cover in climate-driven savannas (Sankaran et al., 2005). The natural variability in precipitation, independent of vegetation, is implemented as additional white noise forcing $P_N(t)$ in the total precipitation

$$P(L_S, t) = \max((P^E(L_S, t) + P_N(t), 0)) . \quad (1.12)$$

1.3.3 Results from the adjusted model

The environmental envelopes for the four AHP plant types are shown in Fig. 1.2. Upper and lower precipitation thresholds mark the growth ranges based on moisture requirements, the limiting and therewith determining factor for plant growth in semi-arid regions (Shelford’s law of tolerance 1913). Since thresholds are derived from empirical relationships between observed species distributions and environmental variables, the implemented envelopes correspond to the “realized niches” or “climatic niches” that are narrower than the potential “fundamental niches” of plant types, as they implicitly account for further abiotic and biotic constraints (Hutchinson, 1957; Pearman et al., 2008). This constrains the comparison between plants interacting individually or together with climate.

In my implementation of the vegetation types described by Hély et al. (2014), plant types range from xeric desert shrubs and grasses ($< 150 \text{ mm yr}^{-1}$) to large tropical trees ($> 1500 \text{ mm yr}^{-1}$). Biome sensitivity assessment studies support this setup of plant sensitivities, suggesting that the percentage of rainfall decrease necessary to shift from one biome

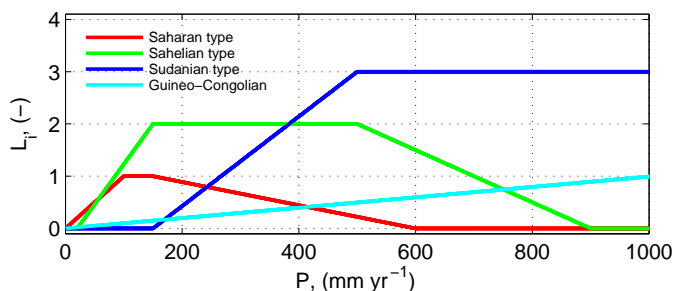


FIGURE 1.2: Environmental envelopes in terms of moisture requirements of four African Humid Period (AHP) plant types in the adjusted set up. The effective leaf area L_i is plotted as a function of mean annual precipitation P for the Saharan type (red), Sahelian type (green), Sudanian type (blue), and Guineo-Congolian type (light blue).

to another seems to be lowest for deciduous forests, followed by semi-deciduous forest, evergreen forest, grasslands, open and finally closed savannas (Hély et al., 2006). It is not clear whether gallery forests are as sensitive to decrease in rainfall as other forest types. Once being established in savannas, positive feedback effects may come into play and stabilize their expansion (Silva et al., 2008). The sensitivities of these plant types to changing environmental conditions are represented by the slopes of the curves in Fig. 1.2. Saharan and Sahelian plant taxa are mainly drought-adapted species that survive until conditions become very harsh, and they respond quickly if precipitation occurs. The Sudanian type includes herbaceous and woody savanna taxa that grow under a wide range of conditions, so the gradual decline with decreasing precipitation

seems reasonable. The prescription of the Guineo–Congolian tropical gallery forest plant type as a linear function of the orbital forcing and local precipitation with relatively low $L_{GC, \max}$ accounts for internal stability.

The effective leaf area L_i introduces an additional degree of freedom in the model, acting as a weighting factor for each plant type in the combined interaction with climate. All surface parameters crucial for climate–vegetation feedback – leaf area, hydrological properties, and albedo – merge in L_i . Tropical plants, especially trees, usually achieve higher leaf areas and higher evapotranspiration rates than grasses or other steppe vegetation. Higher evapotranspiration has in turn a larger impact on atmospheric processes and the formation of precipitation than the low leaf area of steppe vegetation.

Simulations of AHP vegetation interacting individually and together with climate, and the corresponding precipitation curves, are shown in Fig. 1.3. Except for the Guineo–Congolian type, all plant types show an abrupt decline and a pronounced hysteresis effect when they interact individually with climate (Fig. 1.3a). This low stability results from the strong chosen climate feedback coefficient of 140 mm yr^{-1} . The corresponding precipitation curves go in conjunction with the abruptness of L_i decline (Fig. 1.3c). In single interaction with climate, the Guineo–Congolian type declines linearly until it disappears at around year -3000 . The Sudanian type starts with $L_{\text{Sudanian}, \max} = 3$ and collapses abruptly at around year -3600 due to the strong feedback. It develops a hysteresis of around 500 years. The Sahelian type starts with L_{Sahelian} of around 1.2, reaches $L_{\text{Sahelian}, \max} = 2$ at year -4600 and collapses abruptly at around year -2200 . It develops a hysteresis of around 1000 years. The Saharan type gradually increases from an initial L_{Saharan} of around 0.1 to $L_{\text{Saharan}, \max} = 1$ at around year -3200 , before it collapses at around year -2900 . It develops a hysteresis of around 300 years.

When all plant types interact together with climate, I observe more gradual responses to the orbital forcing, changes in appearance over time, and the almost complete disappearance of hysteresis effects (Fig. 1.3d–e). This can be interpreted as an enhancement of system stability (Scheffer et al., 2001). The precipitation curve resulting from feedback with L_S shows a smooth decline (Fig. 1.3f). In combined interaction with the other plant types, the Guineo–Congolian type starts with a higher L_{GC} than alone because this type benefits from local precipitation. The appearance over time does not change as orbital forcing surpasses the beneficial effect from local precipitation enhancement.

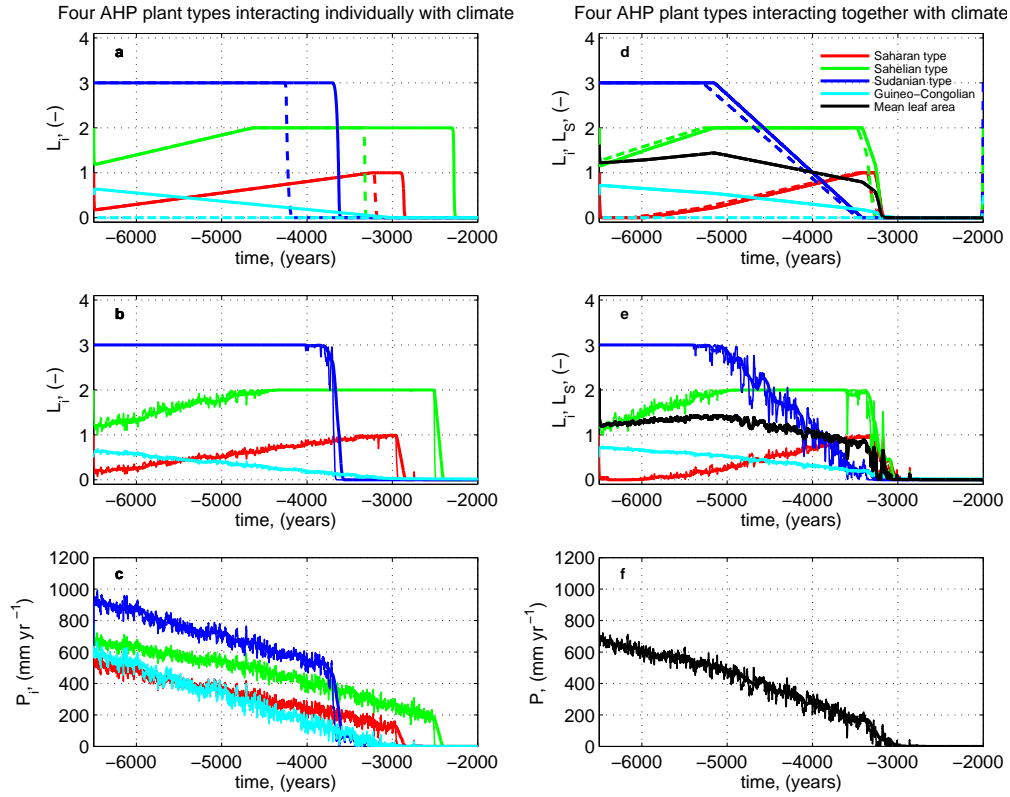


FIGURE 1.3: Transient dynamics of four African Humid Period (AHP) plant types interacting individually (a–c) and together (d–f) with climate. The effective leaf areas L_i and the corresponding precipitation amounts P_i are shown for the Saharan type (red), Sahelian type (green), Sudanian type (blue), and Guineo–Congolian type (light blue). Mean effective leaf area L_S and the corresponding precipitation P are calculated with the niche approach (black) (see Eq. 1.9). Simulations without background noise (a, e) include forward simulations (solid lines) and simulations backward in time (dashed lines). Simulations with background noise are depicted in (b, e) for L_i and L_S , and for precipitation P in (c, f). Thin lines show annual mean values and thick lines show a 100-year running mean.

A high potential effective leaf area puts the Sudanian type in a dominant position in the multi-niche system. L_{Sudanian} starts to decline 1500 years earlier than on its own, but it finally disappears after a more gradual decline around 200 years later than alone. Hence, its abundance is reduced over time due to the presence of other plant types, while its absolute appearance over time is extended. The hysteresis almost disappears. The decline of the Sahelian type starts 1100 years earlier in the combined interaction, happens more gradually and ends around 1000 years earlier than alone. The period of maximum abundance is shifted deeper in the past and the absolute appearance over time is shortened in the considered time frame. The hysteresis almost disappears. The Saharan type starts in combined interaction from $L_{\text{Saharan}} = 0$, increases gradually from year -6000 to its full potential cover at around year -3500 before it disappears again between year -3300 and -3200 . The time span of maximum abundance as well as the

total appearance over time are reduced due to the presence of the other plant types. The hysteresis almost disappears. The Saharan type is largely outcompeted by other plant types in higher precipitation regimes. It only succeeds in the short period of low precipitation amounts.

Under the assumption of a full environmental envelope, the niche approach gives reasonable results for L_S regarding functional diversity. The evolution of L_S can be divided into three main phases (Fig. 1.3e). At the beginning of the simulation, L_S is not at its maximum which could be explained in consideration of the physiognomic community structure in reality. Under a high precipitation regime, the Sudanian type has the largest share of vegetation, including many tree species that outcompete undergrowth. With decreasing precipitation in the first phase from year -6500 to -5200 , tree cover and therewith ground shading effects are reduced and it becomes easier for undergrowth species to establish. While the composition changes substantially under decreasing precipitation, L_S only increases by 0.2. In the second phase between year -5200 and -3400 , L_S slowly decreases by 0.3, slightly below the initial level of 1.1. With the total disappearance of the Sudanian type at around year -3400 , the third phase is initiated and therewith a steeper and fluctuating, but still gradual transition to a “desert” state. The system has now simplified to just two plant types and those are nearing their thresholds, which causes the increase in fluctuations. The increase in fluctuations is one of the proposed early warning signals for regime shifts (Scheffer et al., 2001, 2009). After year -3000 , vegetation is completely absent.

Stepping back to the reconstructions by Hély et al. (2014), my simulations show an evolution of plant diversity similar to reconstructions north of 20° N. Hély et al. (2014) proposed that all these plant types were present around year -6000 , diversity was highest in and within plant types, and tropical types (Guineo–Congolian and Sudanian type) reached their maximum extension and abundance. After year -6000 , pollen abundance and diversity decreased for all plant types. Tropical types apparently declined in conjunction with latitudinal humid surfaces as they grew mainly in gallery forests. Regarding the abundance of pollen in Hély et al. (2014), vegetation was completely absent after year -3000 north of 20° N. All these observations are also true for my simulations, except for the lack of the Saharan type in the beginning of my simulations in year -6000 due to the assumed low maximum precipitation threshold. Quantitative comparison between Hély et al. (2014) and my simulations is not possible because their reconstructions rely

on pollen richness and abundance while I consider the area of growth. High richness and abundance of individual types should not be equated with high plant cover.

So far, I have considered the interaction of AHP plant types interacting individually or all together with climate. I now address the role of plant composition and completeness of required functional types. Claussen et al. (2013) stated that climate–vegetation feedback strength could change if certain plant types were removed or introduced by some external forcing.

Simulations with different combinations of plant types highlight the importance of plant composition on system stability, but I can only make qualitative statements about different scenarios. Figure 1.4 shows L_S computed from Eq. 1.10 with different combinations of plant types. In each simulation, one plant type is absent and its niche is not occupied. The removal of tropical plant types tends to enhance the fluctuations and steepness of the transition while the lack of drought-adapted plant types causes a more gradual

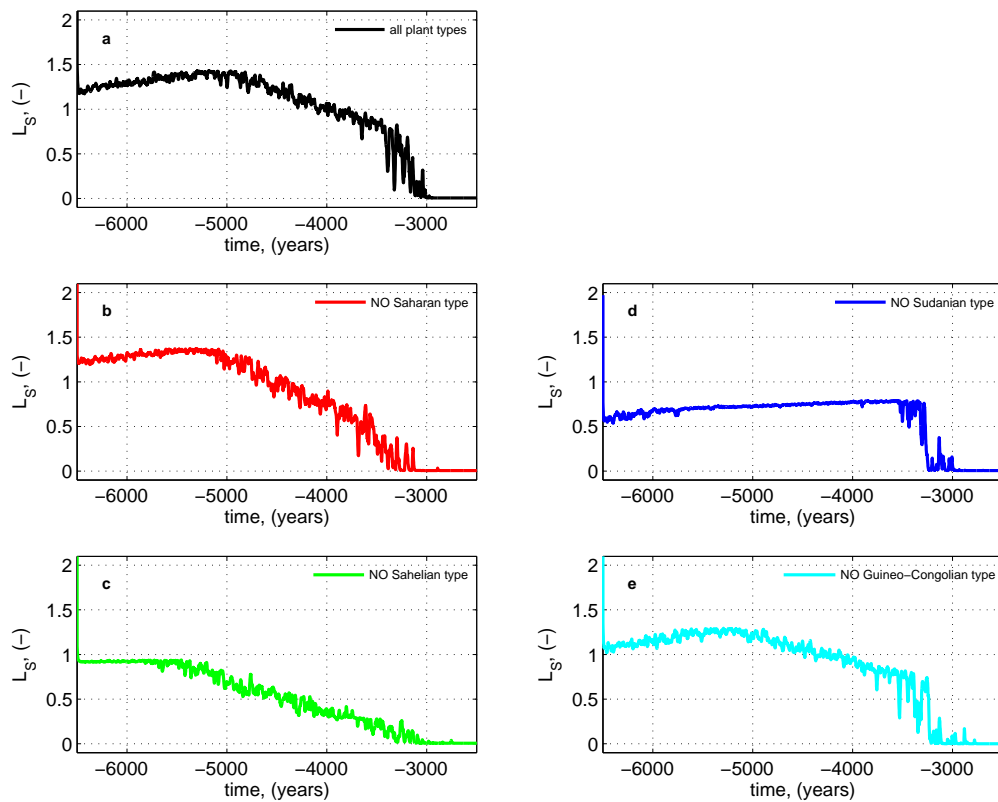


FIGURE 1.4: Transient dynamics of mean effective leaf area L_S illustrate the impact of the removal of plant types. Panels (a–e) show 100-year running means of different simulation set ups. The mean effective leaf area L_S accounting for all plant types ($N = n = 4$ in Eq. 1.10) is shown as a reference (a). In each of the other simulations, one niche is not occupied ($N = 3$ and $n = 4$ in Eq. 1.10): no Saharan type (b), no Sahelian type (c), no Sudanian type (d) or no Guineo–Congolian type (e).

decline that starts earlier. It is not possible to determine with the conceptual approach used here if one of the considered plant types actually played a key role for the stability of the climate–vegetation system during the mid-Holocene, but the Sudanian type seems to have a large impact on my simulations. This is mainly because the Sudanian type was prescribed the highest potential effective leaf area, and its removal leaves the interaction with climate to the Saharan and the Sahelian type, which are both sensitive to changes in precipitation and respond abruptly when their minimum thresholds P_i^{C1} are crossed. Nonetheless, I show that there might be large differences in the mean cover over time depending on the involved plant types, the overlap of environmental envelopes, and the individual response to changing conditions.

1.3.4 Limitations of the adjusted model

The adjustment of the model by Claussen et al. (2013) to AHP plant types reconstructed from pollen (Hély et al., 2014) improved the representation of plant diversity during the mid-Holocene and provides a tool to investigate the impact that different plant types might have on the stability of a climate–vegetation system. Nonetheless, the model’s simplicity limits its application.

As mentioned in Sect. 1.2.2, moisture requirement is an established measure to characterize plant diversity in recent African ecosystems. However, the measure is insufficient to describe plants’ niches and to explain actual vegetation composition and spatial distribution within the considered region, because determinants other than precipitation amounts are not taken into account. I did not explicitly implement additional plant growth determining parameters in the adjusted model, but moisture requirements from empirical data implicitly account for such additional factors. Niches in the model describe “realized niches”, and contributions of determinants such as fire or competition for nutrients cannot be separated from the difference in water requirements. This complicates the comparison between plant types interacting individually or together with climate because the actual simulation of individual growth is not possible. Nonetheless, water is the limiting factor in subtropical Africa and the effects of additional or reduced precipitation due to the presence of other plant types can be considered with my model.

Another shortcoming is the merging of all surface parameters crucial for climate–vegetation feedback – leaf area, albedo, and hydrological properties – in L_i . The individual importance of each of these parameters regarding the effect on atmospheric dynamics and precipitation patterns varies over different latitudes in subtropical Africa (Bathiany et al., 2014): in the Sahara, an increase in plant growth results in a net warming because the surface heating due to albedo decrease surpasses the increase of latent heat flux; the Sahel experiences a net cooling with additional vegetation because evapotranspiration cooling exceeds the albedo warming effect; south of the Sahel, where tree cover and water availability are generally high, the stomatal resistance limits the latent heat flux which results in a net warming. This heterogeneous pattern makes an individual consideration of feedback determinants important, but cannot be performed with my approach as contributions enter the product of L_S and D^B which makes disentangling impossible.

The same applies to the assumption of a homogeneous feedback coefficient D^B for all plant types which does not account for diversity in feedback strength, but it could not be separated from the product with L_S anyway. Another shortcoming of D^B is its arbitrary choice to force strong feedback and abrupt state transition (Liu et al., 2006). Quantitative estimates of the climate feedback coefficient D_i^B based on remote sensing observations of monthly fraction of photosynthetically active radiation showed on average a positive feedback on precipitation in the Saharan region, values ranged in subtropical Africa from -60 to 120 mm yr^{-1} , but little evidence of strong vegetation–precipitation feedback (Liu et al., 2006). Sensitivity studies with various combinations of D_i^B showed only minor changes in the evolution of L_S over time (see Appendix).

1.4 Summary and conclusions

In this chapter, I have critically reassessed the conceptual model by Claussen et al. (2013) in the light of recent ecological literature, and provided an improved version that accounts for plant diversity during the African Humid Period (AHP) as it was reconstructed from pollen by Hély et al. (2014).

Despite its simplicity, the original conceptual model by Claussen et al. (2013) seems to capture the main features of different plant types interacting together with climate,

namely the enhancement of climate–vegetation system stability. The underlying assumptions are reasonable in an ecological context concluded from literature.

The definition of plant diversity in terms of moisture requirements is an established and appropriate approach for semi-arid regions because precipitation is the main determinant of plant growth there. Neglecting further crucial factors for vegetation composition and distribution such as fire or competition is therefore reasonable in the simple approach.

With the niche approach, the effective feedback between vegetation and climate emerges from the interacting properties of different plant types fulfilling specific ecosystem functions. Once a plant type disappears as precipitation drops below the requirements, other plant types cannot occupy its niche (E-space). The prohibition of replacement depicts the fundamental ecological niche in its original sense, but the approach does not allow for a geographically explicit description of vegetation cover evolution. Further, the changes in niches available for occupation that result from substantial changes in the environment over millennia are not implemented.

Regarding the interpretation of transient simulations, the conclusions made by Claussen et al. (2013) fit in the ecological state of knowledge. After decades of debating, ecologists nowadays agree that biodiversity can have a stabilizing effect on ecosystems, especially under changing environmental conditions (see General Introduction). Claussen et al. (2013) concluded that the stability of a climate–vegetation system can determine and arise from plants' appearance over time. Sensitive plants likely benefit from additional water and facilitation effects in a more life-sustaining environment, whereas resilient plants might suffer to a certain degree from additional competition. Claussen et al. (2013) argued ecologically reasonably that it is difficult to determine the origin of system stability as the overall feedback strength depends on species composition. These difficulties are not inconsistent with previous studies that proposed strong climate–vegetation feedback, resulting in abrupt shifts from a stable “green” state to a stable “desert” state. Simulations by Claussen et al. (1999) were performed with the lowest possible number of PFTs, one tree and one grass. The low plant diversity implied a high likelihood for abrupt transitions (Scherer-Lorenzen, 2005; Claussen et al., 2013). In previous studies that focused on multiple stable states of the climate–vegetation system in north Africa, including those of Claussen et al. (1998), Liu et al. (2006), and Bathiany et al. (2012), it was argued that an abrupt change emerging from the loss of stability of one of the stable

climate–vegetation states causes abrupt changes in both the vegetation record and the hydroclimatic record. My study, however, supported the hypothesis of Claussen et al. (2013) that in an ecosystem with rich plant diversity, multiple stable states can exist, even if the hydroclimate record shows a gradual transition. Hence the latter studies did not invalidate the earlier considerations.

When it comes to the application to AHP vegetation reconstructed from pollen data (Hély et al., 2014), the model by Claussen et al. (2013) reaches its limits. The diversity of AHP vegetation in terms of moisture requirements and climate impact cannot be captured. The direct relation between precipitation and plant cover does not hold for highly specialized xeric plant types or tropical plant types indirectly linked to regional precipitation, and the diversity of feedback strength and climate impact arising from different plant properties is not sufficiently reflected in the original model.

The presented modifications refined the model setup such that it accounted for a more realistic spectrum of plant types, interactions, and feedbacks. The extension of environmental envelopes enabled coexistence and superseding of different plant types when conditions and the set of available niches changed. The implementation of the vegetation types described by Hély et al. (2014) provided an insight into plant diversity during the AHP. Plant types ranged from xeric desert shrubs and grasses to large tropical trees. Since precipitation thresholds were derived from observational data, abiotic and biotic constraints could not be completely separated. Together with the full environmental envelopes, the prescribed retreat of tropical gallery forest taxa allowed for the representation of a mosaic-like spatial environment as it was reconstructed from pollen. The effective leaf area introduced an additional degree of freedom that acted as a weighting factor for each plant type in the combined interaction with climate, accounting for differences in leaf area, albedo and hydrological properties.

Simulations with the adjusted model version supported the stabilizing effect of functional diversity on ecosystem performance and precipitation proposed by Claussen et al. (2013), but provided more details on plant turnover. When all plant types interacted together with climate, I observed rather gradual responses to decreasing precipitation, changes in appearance over time and the almost complete disappearance of hysteresis effects. Over a period of around 3100 years, the mean cover varied little while composition changed completely. The disappearance of tropical types initiated the final steeper and

fluctuating, but still gradual, transition to a “desert” state within 400 years. After year -3000 , vegetation was completely absent. The temporal evolution of plant types compared well with reconstructions by Hély et al. (2014) north of 20° N.

The importance of plant composition for the stability of a climate–vegetation system became clear comparing different combinations of plant types. Apparently, the Sudanian type played a leading role for the stability of the climate–vegetation system, but I could not determine if one of the considered plant types actually played a key role during the mid-Holocene with my model. Nonetheless, I could show that there might have been large differences in the mean cover over time depending on the involved plant types, occupied niches and their overlap, and the individual sensitivities to changing conditions.

For further studies on the effect of plant diversity on the stability of climate–vegetation systems, I propose not to complicate the conceptual model any further by introducing more ad hoc tunable parameters, but to transfer the lessons learned from this study to a comprehensive dynamic vegetation model.

The Earth system model MPI-ESM1 did not show abrupt transitions of large-scale vegetation cover in previous transient Holocene simulations, and the understanding I gained in this study can help to investigate whether this was an effect emerging from the representation of plant diversity in the land surface model JSBACH. This process-based model offers the possibility to represent plant diversity in various plant properties, and a variety of interactions with the atmosphere to address the arising questions: could a more complex model depict AHP plant diversity and reproduce the results from my qualitative conceptual study? And further, could changes in plant diversity stabilize or destabilize the climate–vegetation system in coupled GCM simulations?

In conclusion, the assessment of the conceptual approach by Claussen et al. (2013) and the adjustment to AHP plant types supported the hypothesis of plant diversity playing a crucial role for climate–vegetation system stability, and highlighted the importance of plant composition in this context. From this I infer that a deeper understanding of the role plant diversity plays in climate–vegetation interaction and an improved representation of plant diversity based on pollen reconstructions could allow for a more realistic consideration of plant–plant interaction and climate–vegetation feedback in coupled GCM simulations.

Chapter 2

Representation of plant diversity in JSBACH and its impact on the simulated vegetation response to a linear precipitation decline in subtropical Africa

2.1 Introduction

Over the last decades, scientists strove for a better understanding of the transition from the “green” Sahara to the “desert” state towards the end of the African Humid Period (AHP). While some studies indicated an abrupt collapse of vegetation implying a strong climate–vegetation feedback (Claussen, 1994; Claussen & Gayler, 1997; Claussen et al., 1998, 1999), others suggested a gradual vegetation decline thereby questioning the existence of a strong climate–vegetation feedback (Kröpelin et al., 2008; Francus et al., 2013; Lézine, 2009; Lézine et al., 2011). Based on a conceptual modelling study, Claussen et al. (2013) proposed that these different viewpoints are not contradicting if one accounts for plant diversity. High plant diversity could stabilize a climate–vegetation system by buffering strong feedbacks between individual plant types and precipitation,

whereas a reduction in plant diversity might allow for an abrupt regime shift under gradually changing environmental conditions. Hence, climate–vegetation feedback strength would not be a universal property of a certain region but depend on the vegetation composition. An ecological assessment of the conceptual model and an adjustment of the model to AHP plant types endorsed the findings by Claussen et al. (2013), see Chapter 1.

Disregarding the attractiveness of its simplicity, the conceptual model implies severe limitations. The differentiation between plant types’ properties is rather imprecise: crucial surface parameters for climate–vegetation feedback – leaf area, albedo, and hydrological properties – congregate in one parameter and the climate feedback coefficient is assumed to be homogeneous for all plant types. The model leaves out vegetation determinants other than precipitation such as temperature, soil conditions, or fire regime. Additionally, the 2-dimensional approach excludes studies on a large geographical scale that could cover large scale climatic gradients. Since further complication of the conceptual model might add relatively low gain of understanding, it seems convenient to make a step towards a more sophisticated, comprehensive model.

JSBACH, the land surface component of MPI-ESM1, is a process-based Dynamic Global Vegetation Model (DGVM) that offers the possibility to represent plant types accounting for a range of properties, and to simulate their competition. Terrestrial plant diversity is expressed in discrete functional plant classes, the so-called “Plant Functional Types” (PFTs). PFTs are designed to understand ecological processes such as assembly and stability of communities and succession, and to facilitate detection and prediction of responses to environmental change at a range of scales (Duckworth et al., 2000).

But could JSBACH depict AHP plant diversity and reproduce the results from Chapter 1? To address this question, I study in this chapter, as an intermediate step between the conceptual model in Chapter 1 and the coupled ECHAM6/JSBACH in Chapter 3, the representation of plant diversity in JSBACH, its applicability to AHP plant types reconstructed from pollen, and its impact on the simulated vegetation response to a linear precipitation decline in subtropical Africa.

The first section of this chapter provides a brief summary and an assessment of the representation of plant diversity and vegetation dynamics in DGVMs with focus on JSBACH (after Reick et al. (2013)). Considering analogies to Chapter 1, I discuss the applicability of PFTs in JSBACH to AHP plant types.

In the second section, I investigate the effect of PFT diversity on the vegetation response to a gradual desiccation of north Africa performing offline simulations with different PFT combinations. “Offline” means hereinafter that JSBACH runs in a standalone version, uncoupled to the atmosphere. Thereby, I exclude feedbacks with the atmosphere and separate effects emerging from different degrees of PFT diversity. Further, I control precipitation as the main determinant of plant growth similar to the conceptual approach in Chapter 1, but take the advantage of a process based vegetation response in JSBACH.

2.2 Plant diversity and vegetation dynamics in JSBACH

JSBACH is the land component of MPI-ESM1, a comprehensive Earth system model that couples model components for the atmosphere (ECHAM6, Stevens et al. (2013)), ocean (MPIOM, Jungclaus et al. (2013)) and land surface (JSBACH, Raddatz et al. (2007); Reick et al. (2013)) through the exchange of energy, momentum, water and important trace gases such as carbon dioxide. As integral component of ECHAM6, JSBACH provides the lower atmospheric boundary conditions over land as well as biogeochemical and biogeophysical degrees of freedom that arise from terrestrial processes. This chapter focuses on the representation of plant diversity and vegetation dynamics in JSBACH, briefly summarized in the following section.

2.2.1 The concept of Plant Functional Types

Despite the classification of species in PFTs has a long history (see Duckworth et al., 2000), there is no uniform definition of PFTs because of the strong context dependence. In general, PFTs should represent the world’s most important plant types recognized as dominant or major elements in ecosystems, and a set of PFTs should provide a complete, geographically representative coverage of the main vegetation types of the world’s land areas. PFTs should be physiognomically defined, characterized through functional behaviour and attributes, and be qualitatively linked to climatic conditions (Box, 1995).

Common PFT classifications are based on the grouping of species in nonphylogenetic, functional groups according to similarities in resource use and response to environmental

and biotic controls (Wilson, 1999) with either deductive or inductive approaches (McIntyre et al., 1999). For this grouping, characteristic plant traits – observable properties – are chosen to describe common plant physiology, growth form, biogeochemical cycling of water, nutrients, and carbon, and the response to ecosystem disturbance such as fire or windthrow (Midgley et al., 2005). PFTs are of particular interest in regions where the flora remains largely unknown and species based models reach their limits.

In DGVMs, the number of PFTs is usually reduced to a minimum, typically to a set of 5 to 15 PFTs. The standard JSBACH set up provides 21 PFTs representing natural vegetation, crops and pasture. The dynamic vegetation in JSBACH accounts for only 8 PFTs, shown in Tab. 2.1. The concept of PFTs does not consider that plants interact individually with climate, but the loss of information is assumed to be minor compared to the gain of knowledge on global scale (Harrison et al., 2010; Epstein et al., 2001; Meinzer, 2003).

TABLE 2.1: Natural plant functional types in JSBACH, their woodiness type, associated time constants for establishment/mortality τ (in years) (Reick et al., 2013), maximum carboxylation capacities $V_{max,0}$ and electron transport capacities $J_{max,0}$ at 25 °C (in $\mu\text{mol}(\text{CO}_2) \text{ m}^{-2} \text{ s}^{-1}$) (Kattge et al., 2011), specific leaf area SLA (in $\text{m}^2(\text{leaf}) \text{ mol}^{-1}(\text{Carbon})$), and maximum leaf area index LAI_{max} (in $\text{m}^2 \text{ m}^{-2}$).

Plant Functional Type	ID	type	τ	$V_{max,0}$	$J_{max,0}$	SLA	LAI_{max}
Tropical Evergreen Tree	<i>TE</i>	woody	30	39	74.1	0.264	7
Tropical Deciduous Tree	<i>TD</i>	woody	30	31	59.8	0.376	7
Extra-trop. Evergreen Tree	<i>eTE</i>	woody	60	44	83.6	0.110	5
Extra-trop. Deciduous Tree	<i>eTD</i>	woody	60	66	125.4	0.304	5
Raingreen Shrub	<i>SRG</i>	woody	12	61.7	117.2	0.184	2
Deciduous Shrub	<i>SD</i>	woody	24	54	102.6	0.307	2
C3 Grass	<i>C3</i>	grass	1	78.2	148.6	0.451	3
C4 Grass	<i>C4</i>	grass	1	8	140	0.451	3

The geographically explicit representation of vegetation cover as PFTs in JSBACH relies on the model grid cell as the basic unit (Reick et al., 2013). Each grid cell has a predefined geographic location and is split into tiles to allow for the representation of sub-grid scale heterogeneity. These tiles are not specified by location but by their cover fractions of the grid cell. Each tile is associated with one PFT, while not every PFT must be linked with a tile in a particular grid cell.

The area hospitable for vegetation is prescribed for each grid cell as a fraction veg_{max} , in the following referred to as vegetation cover fraction, see Eq. 2.9. Accordingly, $d = 1 - veg_{max}$ is the fraction of inhospitable land in a grid cell, and the area in a grid cell

accessible for vegetation V_{veg} is given by

$$V_{veg} = A \cdot veg_{max} , \quad (2.1)$$

where A is the total area of the grid cell (m^2). Instead of the area, JSBACH uses the fraction of the area covered by vegetation. Denoting by v_i the area covered by the PFT associated with tile i in a grid cell (m^2), such fractions are most naturally introduced by

$$f_i = \frac{v_i}{A}, \quad i = 1, 2, \dots, K , \quad (2.2)$$

where K is the number of tiles in a grid cell. $V_{veg} = \sum_{i=1}^K v_i$ and

$$v_{max} = \sum_{i=1}^K f_i . \quad (2.3)$$

Because of the implicit handling of bare land it is sometimes more convenient to describe land cover only with respect to that part of the grid cell where vegetation can grow. Associated cover fractions are introduced by

$$c_i = \frac{v_i}{V_{veg}} = \frac{f_i}{veg_{max}}, \quad i = 1, 2, \dots, K , \quad (2.4)$$

and they sum up to 1:

$$\sum_{i=1}^K c_i = 1 . \quad (2.5)$$

2.2.2 Natural land cover change and vegetation dynamics in JSBACH

Natural land cover change and vegetation dynamics are simulated in JSBACH by the DYNVEG component. DYNVEG was designed to model the distribution of PFTs based on fundamental understanding of plant ecophysiology. DYNVEG is dynamic in the sense that the time scale over which ecosystem level responses and feedbacks occur is simulated annually, allowing non-equilibrium conditions to exist (Midgley et al., 2005). Natural land cover change and vegetation dynamics in DYNVEG are based on a number of principles that are common for DGVMs, but nonetheless summarized here for the understanding of this work.

The “universal presence principle” implies that each PFT can potentially grow everywhere (“seeds are everywhere”). Physiological constraints define the climatic range within which a certain PFT can exist. Such bioclimatic limits only prevent establishment if conditions are not suitable for a PFT to grow, but do not prevent further existence when values fall out of range. The increase or reduction of land cover is determined by two processes. First, PFT cover can be reduced by natural death or disturbance and increased by migration into space opened in this way, so-called “uncolonized land”. The different PFTs compete for this uncolonized land while vegetation establishment is generally only possible when net primary production (NPP) is positive at least in some years. Competition is considered in DYNVEG by growth form and by productivity. After disturbances, grasses have an advantage because they quickly migrate in the new space while trees and shrubs regrow slowly. The ratio of grass and woody PFTs depends on the rate of disturbances. Within the woody PFTs, competition is regulated by productivity: higher NPP means a competitive advantage if not other aspects such as growth form are dominating. PFTs with higher NPP migrate faster into uncolonized land. In absence of disturbance, woody PFTs (trees and shrubs) are dominant (light competition) over grasses. The second possibility for land cover to increase or decrease is that inhospitable regions can expand or shrink. This change in area available for growth affects the cover of all PFTs.

The dynamic modelling of natural vegetation is based on fractions of unit area in a grid cell as the basic dynamic variables in DYNVEG. A composition of woody (w_i), grass (g_i), and uncolonized (u) fractions compose the full grid cell:

$$u + \sum_{i=1}^{N^w} w_i + \sum_{i=1}^{N^g} g_i = 1 , \quad (2.6)$$

where N^w and N^g are the number of woody and grass PFTs, respectively. The dynamics of the cover fractions are governed by the coupled set of differential equations that account for establishment, natural mortality, and disturbances (fire, wind throw), acting on characteristic timescales for woody and for grass types (see Reick et al., 2013). The result is the potential natural vegetation cover in a world without humans. DYNVEG also includes a sophisticated approach to account for a human aspect, but I do not consider anthropogenic land cover change here.

The dynamics of inhospitable land $d = 1 - veg_{max}$ in DYNVEG are calculated with a submodel in order to determine the extent of cool deserts like arctic or hot deserts like the Sahara. The extent of d determines the fraction of a grid cell veg_{max} where vegetation can grow. The model is based on the idea that deserts develop when NPP exceeds a threshold so that vegetation cannot establish a canopy at least once a year. The fraction f with substantial vegetation cover at least once in year y is

$$f(y) = \sum_{i \in W} w_i (1 - e^{-a(LAI_i^{max})^b}) + \sum_{i \in G} g_i \frac{g + u}{g} (1 - e^{-a(LAI_i^{max})^b}), \quad (2.7)$$

where $g = \sum_{i \in G} g_i$ is the total grass fraction of vegetation, and LAI_i^{max} is the maximum leaf area that appeared during the year y . LAI_i^{max} is determined from the maximum biomass in leaves by

$$LAI_i^{max}(y) = SLA_i \cdot C_{G,i}^{max} / 3, \quad (2.8)$$

where $C_{G,i}^{max}$ is the maximum living biomass found in PFT i in the considered year. One third of the biomass is assumed to be in the leaves, and the specific leaf area SLA_i relates the carbon content of leaves to their area. The parameter $a = 1.95$ was chosen such that the simulated distribution of hot and cold deserts matches observations. The parameter $b = 2$ describes steepness of the transition between vegetation and desert and was chosen to give the realistic distribution of deserts. However, one year of low growth does not make a desert. Indeed, a delay development is assumed: for the year y

$$veg_{max} = \sum_{y'=-\infty}^y \frac{f(y')}{\tau_{desert}} e^{-\frac{y-y'}{\tau_{desert}}}, \quad (2.9)$$

where the time scale for development of inhospitable conditions is chosen as $\tau_{desert} = 50$ years.

Since one of the further on presented simulation involves modifications of the photosynthetic parameters “standard maximum carboxylation rate” $V_{max,0}$ and “standard maximum electron transport rate” $J_{max,0}$, I here provide the fundamental equations for the calculation of photosynthesis in JSBACH. For a detailed description including temperature dependence, nitrogen scaling, stomatal conductance, and assimilation under water stress, see Reick et al. (2014).

For C3 plants, photosynthesis is derived with the Farquhar model (Farquhar et al., 1980). On the basis of observations, the model assumes the gross carbon assimilation rate in plants' chloroplasts to be limited either by the carboxylation rate J_C of the enzyme RuBisCO, or by the transport rate J_E of the two electrons freed during the photo reaction. Gross carbon assimilation is reduced by the so-called "dark respiration" R_d , which is the loss of CO_2 from mitochondrial respiration required to supply the metabolic energy for the plant. The total net rate of carbon fixation ("productivity") A_C is thus

$$A_C = \min(J_C, J_E) - R_d . \quad (2.10)$$

The carboxylation rate J_C of the enzyme RuBisCO is not only determined by the CO_2 availability, but also by O_2 concentration. As indicated by its name "Ribulose-1,5-bisphosphate-carboxylase/-oxygenase", the enzyme is sensitive to both molecules and a high O_2 concentration reduces the carboxylation rate as follows:

$$J_C = V_{max} \frac{C_i - \Gamma_*}{C_i + K_C(1 + O_i/K_O)} . \quad (2.11)$$

V_{max} is the maximum carboxylation rate, C_i and O_i are the leaf internal CO_2 and O_2 concentrations. Γ_* is the so-called CO_2 compensation point representing the CO_2 concentration where CO_2 assimilation ("photosynthesis") and loss ("respiration") are in equilibrium. K_C and K_O are Michaelis-Menten constants parametrizing the dependance of J_C on CO_2 and O_2 concentrations.

The electron transport rate J_E is given by

$$J_E = J(I) \frac{C_i - \Gamma_*}{4(C_i + 2\Gamma_*)} , \quad (2.12)$$

$$J(I) = J_{max} \frac{\alpha I}{\sqrt{J_{max}^2 + \alpha^2 I^2}} , \quad (2.13)$$

where I is the radiation intensity in the photosynthetically active band (computed by the canopy radiation model), J_{max} is the maximum electron transport rate, and α is the quantum efficiency for photon capture.

Dark respiration R_d is under standard conditions (25 °C, indicated by an index "0" in the following) determined as

$$R_{d,0} = \gamma_d \cdot V_{max,0} , \quad (2.14)$$

with $\gamma_d = 0.011$ (after Farquhar et al. (1980)), for temperature dependent R_d see Reich et al. (2014). $V_{max,0}$ is used here as a zeroth order estimate for $R_{d,0}$ based on the assumption that $V_{max,0}$ indirectly depends on nitrogen through the maximum carboxylation rate parameter and thereby reflects the typical nitrogen status of the plant which cannot be modelled in the Farquhar model.

For C4 plants, photosynthesis is derived with the Collatz model (Collatz et al., 1992). The structure of the Collatz model is similar to the Farquhar model described above, except that the equations for the carboxylation rate, and the electron transport rate are replaced by the following:

$$J_C = k \cdot C_i , \quad (2.15)$$

$$J_E = \frac{1}{2\theta_S} (V_{p,max} + J_i - \sqrt{(V_{p,max} + J_i)^2 - 4\theta_S \cdot V_{p,max} \cdot J_i}) , \quad (2.16)$$

$$J_i = \alpha_i \cdot \frac{I}{E_{PAR}} . \quad (2.17)$$

$V_{p,max}$ corresponds to the maximum carboxylation rate of the enzyme PEPCase (Phosphoenolpyruvatcarboxylase) in C4 plants, k is the PEPCase CO_2 specificity, and α_i is the integrated C4 quantum specificity. θ_S describes the curve parameter for J_E and E_{PAR} stands for the photosynthetic photon flux density. Just like for C3 plants, $R_{d,0}$ is assumed to be proportional to the maximum carboxylation rate, but here $\gamma_d = 0.042$ (after Knorr (1998)):

$$R_{d,0} = \gamma_d \cdot V_{P,max,0} . \quad (2.18)$$

2.2.3 General assessment of the PFT concept in JSBACH

The main advantages of the PFT concept are its simplicity, its large scale to global applicability, and its reasonable reproduction of the global biome distribution, also in fully coupled simulations with GCMs (Scheiter et al., 2013). JSBACH was in the past successfully applied to reproduce global vegetation (see e.g. Brovkin et al., 2009; Giorgetta et al., 2013) and served for numerous studies related to vegetation cover, for example studies on climate carbon cycle feedbacks (Friedlingstein et al., 2006; Raddatz et al., 2007; Arora et al., 2013), land use and land cover change (Pongratz et al., 2008; Boysen et al., 2014; Wilkenskjaeld et al., 2014), biogeophysical and biogeochemical feedbacks of vegetation and atmosphere (Otto et al., 2009; Dallmeyer et al., 2010; Bathiany et al.,

2010), volcanic eruptions (Brovkin et al., 2010; Segschneider et al., 2013), boreal wetlands and permafrost (Schuldt et al., 2013; Ekici et al., 2014), and the role of fire in the Earth System (Lasslop et al., 2014; Bruecher et al., 2014) under past, present and future conditions.

The main disadvantages of the PFT concept arise from oversimplification due to limited computational resources and the lack of data and theory: loss of information with discrete PFT classification, limited set of plant attributes to define a limited number of mostly static PFTs that seldom account for plasticity in plant traits along geographic and environmental gradients, limited representation of (especially) sub-/tropical plant diversity, and the poor representation of sub-grid ecological interaction and competition concerning age stages, roots, light, nutrients, and others (Fisher et al., 2010; Scheiter et al., 2013). The study by Pavlick (2012) named a main drawback: “Field ecology community has shown that for many plant traits there is a large amount of variation within PFTs, and that for several important traits, there is greater variation within PFTs than between PFTs (Wright et al., 2005; Reich et al., 2007; Kattge et al., 2011). This trait variation may play an important role for many ecosystem functions (Díaz & Cabido, 2001; Westoby et al., 2002; Ackerly & Cornwell, 2007) and for ecosystem resilience to environmental change (Díaz et al., 2006)”. Another large uncertainty arises from the assumption of a constant relation between species distribution and environmental variables, typically climate variables, over time. Assumptions about changes in plant distributions are simplified, and not all plants shift their ranges in the expected way: “range contractions (Zhu et al., 2012), shifts in the opposite direction (Crimmins et al., 2011), or significant time lags (Bertrand et al., 2011) are just some examples” (Snell et al., 2014). Since most DGVMs are not designed for tropical systems (House et al., 2003) and do not include internal feedbacks of these biomes (Moncrieff et al., 2013), these models display high uncertainty in predicting vegetation for the forest, savanna, and grassland biomes due to the complexity of tree-grass coexistence (Bonan et al., 2003; Hély et al., 2006; Baudena et al., 2015). Three critical processes that require special consideration to improve the modelling of tropical biomes are phenology, root-water uptake, and fire disturbance (Whitley et al., 2016).

In comparison to other DGVMs, JSBACH has a simple representation of ecosystem processes and implies a limited number of interactions. Other DGVMs explicitly account for root competition (e.g. TEM-LPJ, Pan et al. (2002)), light competition and shading effects (e.g. LPJ-DGVM, Sitch et al. (2000); LSM-DGVM, Bonan et al. (2003)), Lotka–Volterra type differential equation models (e.g. TRIFFID, Cox (2001)), PFT-dependent fire resistance (e.g. LPJ-DGVM, Sitch et al. (2000)), recruitment and age classes (e.g. LPJ-GUESS, Smith et al. (2001)), different sets of PFTs, growth and competition among individual plants (e.g. LPJ-GUESS, Smith et al. (2001)), or trait flexibility “everything is everywhere, but the environment selects” (JeDi-DGVM, (Pavlick, 2012)). These refinements better capture ecological interactions, water-limited tree growth, and a positive grass-fire feedback as observed in reality. Drought sensitivity, an important trait in semi-arid regions, is in JSBACH assumed to be equivalent for all PFTs although it varies in reality considerably among plants from different climate zones, shown to be relevant in a study on drought response with the CABLE LSM (De Kauwe et al., 2015). Baudena et al. (2015) showed that JSBACH overestimates tree cover because competition via only *NPP* favors trees irrespective of water availability, and fire is fostered disproportionately by woody vegetation as compared to grasses, resulting in a negative grass-fire feedback. At the same time, competition between neighboring plants cannot be explicitly represented in JSBACH. An example of an adjusted model is the aDGVM – specifically designed for African vegetation and savannas – including functional variation within PFTs (e.g., phenology, allocation and physiology adapt to changing environmental conditions) (Scheiter & Higgins, 2009). Scheiter et al. (2013) presented a “trait- and individual-based vegetation model (aDGVM2) that allows individual plants to adopt a unique combination of trait values”, dealing “with functional diversity and competition fundamentally differently from current DGVMs”. However, the high computational demand limits the application to palaeo studies.

In summary, the PFT set in JSBACH designed for global application has only a limited applicability for detailed studies on the role of plant diversity in subtropical semi-arid regions. Compared to other DGVMs, JSBACH has a very simple and limited representation of plant diversity and vegetation dynamics. However, JSBACH is designed such that plant diversity can be increased and PFT specific traits can be modified.

2.2.4 Analogy between plant diversity in JSBACH and in the conceptual model in Chapter 1

A necessary prerequisite for the transfer of knowledge gained from the conceptual model in Chapter 1 to JSBACH is the assurance of their comparability concerning their overall goals, basic vegetation units, reconstruction scales, and the consideration and determination of plant diversity. First, I briefly recapitulate the concepts of White (1983) and Hély et al. (2014) because they served as references for the model adjustment in Chapter 1. The comparison of the conceptual model from Chapter 1 and the PFT concept from JSBACH (Reick et al., 2013) subsequently follows.

The most specified vegetation classification that served as a basis for many studies on plant diversity in Africa is the classification after White (1983). “White’s vegetation map of Africa” (Fig. 2) was designed based on recent vegetation and considers two aspects of vegetation: first the mapping units in a regional framework that consider clearly distinguishable vegetation types resulting from characteristic physiognomy (e.g. forest, grassland, steppe, ...), and second phytochoria in a trans-regional framework that are based on characteristic compositions of species in restricted regions (e.g. Guineo–Congolian regional centre of endemism, Sudanian regional centre of endemism, Sahara regional transition zone, ...). Each phytochorion relates to a certain range of mean annual precipitation and can be composed of different vegetation types. The basic units are species themselves that can occur in certain growth forms in certain regions. The reconstruction scale ranges from species level to phytochoria on continental scale. Plant diversity is considered maximally with the registration of every single species.

Hély et al. (2014) used White’s classification to group paleobotanical data from different sites in Africa to discuss the relation between available surface water, monsoon rainfall and vegetation distribution in West Africa during the Holocene. The authors concentrated on four main phytochoria: Guineo–Congolian type, Sudanian type, Sahelian type, and Saharan type. The basic units in their study were the parent species to the pollen samples characteristic for each phytochorion. In their reconstruction approach they focused on changes in longitudinal distribution of phytochoria that imply characteristic species, but the physiognomy and related functionalities were not of explicit importance. Plant diversity was considered in terms of absolute species richness and in terms of mixture of phytochoria within regions.

The land surface model JSBACH was designed to simulate vegetation distribution on a global scale in the geographical space (G-space), accounting for the most important functionalities of vegetation and its interaction with the atmosphere. In comparison to the approaches above, characteristic species and their individual ecology are of minor importance. The basic units are PFTs whose ratios can be translated into biomes. Previous reconstructions typically focused on the longitudinal shifts of biomes, upscaled from the distribution of PFTs. Species diversity is not considered with the PFT concept and the method to derive biomes via PFT ratios excludes the possibility of deriving mixtures of phytochoria in a grid cell.

The conceptual model described in Chapter 1 was designed to study how plant diversity affects the stability of a climate–vegetation system in the ecological space (E-space). In contrast to the approaches above, the model does not operate on continental scale but is limited to a much smaller area that experiences a homogeneous climate. Longitudinal vegetation gradients are therefore not observable. The basic units are plant types derived from White’s phytochoria, mainly characterized by specific moisture requirements and maximum effective leaf area, which points to their overall physiognomy. Reconstructions can only focus on the change in phytochoria composition within a limited region caused by changes in mean annual precipitation in this particular area, not on the longitudinal shift of phytochoria or biomes. Plant diversity is considered in terms of mixture of phytochoria within the simulated region.

The attempt to compare the approaches above faces several problems due to large discrepancies, especially in the spatial dimension (E-space vs. G-space) and the consideration of plant diversity. The conceptual model described in Chapter 1 deals with plant diversity as a mixture of phytochoria composed of several vegetation types within a region in the order of a GCM grid cell. These vegetation types include regional variations of functional types (Guineo–Congolian tree, Sudanian tree, Sahelian grass, Saharan grass, ...). JSBACH deals with plant diversity between grid cells and determines vegetation types composed of PFTs, which are homogeneous for all regions. The plant types of the conceptual model described in Chapter 1 can further not directly be compared to the PFTs in JSBACH because their definition is based on discrete precipitation thresholds that are not explicitly implemented in JSBACH. Environmental envelopes with discrete precipitation thresholds in the conceptual model allow for a clear distinction between plant types with defined properties and enable the implementation of AHP vegetation

based on moisture requirements. In JSBACH in contrast, the growth ranges of PFTs rely on a range of factors that interact in a nonlinear manner. This implies a loss of control in a conceptual sense, and AHP plant types distinguished by discrete precipitation thresholds cannot be depicted. A mosaic-like environment as reconstructed from pollen cannot be simulated with the tiling approach because tiles have no explicit geographic location in the grid cell. Some characteristic functional plant groups do not find corresponding PFTs in JSBACH such as perennial grasses, subtropical evergreen shrubs or monsoon forest trees. However, JSBACH simulates a more process-based plant behaviour and might capture plant features that the conceptual model is not capable of such as sensitivities to temperature, fire, and competition.

In summary, the comparison of plant diversity in the conceptual model in Chapter 1 and JSBACH reveals profound differences. AHP plant types defined based on moisture requirements cannot be represented in JSBACH, and their coexistence in a mosaic-like environment (especially gallery forests) cannot be depicted. However, since JSBACH is a process-based model, qualitatively comparable results from simulations with different PFT compositions could substantiate the conclusions from the conceptual study in Chapter 1 which are supported by ecological literature.

2.3 PFT response to a linear precipitation decline

In the conceptual model in Chapter 1, the sensitivity of plant types is determined by their individual precipitation thresholds and depicted in the slopes in the V–P diagram (Fig. 1.1) or rather the L_i -P diagram (Fig. 1.2). This direct linear relationship makes plant growth predictable as a function of precipitation. In JSBACH in contrast, the growth of plant types is not directly related to explicit precipitation requirements but results from a combination of processes in the model, some of them are nonlinear. Therefore, plant behaviour with changing precipitation patterns and the role of plant diversity in this context are not always predictable. To improve the understanding of PFT behaviour, I study here the vegetation performance along a prescribed precipitation decline using an offline version of JSBACH. Neglecting interactions with the atmosphere, and therewith excluding potential feedbacks, I can separate the effects emerging from different degrees of plant diversity.

2.3.1 Model set up

Palaeo simulations over thousands of years require enormous computing time, even in offline simulations. To minimize computation, I reduce the land area to the study domain in north Africa (12 to 34° N, -15 to 40° E) by modifying the land-sea mask, see Fig. 2.1.

JSBACH runs with dynamic vegetation at a low horizontal atmospheric resolution (T63, approximately 1.88°). The model simulates land surface properties interactively in terms of soil moisture, snow cover, leaf area index, and vegetation distribution. Soil properties originate from the FAO digital soil map of the world (FAO/UNESCO, 1974) and remain constant over the simulated period.

I provide the atmospheric boundary

conditions from modified observational data. The original data set is a 30 years period (1950 to 1979) from CRUNCEP, a data set combined of two existing data sets: The CRU TS.3.1 0.5° x 0.5° monthly climatology (1901 to 2012) and the NCEP reanalysis 2.5° x 2.5° 6 hours time step beginning in 1948 and available in near real time.

For the initial high precipitation P for the simulations, I calculate the mean annual cycle of P from 12 to 14° N, -15 to 40° E and add daily values (in total 633.5 mm yr⁻¹) to latitudes between 12 and 34° N. The resulting P ranges from around 650 mm yr⁻¹ in the Sahara to up to 1500 mm yr⁻¹ at the southern edge of the domain. This is much higher than reconstructed for the mid-Holocene (from 250 to 400 mm yr⁻¹ (Baumhauer & Runge, 2009) to >500 mm yr⁻¹ in some locations (Bartlein et al., 2011)), but for this idealized set up, it allows to cover extreme scenarios. All other atmospheric variables such as temperature and specific air humidity remain unchanged. Orbital parameters and greenhouse gas concentrations remain constant conforming to the standard preindustrial set up of MPI-ESM1 (see 0 ky set up in Tab. 3.1). Limitations of this set up will be discussed in Sect. 2.3.4.

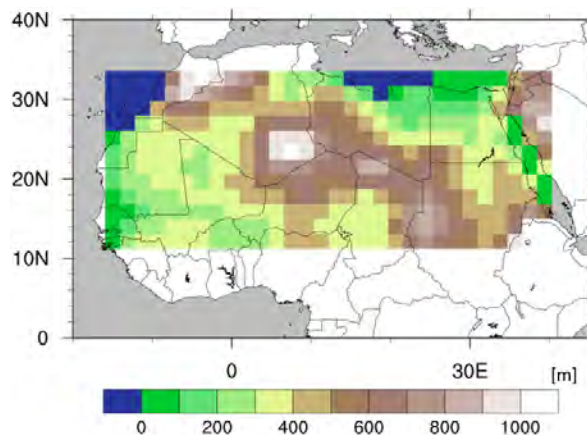


FIGURE 2.1: Mean orography (in m) of the simulated study domain in north Africa at 12 to 34° N, -15 to 40° E.

As a reference, I set up a control simulation EXP_{ALL} with all natural PFTs available in JSBACH (see Tab. 2.1) and linearly decreasing P . To analyze individual behaviour, I exclude in the next step all woody PFTs and their competition from the study domain in a grass only experiment. As $C4$ Grass is by far the dominant grass PFT in the study domain, apart from the latitudes north of 32°N where $C3$ Grass substantially contributes to the veg-

etation cover, this experiment can be considered as a single-PFT experiment with $C4$ Grass only (EXP_{C4}). Simulations with woody PFTs only are not straight forward to implement in JSBACH since the model is constructed such that bare land is immediately occupied by grasses. With respect to reality, this is a reasonable assumption since some herbaceous vegetation is always present in the study domain if P allows tree growth. In a next step, I increase the number of PFTs to two in the experiments EXP_j ($EXP_{TE,C4}$ and $EXP_{SRG,C4}$). Finally, I strongly increase the number of PFTs to 58 for a high plant diversity experiment EXP_{HIDI} . I vary the default PFTs for TE , SRG , $C3$, and $C4$ in maximum carboxylation capacities $V_{max,0}$ and electron transport capacities $J_{max,0}$ at 25°C within the range of observations (Kattge et al., 2011; Verheijen et al., 2013). I also vary the establishment/mortality timescale τ of TE and SRG , standard values can be found in Tab. 2.1. This results in 15 different TE (TE_{1-15}), 15 different SRG (SRG_{1-15}), 10 different $C3$ ($C3_{1-10}$), 10 different $C4$ ($C4_{1-10}$), and the standard PFTs TE , TD , eTE , eTD , SRG , SD , $C3$, and $C4$, see Tab. A1. In all simulations, initial cover fractions are equally distributed over all included PFTs.

To bring vegetation in an equilibrium, I run a spin up of 600 years. After this period, I start the actual experiment by reducing the added precipitation field by 1% per 30 years cycle. After 100 cycles, which correspond to 3000 simulated years, P reaches the level observed in the input forcing period (1950 to 1979).

TABLE 2.2: List of performed offline simulations, the number of included PFTs, and the considered dynamics.

experiment	PFTs	dynamics
EXP_{ALL}	8	dynveg
EXP_{C4}	1	grass only
$EXP_{TE,C4}$	2	dynveg
$EXP_{SRG,C4}$	2	dynveg
EXP_{HIDI}	58	dynveg

2.3.2 Results

The performed simulations provide time series of vegetation cover fractions veg_{max} , PFT cover fractions f_i and precipitation P for each grid cell (360 in total), presented in the following. For a clearer illustration of the results, I discuss example grid cells to highlight the fundamental differences between simulations. All presented curves are smoothed with a 30-years unweighted running average.

With high P at the beginning of EXP_{ALL} , vegetation is widely spread all over the study domain in north Africa (Fig. 2.4). In the northernmost regions (30 to 34° N), vegetation is composed of $C4$ or $C3$, eTE , and SRG . In the Sahara region (18 to 30° N), $C4$ has the largest share beneath eTE or SRG . In Sahelian and Sudanian regions (12 to 18° N), vegetation is mainly characterized by the coexistence of $C4$ and TE . This represents a north-south gradient from steppe over savanna to tropical forest. In the course of the experiment, $veg_{max,ALL}$ retreats faster than the linear P forcing, except for the southernmost latitudes where P is generally high enough to sustain plant growth (Fig. 2.3a, 2.4). Retreating PFTs are replaced by less productive ones when conditions become too harsh to sustain growth (Fig. 2.4).

In the experiment with grass only (EXP_{C4}), vegetation fully covers all grid cells at the beginning of the experiment (Fig. 2.5). Throughout the experiment, $veg_{max,C4}$ retreats much faster than P , except for the southernmost latitudes where P is generally high enough to sustain plant growth (Fig. 2.2a, 2.3b, 2.5).

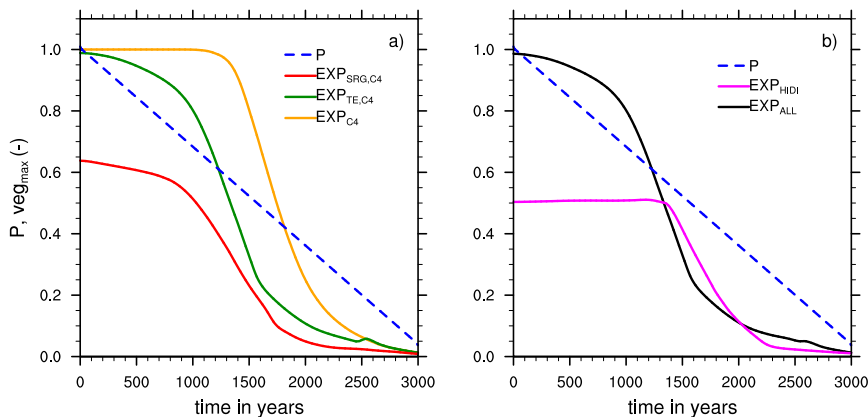


FIGURE 2.2: Vegetation cover fraction veg_{max} and precipitation P for simulations with different PFT compositions for one selected grid cell (19.58° N, -3.75° E). Curves depict the transient behaviour of EXP_{C4} (a; orange), $EXP_{TE,C4}$ (a; dark green), $EXP_{SRG,C4}$ (a; red), EXP_{ALL} (b; black), and EXP_{HIDI} (b; magenta). P (blue dashed) is scaled to 100% at the beginning of the simulation period.

With an increasing number of PFTs in $EXP_{TE,C4}$ and $EXP_{SRG,C4}$, the area covered with vegetation $veg_{max,j}$ is reduced compared to $veg_{max,C4}$ in the single-PFT experiment (Fig. 2.2a, 2.5). This reduction is stronger in $EXP_{SRG,C4}$ than in $EXP_{TE,C4}$. In the course of the experiments, $veg_{max,j}$ retreat faster than P , except for the southernmost latitudes where P is generally high enough to sustain plant growth (Fig. 2.3c, d, 2.5). $veg_{max,TE,C4}$ declines faster than $veg_{max,C4}$ and $veg_{max,ALL}$ in the northern part of the domain (north of 20° N) while the transition is slower in the southern part. $veg_{max,SRG,C4}$ retreats everywhere slower than $veg_{max,C4}$ and $veg_{max,ALL}$ (Fig. 2.2a, 2.3c, d).

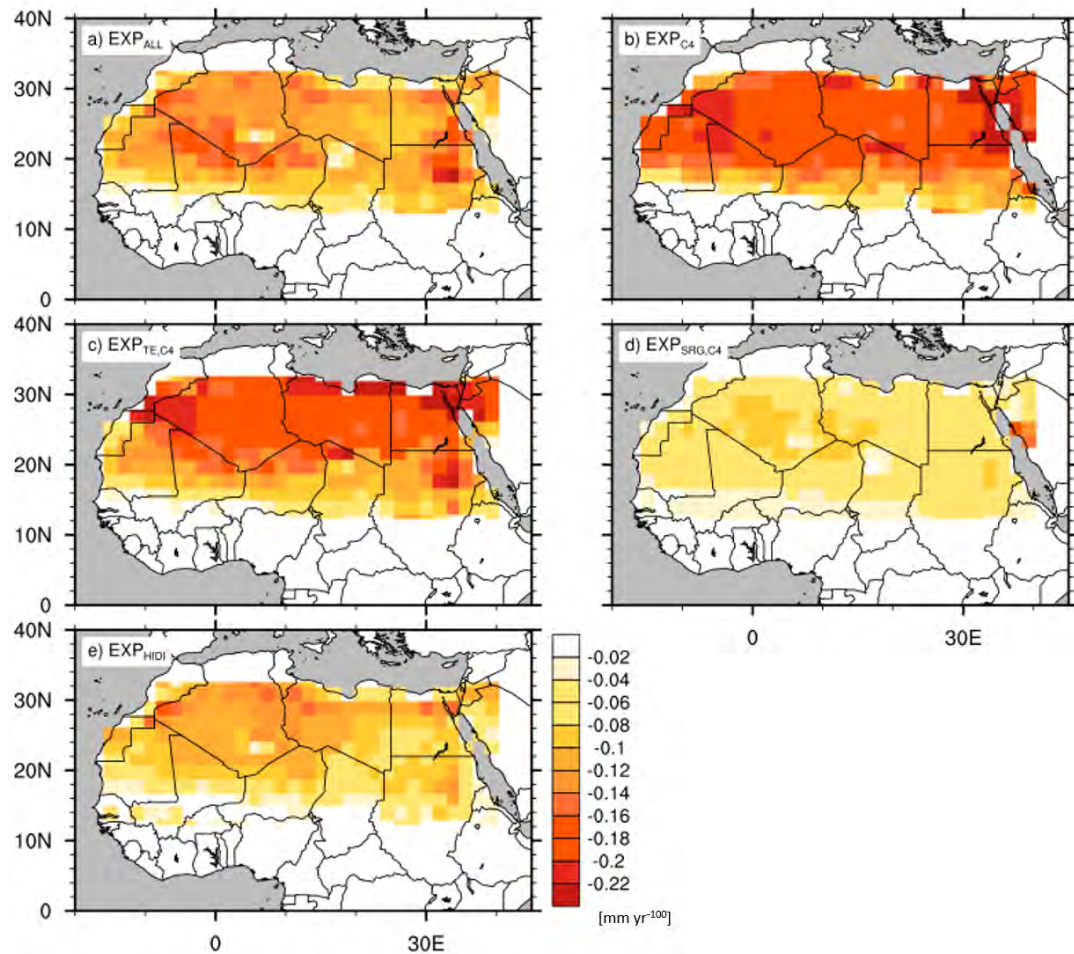
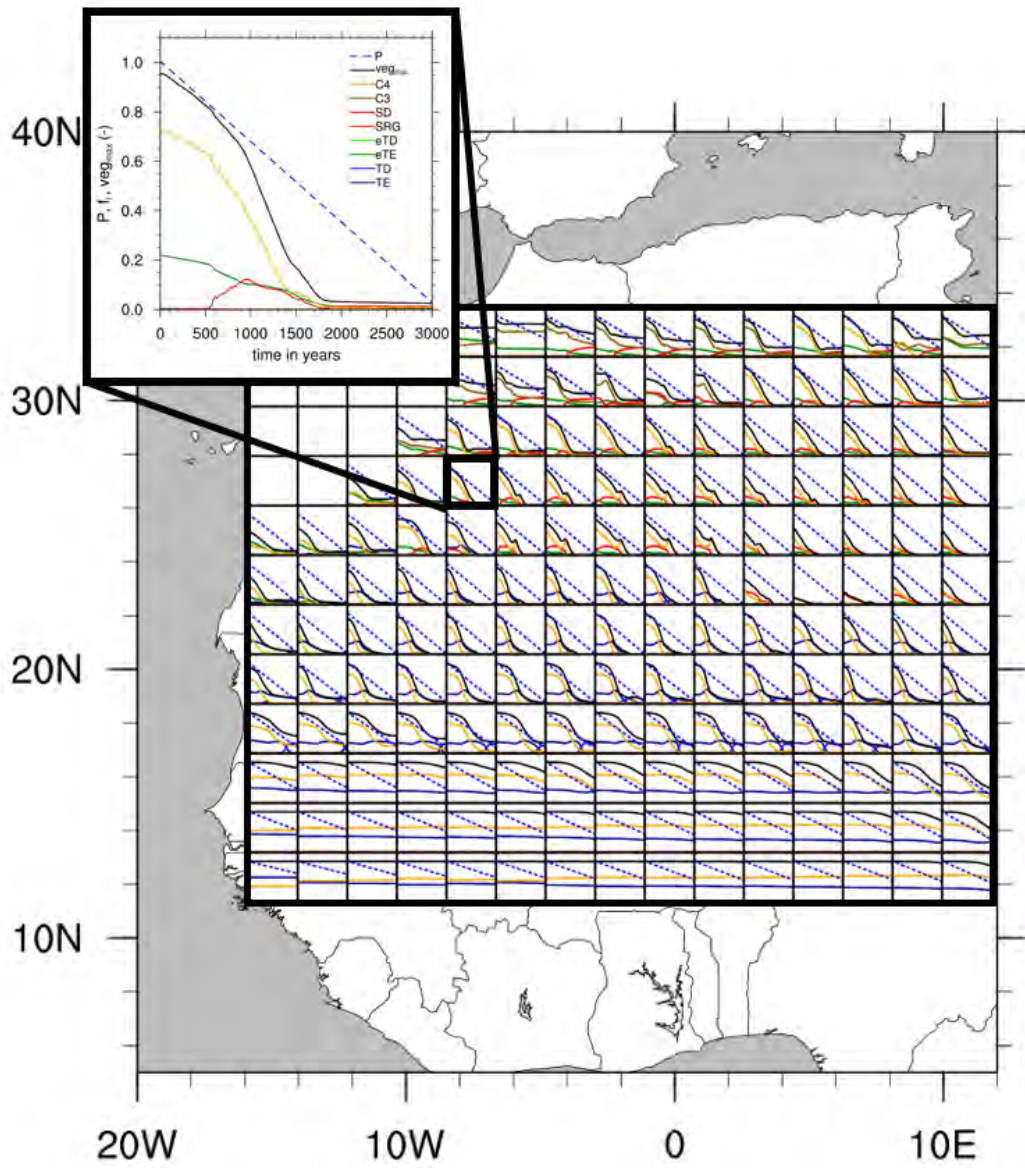


FIGURE 2.3: Maximum slope of vegetation cover fractions veg_{max} over a 100-years running window for EXP_{ALL} (a), EXP_{C4} (b), $EXP_{TE,C4}$ (c), $EXP_{SRG,C4}$ (d), and EXP_{HIDI} (e). The slope of precipitation P decline is in all simulations $0.03\% yr^{-1}$. Yellowish colors indicate that the slope of veg_{max} is slightly steeper than the slope of P , reddish colors represent grid cells where the slope of veg_{max} is much steeper than the slope of P .



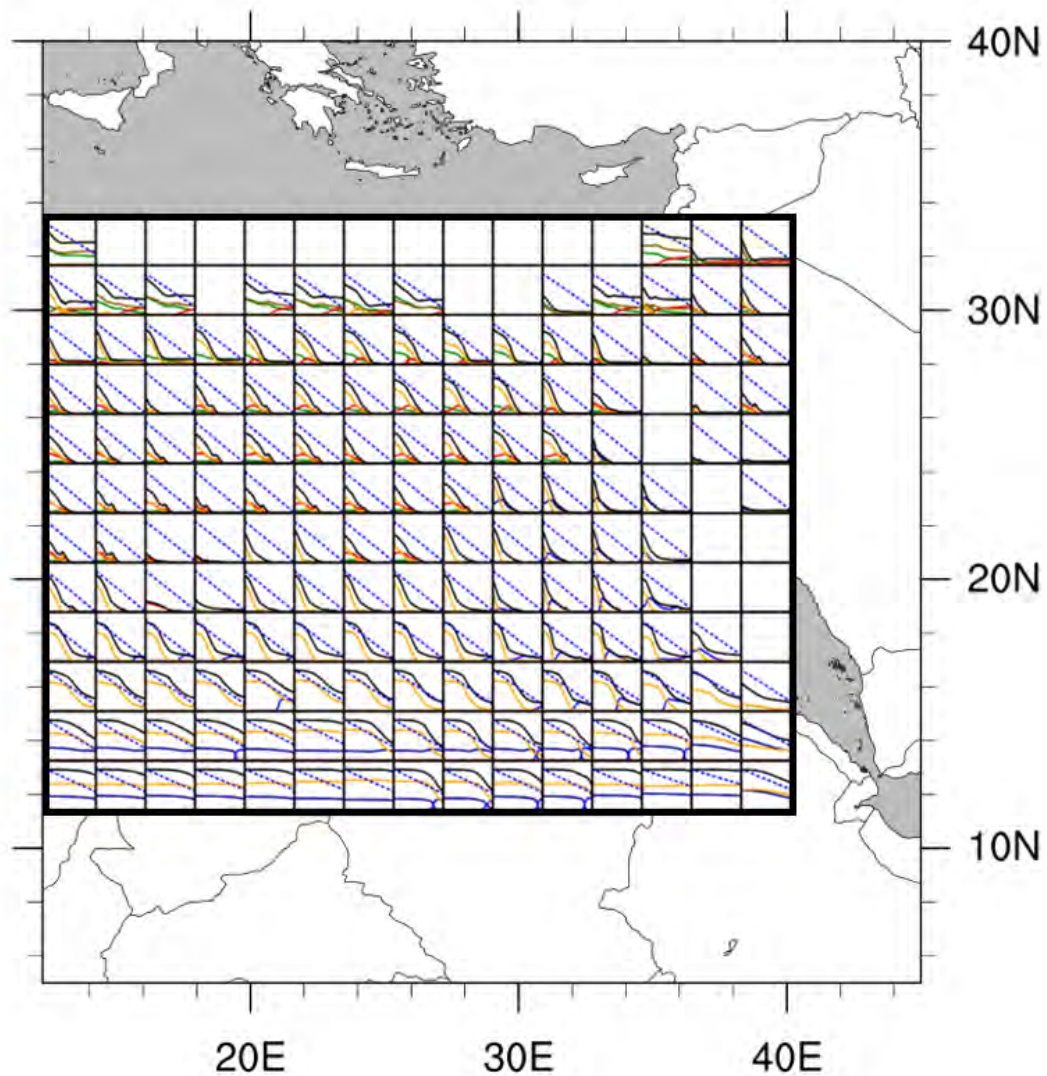
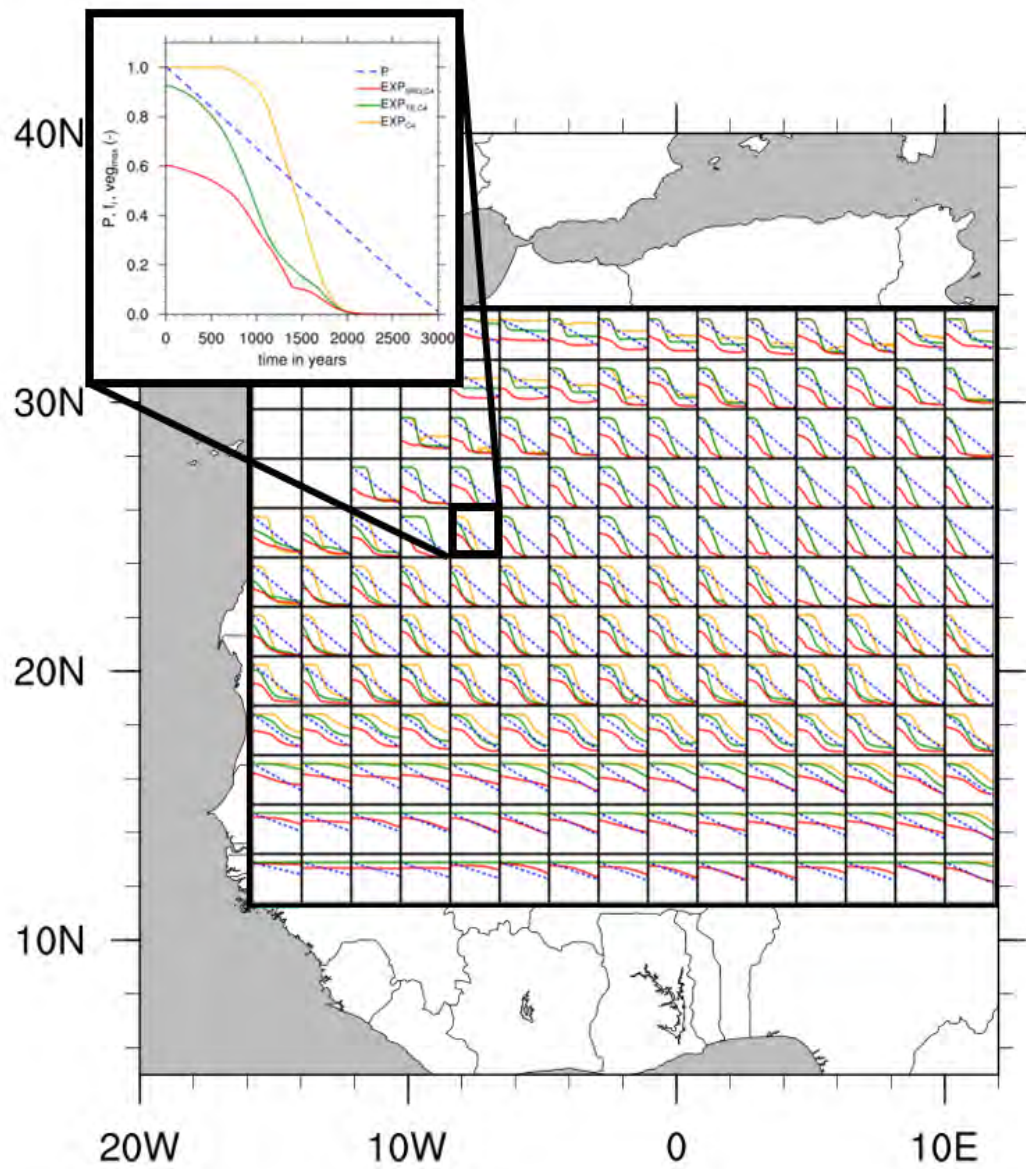


FIGURE 2.4: Vegetation cover fraction $veg_{max,ALL}$, cover fractions f_i of PFTs i and precipitation P of a simulation with the standard PFT set up (EXP_{ALL}) at 12 to 34° N, -15 to 40° E. P (blue dashed) is scaled to 100% at the beginning of the simulation period for each grid cell individually. f_i are shown for PFTs relevant in the study domain: Tropical Evergreen Tree (TE ; dark blue), Tropical Deciduous Tree (TD ; light blue), Extratropical Evergreen Tree (eTE ; green), Shrub Raingreen (SRG ; red), C3 Grass ($C3$; brown), C4 Grass ($C4$; orange).



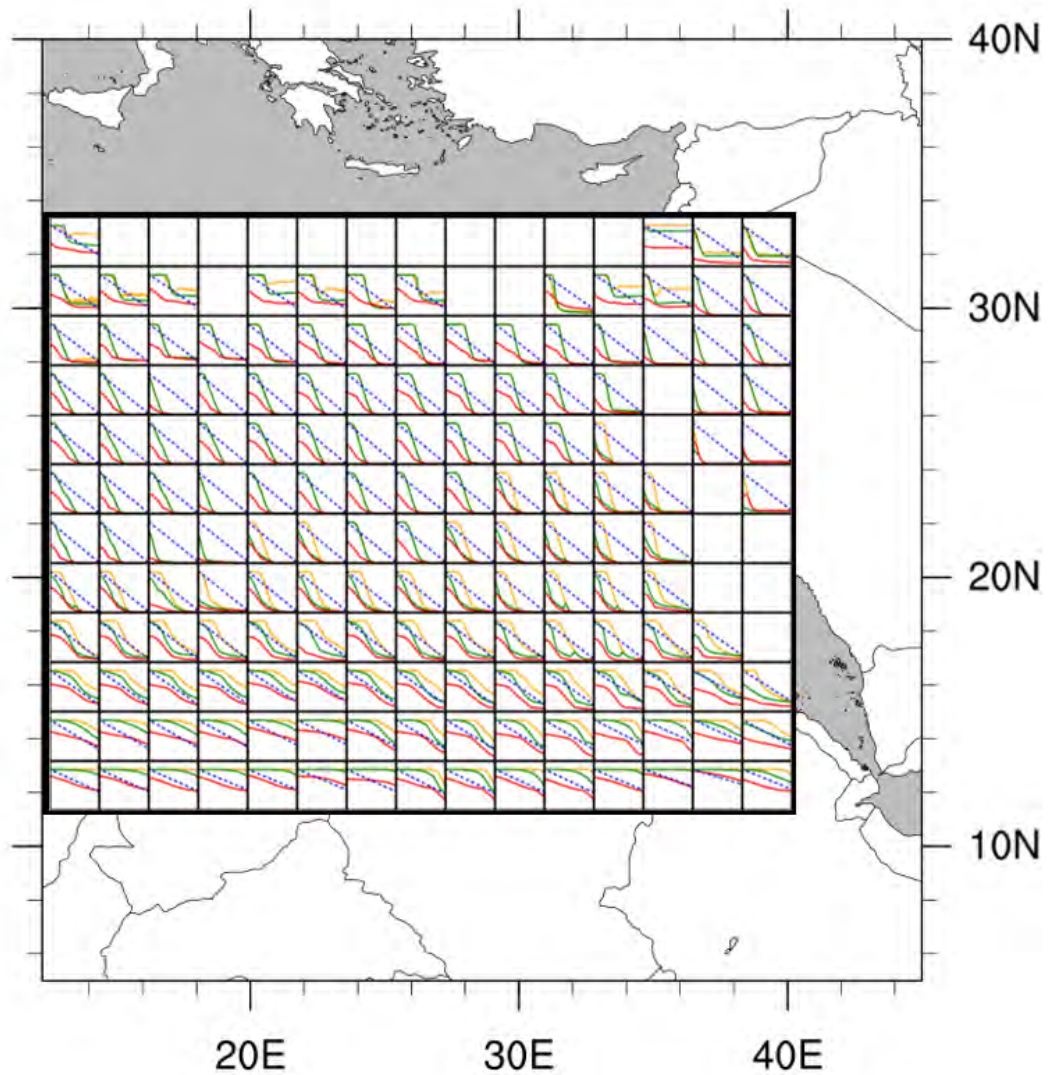
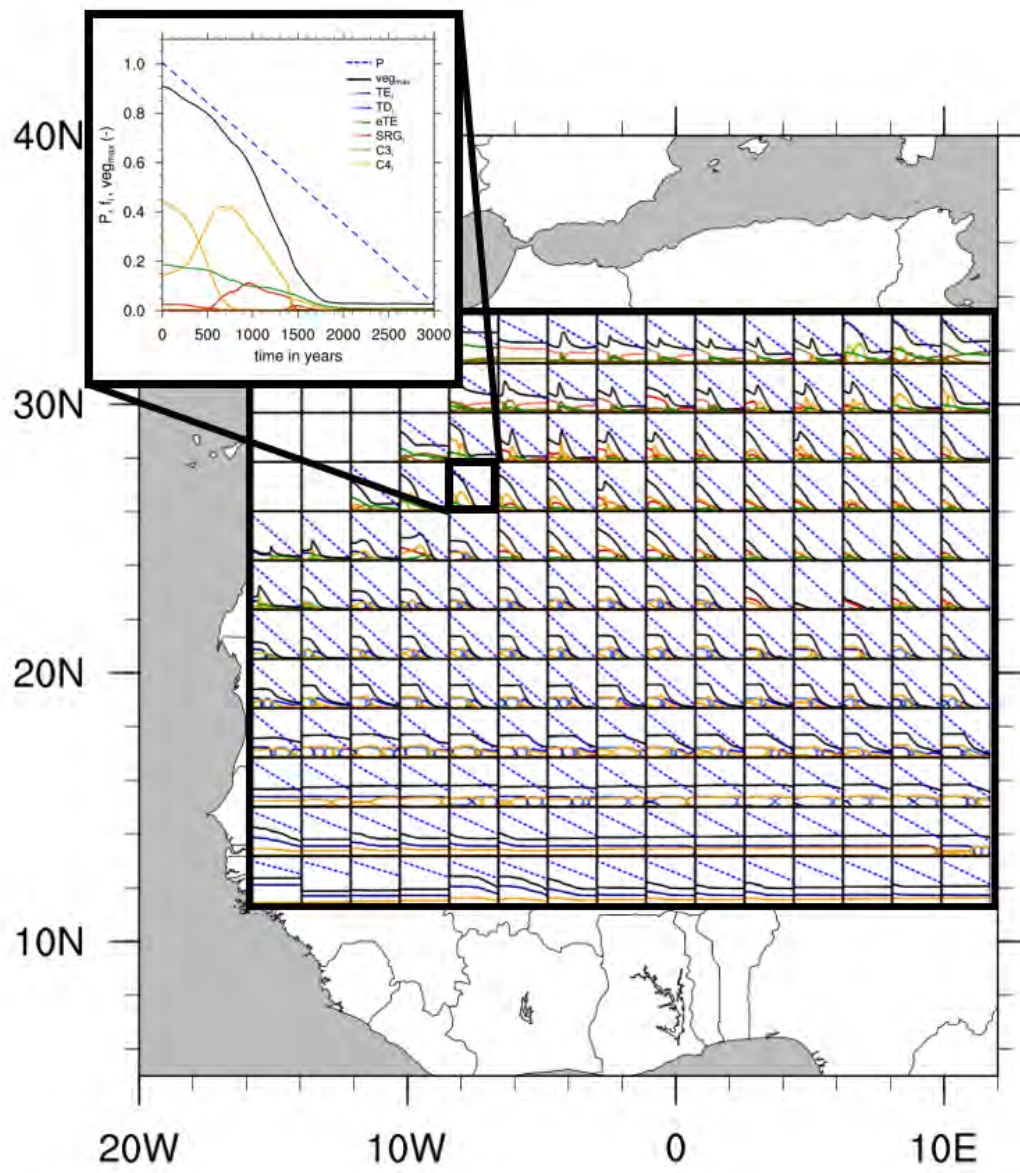


FIGURE 2.5: Vegetation cover fraction veg_{max} and precipitation P for single-PFT and two-PFT simulations at 12 to 34° N, -15 to 40° E. Curves depict the transient behaviour of C4 Grass only in EXP_{C4} (orange), Tropical Evergreen Tree and C4 Grass in $EXP_{TE,C4}$ (dark green), and Raingreen Shrub and C4 Grass in EXP_{SRG} (red). P (blue dashed) is scaled to 100% at the beginning of the simulation period for each grid cell individually.



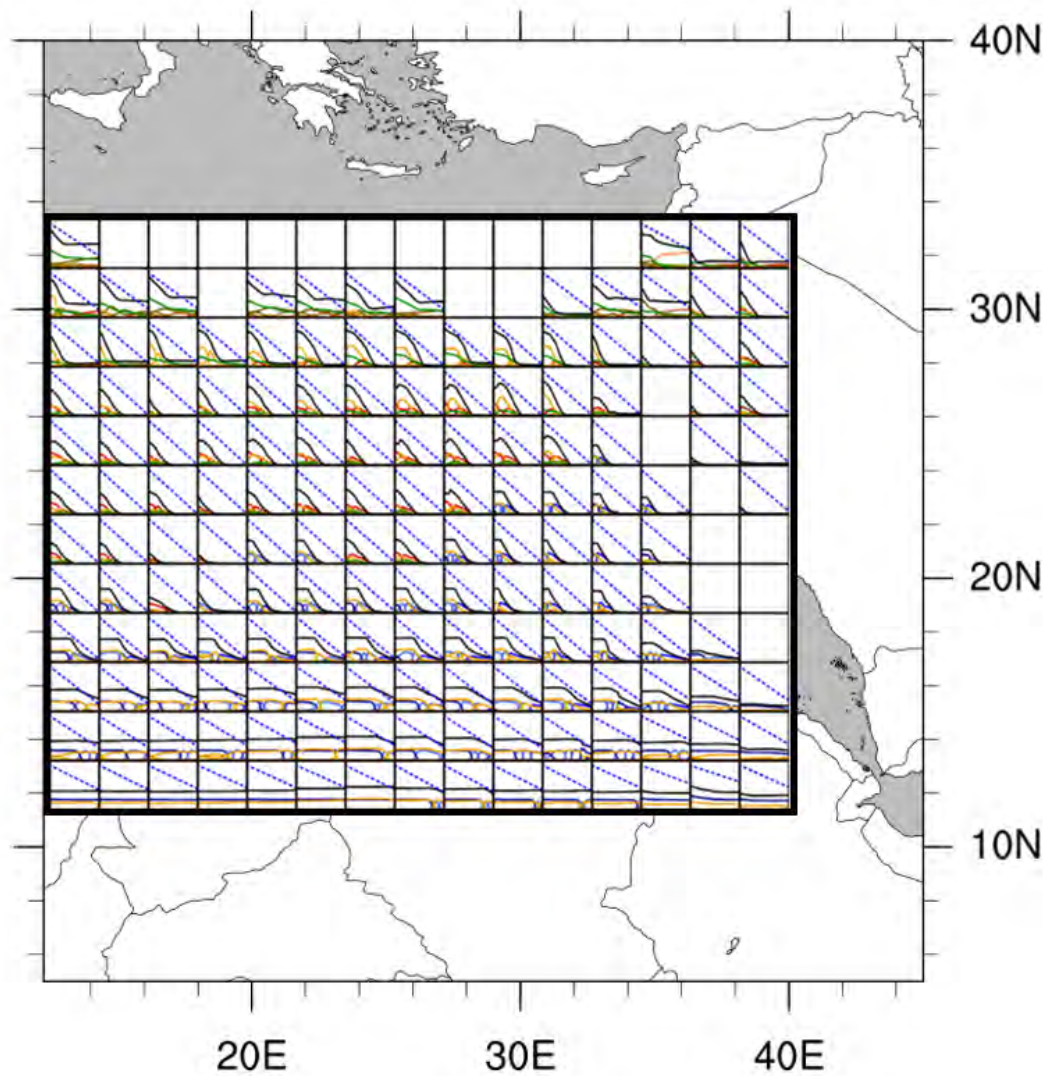


FIGURE 2.6: Vegetation cover fraction $veg_{max,HIDI}$, cover fractions f_i of PFTs i and precipitation P of a simulation with the high PFT set up (EXP_{HIDI}) at 12 to 34° N, -15 to 40° E. P (blue dashed) is scaled to 100% at the beginning of the simulation period for each grid cell individually. f_i are shown for modified and standard PFTs relevant in the study domain: Tropical Evergreen Tree (TE , TE_i ; blue), Tropical Deciduous Tree (TD , TD_i ; light blue), Extratropical Evergreen Tree (eTE ; green), Shrub Raingreen (SRG , SRG_i ; red), C3 Grass ($C3$, $C3_i$; brown), C4 Grass ($C4$, $C4_i$; orange) with dark colour shade indicating high photosynthetic capacity and light colour shade indicating low photosynthetic capacity.

At the beginning of EXP_{HIDI} , vegetation is widely spread all over the study domain (Fig. 2.6). The PFT composition is overall the same as in EXP_{ALL} . From the variations within one PFT, the PFT with the highest photosynthetic capacity and shortest τ always outcompetes the others. Compared to EXP_{ALL} , $veg_{max,HIDI}$ is strongly limited especially in the southernmost latitudes (Fig. 2.6). With decreasing P , $veg_{max,HIDI}$ does not respond uniformly in the study domain. In the northeastern part (around 28 to 34° N, -6 to 6° E), $veg_{max,HIDI}$ declines slowly before it increases abruptly by more than 0.2 after around 500 to 1000 years of the experiment (Fig 2.6, 2.7a). After that peak, $veg_{max,HIDI}$ declines faster than P , closely following $veg_{max,ALL}$ (Fig. 2.2d). In the central and eastern part of the domain (around 23 to 28° N, 4 to 30° E) $veg_{max,HIDI}$ retreats monotonously and faster than P . In the transition zone between steppe and savanna (18 to 23° N, -15 to 6° E and 18 to 21° N, 6 to 30° E), $veg_{max,HIDI}$ stagnates on at plateau at 40 to 60% and starts a delayed decline around 500 to 1000 years later than $veg_{max,ALL}$. In the following, the curves of $veg_{max,HIDI}$ and $veg_{max,ALL}$ are almost congruent, decreasing faster than P (Fig. 2.2d). South of 18° N, $veg_{max,HIDI}$ is constant in most grid cells with values never exceeding 0.6. If $veg_{max,HIDI}$ is not constant, the decline is slower than P . Looking into changes in PFT composition, initially established PFTs are replaced by less and less productive ones. The overturning of PFTs with different productivities smooths $veg_{max,HIDI}$ relative to f_i , see Fig. 2.6, 2.7.

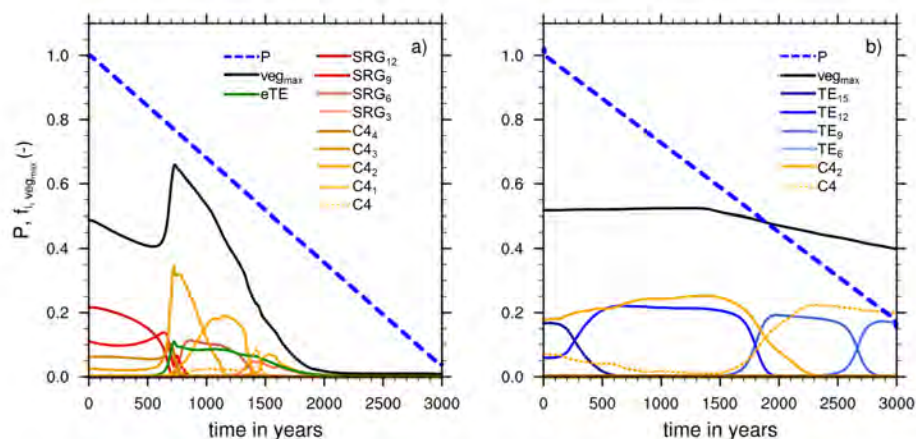


FIGURE 2.7: Vegetation cover fraction $veg_{max,HIDI}$, cover fractions f_i of PFTs i and precipitation P (in mm yr^{-1}) of a simulation with the high PFT set up (EXP_{HIDI}) for two example grid cells at 30.77° N, 5.625° E (a) and 17.72° N, -11.25° E (b). P (blue dashed) is scaled to 100% at the beginning of the simulation period for each grid cell individually. f_i are shown for modified and standard PFTs relevant in the grid cells: Tropical Evergreen Tree (TE_i ; blue), Extratropical Evergreen Tree (eTE ; green), Shrub Raingreen (SRG_i ; red), C4 Grass ($C4$, $C4_i$; orange) with dark (light) colour shade indicating high (low) photosynthetic capacity.

2.3.3 Discussion

Offline simulations with different sets of PFTs show that the expansion of vegetation with high P at the beginning of the simulations as well as the slope of vegetation retreat differ between single-PFT and multi-PFT simulations.

The differences in initial cover arise from the different productivities of occurring PFTs, their competition and disturbances. In the single-PFT simulation, $veg_{max,C4}$ results from only $C4$'s productivity and its capability to suppress desert expansion, see Eq. 2.7, 2.8. The value by how much $veg_{max,i}$ of any individual PFT deviates from $veg_{max,j}/ALL/HIDI$ is determined by the ratio of involved PFTs resulting from competition. The more competitive and productive a PFT, the larger is the grid cell fraction this PFT covers and the larger is its weight in the calculation of $veg_{max,j}/ALL/HIDI$ in Eq. 2.7.

What is striking is the strong limitation of veg_{max} in simulations with dynamic vegetation that include SRG . The explanation lies in the parameterization of SRG in JSBACH. Due to a low SLA (see Tab. 2.1) SRG requires a higher productivity to cover the same area as other PFTs; for example to cover 1 m² area with 1 m² leaves, SRG needs around 50% more NPP than TE and around 260% more than $C4$ (derived from Eq. 2.7, 2.8). Reaching comparatively high NPP as other PFTs is impeded by SRG 's comparatively low productivity. SRG thereby acts as desert promoter. The lack of SRG in EXP_{C4} and $EXP_{TE,C4}$ in turn reduces the competitive pressure on other PFTs and their higher SLA facilitates their expansion and the repression of desert. In $EXP_{SRG,C4}$, SRG outcompetes grasses, but since growth conditions are not optimal, SRG cannot fill the green pools over the growing season which leads to negative feedback and an expansion of desert. With respect to literature, the role of SRG as desert promoter seems reasonable despite mechanisms are not explicitly implemented in JSBACH. Eldridge et al. (2011) summarized "Shifts from grassland to shrubland have been shown to be associated with changes in the spatial distribution of soil resources (Schlesinger et al., 1996), altering the patterns of resource flow between shrubs and their interspaces (Li et al., 2008) and reinforcing the persistence of shrubs (D'Odorico et al., 2007). Wind- and water-transported nutrients, detritus and seeds accumulate under shrub canopies, leading to higher levels of infiltration capacities (Bhark & Small, 2003), while the bare interspaces experience higher temperatures and evapotranspiration, retarded organic N incorporation, denitrification, ammonia volatilization and increased erosion (Schlesinger

et al., 1990). The combined effect of these processes is a strengthening of the “fertile island” effect around shrubs, making shrublands extremely resistant to change and enhancing the persistence and development of shrublands at the expense of grasslands (Schlesinger et al., 1996; Whitford, 2002). Losses of grassland biota with encroachment have been shown to reinforce the shrub-dominant state (Eldridge et al., 2009).”

Similar to the initial cover, the slope in multi-PFT simulations is determined by the ratio of involved PFTs. The main aspects shaping the slope are their productivities under the new given P conditions and their establishment/mortality time scales (τ). The smaller a PFTs productivity and τ , the faster the transition to the “desert” state. This is very pronounced in EXP_{C4} since $C4$ has the lowest productivity and the smallest τ of 1 year. Another aspect influencing the slope is the initial cover. Starting with a comparatively low cover does not inherit the potential for a sharp decline of several tenths. This effect becomes visible in $EXP_{SRG,C4}$ especially in the northern part of the domain (Fig. 2.5). Due to unfavourable conditions, the initial cover is relatively low and the large τ of 12 years favours a smooth transition.

Comparing the results to Chapter 1, the offline simulations reflect plants’ sensitivities described and observed in the conceptual study. Similar to the conceptual approach in Chapter 1, veg_{max} is in JSBACH offline simulations high at the beginning with high P and retreats with P decline. Saharan and Sahelian plant taxa – $C4$ in JSBACH – are mainly drought-adapted species that survive until conditions become very harsh, and they respond quickly if P crosses the minimum threshold. However, the individual response of woody PFTs cannot be simulated with the current JSBACH version. Further, the special behaviour of the Guineo–Congolian tropical gallery forest plant type and its association with open water cannot be depicted with JSBACH due to the lack of spatial explicitness in the coarse resolution.

The buffering effect of higher plant diversity on veg_{max} described in Chapter 1 can be observed in some regions in JSBACH offline simulations, for example in Fig. 2.7, despite the underlying cause is different. In Chapter 1, the buffering effect of high plant diversity is a result of the niche approach. By averaging over the E-space covered by different plant types, the effective vegetation cover interacting with the atmosphere is smoothed over time. The smoothing in JSBACH arises from the weighting of PFT contributions in the calculation of the desert extent in Eq. 2.7. PFTs occupy the G-space and the

atmosphere sees the sum of PFTs which is similar to the “potential vegetation coverage” approach by Claussen et al. (2013). When a PFT disappears in JSBACH, its space can be occupied by another PFT that grows better under the new conditions, other than assumed in the conceptual model (see “niche conservatism” in Sec. 1.2.1).

Another common result of Chapter 1 and JSBACH offline simulations is the importance of plant composition. In both approaches, I observe large differences in the vegetation cover fraction and its response to declining precipitation depending on the involved plant types and their individual sensitivities to changing conditions.

However, one elementary aspect is missing in offline JSBACH simulations: the effect emerging from feedbacks between vegetation and the atmosphere. Do sensitive plants benefit from additional water and facilitation effects in a more life-sustaining environment, whereas resilient plants might suffer to a certain degree from additional competition? To address this question, simulations with the coupled land-atmosphere model are indispensable.

Recapitulatory, the initial composition of vegetation is mainly determined by bioclimatic limits, the prevailing P regime and competition. The same holds for the rate of transition from a wet “green” to a dry “desert” desert. Whether PFTs are stronger (wider expansion and longer persistence) or weaker (less expansion, shorter persistence) when plant diversity increases depends on the combination and individual productivities per area. A very important player in this context is SRG which acts as a desert promoter. Despite large differences in the underlying assumptions, offline JSBACH simulations support the results from Chapter 1: high plant diversity could have a buffering effect on mean vegetation cover when precipitation decreases and plant composition plays a crucial role for the climate–vegetation system stability.

2.3.4 Limitations

The main limitation in terms of representing realistic mid-Holocene conditions is the handling of precipitation. The assumed P is considerably higher than reconstructed for the mid-Holocene (Baumhauer & Runge, 2009; Bartlein et al., 2011). The intention behind this exaggeration was to capture the extreme case and make sure that I get a very “green” Sahara. The technique to add P to the domain does not realistically

capture the changes in P patterns for the mid-Holocene induced by changes in orbital forcing. Reconstructions indicate that P did not increase homogeneously all over north Africa, but suggest a northward shift of the rain belt, leaving southern areas relatively dry compared to today (Hély et al., 2014; Shanahan et al., 2015). This implies changes in seasonality of rainfall which affect the length of the growing season and the duration of water availability.

Although P seems to be the main determinant of plant growth in the study domain on the considered scale of the order of 100 km² (Coughenour & Ellis, 1993), the prescription of only P changes implies several limitations. Leaving other atmospheric variables such as specific air humidity, temperature, and greenhouse gasses unchanged can affect the model outcome especially regarding fire intensity and frequency, and plant productivity.

Numerous studies highlighted the importance of fire as a determinant of tree-grass co-existence in savanna ecosystems (e.g. Scholes & Archer, 1997; Jeltsch et al., 2000; House et al., 2003; Sankaran et al., 2004, 2005). For wildfires to happen in JSBACH, sufficient above ground plant litter has to be available for combustion, and the litter needs to be sufficiently dry, meaning below a threshold, to catch fire. Fire disturbance rate is assumed to increase linearly with decreasing humidity, and depends on the extent of woody types w and grasses g via the value of the above ground litter obtained from the cover fractions c_i (Reick et al., 2013). Since air humidity remains unchanged despite high P , litter dryness reaches the threshold more likely and fire ignition might be over-estimated. On the other hand, the resulting underestimation of tree cover might cause a lack of litter which in turn might underestimate fire. Recently, the process-based SPIT-FIRE model (Thonicke et al., 2010; Lasslop et al., 2014) was implemented in JSBACH and a study on fire-vegetation feedback showed that multiple stable states of tree cover could occur in the transition zones between grasslands and forests in Africa (Lasslop et al., 2016). At the time I performed the simulations for this thesis, only the simple fire algorithm (Reick et al., 2013) was available and evaluated for simulations with dynamic vegetation. For future studies on plant diversity and vegetation dynamics in semi-arid regions, I highly recommend to use SPITFIRE.

Temperatures during the AHP were about 3 to 5 °C higher in summer and 1 to 4 °C cooler in winter compared to present day in north Africa (Wu et al., 2007). Temperatures

in the forcing data set are generally in a range that favours growth of tropical and subtropical PFTs in the southern part of the study domain, but reach the bioclimatic limits for tropical PFTs thereby excluding them from growing north of 18° N. Enhancement of P and related evaporation would naturally cause a surface cooling which reduces respiration and increases the NPP due to the temperature dependence of the photosynthesis (Reick et al., 2014). This cooling was not considered in this model set up. However, model studies on “greening the desert” with irrigated plantations in Oman (Groner, 2013; Wulfmeyer et al., 2014), Israel (Branch et al., 2014), and Sonora (Wulfmeyer et al., 2014) showed that the cooling effect is small on daily average (1 to 2 K) but can be large during nighttime (up to 5 K). Since these studies assumed tropical tree cover, NPP might be only slightly underestimated in this “savanna” study.

Greenhouse gas concentrations in the atmosphere affect the radiation balance and therefore the surface energy balance (greenhouse effect). This effect vanishes in offline simulations since atmospheric variables are prescribed. However, CO_2 concentrations also affect the productivity of vegetation and the competition between C3 and C4 PFTs. High CO_2 concentrations have a fertilization effect on vegetation and favor C3 plants, see e.g. Körner et al. (2007) for a review. At low CO_2 concentrations, C4 plants have an advantage over C3 plants due to their superior water use efficiency (see e.g. Black et al., 1969; Ehleringer et al., 1991). At 6 k, CO_2 concentrations were on average 20 ppm lower than at 0 k (Joos, 2016) which implies that plant productivity might be overestimated in the presented simulations and the ratio between C3 and C4 plants might be shifted in favor of C3 vegetation.

Another shortcoming is that the soil map in JSBACH was initially not adjusted to AHP but reflected present day conditions. Due to lack of paleosol data, I was obliged to assume that the soil characteristics have not changed during the considered period. Soils in the present day Sahara have a very low water holding capacity making growth difficult for PFTs with high moisture requirements even though provided precipitation is sufficient. Given a higher availability of paleosol data, the consideration of soil reconstructions to create model input could partly solve this problem, but points straight to a further limitation: the non-dynamic handling of physical land/soil characteristics (discussed in more detail later on in Sec. 3.5).

2.4 Summary and Conclusions

In summary, the PFT set in JSBACH – designed for global application – has only a limited applicability for detailed studies on the role of plant diversity in subtropical semi-arid regions. The main advantages of the PFT concept are its simplicity, its large scale to global applicability, and its reasonable reproduction of the global biome distribution, also in fully coupled simulations with GCMs (Scheiter et al., 2013). The main disadvantages of the PFT concept arise from oversimplification due to limited computational resources and the lack of data and theory: loss of information with discrete PFT classification, limited set of plant attributes to define a limited number of mostly static PFTs that seldom account for plasticity in plant traits along geographic and environmental gradients, limited representation of (especially) sub-/tropical plant diversity, and the poor representation of sub-grid ecological interaction and competition in terms of age stages, roots, light, nutrients, and others (Fisher et al., 2010; Scheiter et al., 2013). Effects emerging from local plant diversity in a plants' neighborhood can only implicitly be assumed, JSBACH does not explicitly capture competing or facilitating interactions of neighboring plants and PFTs have no geographically explicit growth area in a grid cell. Since most DGVMs are not designed for tropical systems (House et al., 2003) and do not include internal feedbacks of these biomes (Moncrieff et al., 2013), these models display high uncertainty in predicting vegetation for the forest, savanna, and grassland biomes due to the complexity of tree grass coexistence (Bonan et al., 2003; Hély et al., 2006; Baudena et al., 2015). Another large uncertainty arises from the assumption of a static relation between species distribution and environmental variables, typically climate variables, over time. In comparison to other DGVMs, JSBACH has a simple representation of ecosystem processes and a limited number of interactions are implemented.

The attempt to compare the PFT concept in JSBACH with the conceptual approach in Chapter 1 faced several problems due to large discrepancies, especially in the spatial dimension (E-space vs. G-space) and the consideration of plant diversity. The conceptual model described in Chapter 1 deals with plant diversity as a mixture of phytochoria composed of several vegetation types within a region in the order of a GCM grid cell. These vegetation types include regional variations of functional types (Guineo–Congolian tree, Sudanian tree, Sahelian grass, Saharan grass, ...). JSBACH deals with plant diversity

between grid cells and determines vegetation types composed of PFTs, which are homogeneous for all regions. The AHP plant types of the conceptual model described in Chapter 1 can further not directly be compared to the PFTs in JSBACH because their definition is based on discrete precipitation thresholds that are not explicitly implemented in JSBACH. Some functional plant groups characteristic for Africa do not find corresponding PFTs in JSBACH such as perennial grasses, subtropical evergreen shrubs or monsoon forest trees. Thus, JSBACH is not capable to capture AHP plant types in terms of moisture requirements, species diversity or ratios between physiognomic types after White (1983), and cannot depict mosaic-like environments as reconstructed from pollen by Hély et al. (2014).

However, as a process-based model JSBACH provides a range of features that allow for basic studies on range shifts and plant responses to decreasing precipitation as a function of plant diversity. Offline simulations with different PFT combinations showed that the expansion of veg_{max} with high P at the beginning of the simulations as well as the slope of vegetation retreat differed between single-PFT and multi-PFT simulations. The initial composition of vegetation was mainly determined by bioclimatic limits, the prevailing P regime and competition via growth form and by productivity. In absence of disturbance, woody PFTs (trees and shrubs) were dominant (light competition) over grasses. After disturbances, grasses had an advantage because they quickly migrated in the new open space while trees and shrubs grew more slowly. Within the woody PFTs, competition was regulated by productivity: higher net primary productivity implied a competitive advantage if no other aspects such as growth form were dominating. Similar to the initial cover, the slope of vegetation decline was determined by the ratio of involved PFTs and their properties. Their productivities under the new given P conditions and their establishment/mortality time scales shaped the slope. In a single-PFT simulation with only C4 Grass, vegetation responded non-linearly, retreating faster than the prescribed P decline. Multi-PFT simulations showed that the rate of transition did not necessarily decrease with the number of PFTs: Whether PFTs were stronger (wider expansion and longer persistence) or weaker (less expansion, shorter persistence) when plant diversity increased finally depended on their combination and individual productivities per area. The more productive a PFT was under the given conditions, the larger was the grid cell fraction covered by this PFT, and the stronger its weight in the calculation of veg_{max} . In high plant diversity experiments (8 or 58 PFTs), the replacement of retreating PFTs by

others that grew better under new conditions smoothed on the decline of mean veg_{max} , comparable to the niche approach in Chapter 1. Fast retreats of individual PFTs were buffered before the final breakdown. On the other hand, competition via differences in growth form and productivity weakened individual PFTs and limited their expansion and persistence in multi-PFT simulations. This supported the outcome of Chapter 1. So did the regional differences in vegetation decline attributed to PFT composition. In most regions, the response to P decline was driven by $C4$ having the largest share of veg_{max} . If present, SRG acted as desert promoter.

One elementary aspect of the conceptual model in Chapter 1 could not be observed in offline JSBACH simulations: the effect emerging from feedbacks between vegetation and the atmosphere. The presented study only considered how plant diversity influences the vegetation response to a prescribed precipitation regime, but to understand how precipitation is in turn affected by the diversity of vegetation cover and how the interaction between terrestrial biosphere and atmosphere could have affected the stability of the “green” Sahara and the transition to the “desert” state, simulations with a coupled land-atmosphere model and different degrees of plant diversity are indispensable.

In conclusion, this chapter highlighted that JSBACH is not capable to capture AHP plant types in terms of moisture requirements, species diversity and ratios between physiognomic types after White (1983), and cannot depict mosaic-like environments and gallery forests as reconstructed from pollen by Hély et al. (2014). However, despite large differences in the underlying assumptions, JSBACH as a process-based model qualitatively reproduced the results from the conceptual model in Chapter 1 therewith substantiating the conclusions supported by ecological literature: high plant diversity could have a buffering effect on mean vegetation cover when precipitation decreases while plant composition plays a crucial role for the climate–vegetation system stability.

Chapter 3

Effects of plant diversity on simulated climate–vegetation interaction towards the end of the African Humid Period

3.1 Introduction

The main source of precipitation in the Sahel region is the West African Monsoon (WAM), an atmospheric phenomenon characterized as a pronounced seasonal wind shift induced by thermodynamic contrasts between the land (i.e., the Sahara) and ocean (i.e., the equatorial Atlantic) (Nicholson, 2013). The classic picture of the WAM associated rainfall in the Sahel with the position of the InterTropical Convergence Zone (ITCZ); rain production was assumed to result from local thermal instability, facilitated by the low-level wind convergence within the ITCZ (see e.g. Griffiths, 1972). The term “ITCZ” is ambiguous since literature provides very different definitions based on wind convergence, surface air pressure and rainfall or outgoing longwave radiation. Hereinafter, I refer to the ITCZ as the surface feature over the African continent that marks the convergence of northeasterly Harmattan winds that originate in the Sahara and the southwest monsoon flow that emanates from the Atlantic, also named InnerTropical Front (ITF).

A revised picture of the WAM diminishes the importance of the ITCZ for Sahelian rainfall, but suggests that the intensity, extent and variability of rainfall result from a complex interplay of a number of atmospheric features: the upper-level Tropical Easterly Jet (TEJ), the mid-level African Easterly Jet (AEJ), low-level equatorial westerlies associated with the southwest monsoon flow (LLW), African Easterly Waves (AEW), and the Saharan Heat Low (SHL) (Nicholson, 2009, 2013). Superimposed upon the zonal flows are two meridional overturning circulations: a deep circulation associated with low-level contrasts in deep moist convection and a shallow circulation associated with contrasts in dry convection (Thorncroft et al., 2011). Fig. 3.1 provides a schematic overview over the WAM system.

The WAM includes two areas of peak moisture flux and vertical motion (Nicholson, 2008; Thorncroft et al., 2011). The first one is located between the AEJ and TEJ and is associated with the core of the tropical rain belt (Nicholson & Grist, 2003). It also corresponds to the southerly track of AEW (Nicholson, 2013). The second area is located around 8° polewards of the rainfall maximum and coincides with the ITCZ. This area is associated with the SHL (Thorncroft et al., 2011) and corresponds to the northerly track of AEW (Nicholson, 2013). Here, convergence is not strong enough to induce convection.

The two regions are separated by a region of large scale subsidence: the Sahara. In addition to the large scale subsidence, the radiative cooling above the bright, nearly cloud-free desert is compensated by adiabatic warming of descending air-masses which further suppresses convection and rain formation. Therewith, the ITCZ and the tropical rain belt are effectively decoupled in the revised picture of the WAM (Nicholson, 2013). A detailed review on the aforementioned features, their variability and interactions as well as the consequences for rainfall is given by Nicholson (2013). A general observation is that wetter years in the Sahel are linked

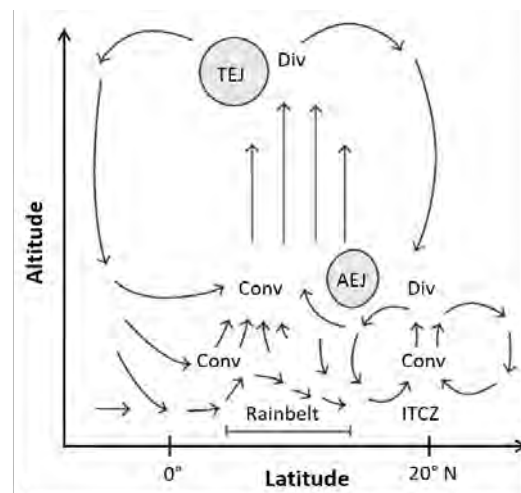


FIGURE 3.1: Schematic view of the West African Monsoon including some of its key features: the upper-level Tropical Easterly Jet (TEJ), the mid-level African Easterly Jet (AEJ), the InnerTropical Convergence Zone (ITCZ) and the position of the tropical rain belt (adjusted from Nicholson (2009)).

to a weaker and northward shifted AEJ (Nicholson & Grist, 2003; Nicholson, 2013), a stronger TEJ (Grist & Nicholson, 2001; Jenkins et al., 2005; Nicholson, 2008; Hulme & Tosdevin, 1989), and a stronger SHL (Parker et al., 2005; Lavaysse et al., 2010). Dryer years are in contrast linked to a stronger and southward shifted AEJ, a weaker TEJ, and a weaker SHL. The latitudinal position of the TEJ core varies little from year to year, while the AEJ shows a considerable intra- and inter-annual variability (Nicholson, 2008, 2013). Overall, the shape of the meridional temperature and moisture gradient between the equator and the northern Tropics is a good indicator of how far north the monsoon flow penetrates into Africa (Bonfils et al., 2001).

On longer timescales, the intensity and northward extent of the WAM are affected by changes in orbital forcing. One prominent example is the African Humid Period (AHP), an era when changes in the Earth's orbit led to a stronger insolation and higher temperatures in the boreal summer resulting in an intensification of the WAM (Kutzbach, 1981; Kutzbach & Guetter, 1986) accompanied by a "greening" of the Sahara (Ritchie & Haynes, 1987; Jolly et al., 1998; Watrin et al., 2009; Hély et al., 2014). However, modelling studies showed that the increase in insolation alone is insufficient to explain the rainfall necessary to sustain the vegetation coverage reconstructed from palaeo records (see Yu & Harrison, 1996). It has been demonstrated that a positive climate–vegetation feedback could have amplified the effects of orbital forcing via albedo (Claussen & Gayler, 1997; Claussen, 2009) or evapotranspiration (Rachmayani et al., 2015) anomalies. Because the atmosphere is instantly coupled to the land surface through the exchange of energy, momentum, water, and trace gases such as carbon dioxide, changes in land surface properties alter the atmospheric circulation and consequently the location and intensity of rainfall. Following the hypothesis of a positive climate–vegetation feedback, the effect of vegetation on climate can be explained by the following mechanism (Kleidon et al., 2000): the lower albedo of vegetation relative to bare soil enhances the absorption of solar energy available for evapotranspiration which accelerates energy and water cycling. Vegetation has access to water from deeper soil layers which increases the amount of water available for evapotranspiration compared to soil evaporation only. Further the leaf area of vegetation provides an area for interception water that can be directly evaporated and is not lost to runoff. Those factors together boost moisture available in the atmosphere. The enhanced evapotranspiration leads to high latent heat flux which can – if strong enough – cool the surface and compensate the excess absorbed solar

energy. Cooler temperatures reduce the atmospheric demand for evapotranspiration and consequently water stress. The higher surface roughness of vegetation compared to bare soil strengthens turbulent fluxes of heat, water and momentum. Stronger turbulent fluxes extend the planetary boundary height and atmospheric instability, and therewith the likelihood of reaching the lifting condensation level and the initiation of convection (Adler et al., 2011; Wulfmeyer et al., 2014). Those factors together increase the probability of rain events and thereby the amount of precipitation. The concurrently increasing cloud cover counteracts this mechanism by reducing the amount of solar radiation reaching the surface. Large scale changes of vegetation cover alter the meridional temperature and moisture gradient between the equator and the northern Tropics which affects the position of the ITCZ and the AEJ, and consequently the position and intensity of the tropical rain belt.

This positive climate–vegetation feedback provides a mechanism that might allow for the existence of multiple stable equilibria in north Africa, namely a “green” state with high vegetation cover and a “desert” state without vegetation (Brovkin et al., 1998; Bathiany et al., 2012). The potential non-linearity of this feedback might cause an abrupt transition between these states when the system reaches a “tipping point” (Williams et al., 2011). Over the last decades, there have been several model studies on climate–vegetation interaction towards the end of the AHP in north Africa. Studies ranged from models of intermediate complexity (Texier et al., 1997; Claussen & Gayler, 1997; Claussen et al., 1999; Jolly et al., 1998; Prentice & Jolly, 2000; de Noblet-Ducoudré et al., 2000; Renssen et al., 2003, 2006) to General Circulation Models (GCMs) coupled with Dynamic Global Vegetation Models (DGVMs) (Doherty et al., 2000; Bonan et al., 2003; Liu et al., 2007; Notaro et al., 2008; Hély et al., 2009; Baudena et al., 2015; Rachmayani et al., 2015). Some studies indicated an abrupt collapse of vegetation associated with a strong climate–vegetation feedback at the end of the AHP, while others suggested a gradual decline or attributed the collapse to other triggers.

However, none of the aforementioned studies took the role of plant diversity explicitly into account. It is worth considering plant diversity in the context of climate–vegetation system stability because ecologists nowadays agree that diversity might on average increase the stability of ecosystem functioning (McCann, 2000; Scherer-Lorenzen, 2005), in particular under changing environmental conditions. Conceptual modelling studies showed that high plant diversity can further stabilize the climate–vegetation system in

semi-arid regions when precipitation decreases due to external forcing (Claussen et al. (2013), Chapter 1).

Thus, it remains an open question how the diversity of Plant Functional Types (PFTs) in a comprehensive land surface model like JSBACH affects the simulated interaction between terrestrial biosphere and atmosphere and therewith the stability of the “green” Sahara and the transition to the “desert” state. To address this question, I perform coupled simulations with different degrees of diversity for a series of time slices between mid-Holocene and preindustrial using ECHAM6/JSBACH which is part of the Earth System Model MPI-ESM1.

In the first section, I briefly introduce the model MPI-ESM1 and summarize the set ups for the series of performed simulations.

Second, I consider simulations with different PFT combinations for mid-Holocene conditions (8 ky = 8000 years before present) to discuss the potential effects of PFT diversity on the extent of the “green” Sahara as well as on climate–vegetation interaction during the AHP. The analysis focuses on changes in land surface parameters, hydrological cycle, surface energy budget, and atmospheric circulation patterns.

In the third section, I look into differences between consecutive time slices between 8 ky and 0 ky for all simulations with different PFT combinations to estimate the effect of PFT diversity on the timing and rate of transition from the “green” Sahara to the “desert” state.

3.2 Model set up

3.2.1 MPI-ESM1

MPI-ESM1 is a comprehensive Earth System Model that couples model components for the atmosphere (ECHAM6, Stevens et al. (2013)), ocean (MPIOM, Jungclaus et al. (2013)) and land surface (JSBACH, Raddatz et al. (2007); Reick et al. (2013)) through the exchange of energy, momentum, water and important trace gases such as CO₂. This study focuses only on the coupling between the atmospheric component and the land surface component in simulations with an atmosphere-land version of MPI-ESM1.

ECHAM6 is an atmospheric General Circulation Model (GCM) which was developed at the Max Planck Institute for Meteorology (MPI-M) in Hamburg, Germany. The model focuses on the coupling between diabatic processes and large-scale circulations which are both driven by solar insolation. For each time step the model determines the large-scale horizontal circulation with a spectral hydrostatic dynamical core. Additionally, other physical processes (turbulent diffusion, convection, clouds, precipitation, gravity wave drag, diabatic heating by radiation) are calculated for each vertical column of the Gaussian grid associated with the truncation used in the spectral dynamical core. These processes are coupled with the horizontal circulation each time step by transforming the variables representing the atmospheric state from the spectral representation to the Gaussian grid and back. Radiative transfer is computed extensively only once per hour for solar radiation (14 bands) as well as terrestrial radiation (16 bands).

As integral component of ECHAM6, JSBACH provides the lower atmospheric boundary conditions over land as well as biogeochemical and biogeophysical degrees of freedom that arise from terrestrial processes. JSBACH simulates land-surface properties interactively in terms of soil moisture, snow cover, leaf area index, and vegetation distribution. Natural land cover change and vegetation dynamics are simulated in JSBACH by the DYNVEG component, described in Chapter 2.

3.2.2 Set up of simulations

I perform global coupled land-atmosphere simulations with a horizontal resolution of approximately 1.88° (T63) and 47 vertical levels. ECHAM6/JSBACH runs with dynamic vegetation for the periods 8 ky, 6 ky, 4 ky, 2 ky, and 0 ky for 300 years with the first 200 years corresponding to the spinup period; the first 100 years of the spin up period run with accelerated vegetation dynamics. In the standard JSBACH configuration, the seasonal canopy albedo is calculated as a function of leaf area index, whereas the background albedo is a grid cell constant derived from satellite measurements. To account for darker soils below vegetation, I implement for the study domain (12 to 34° N, -15 to 40° E, see Fig. 2.1) a simple albedo-scheme that reduces the soil albedo according to the mean net primary productivity of the preceding five years (Zink, 2014). Soil properties originate from the FAO digital soil map of the world (FAO/UNESCO, 1974). Due to lack of palaeo soil data, I am obliged to assume that the soil characteristics

remain constant during the considered period. To attain equilibrium states, I set orbital parameters (Berger, 1978) and CO₂ concentrations (Joos, 2016) to fixed values for each time slice experiment, see Tab. 3.1. Other atmospheric boundary conditions (trace gas concentrations, aerosol distribution, spectral solar irradiance, orography) remain unchanged over time. Moreover, I prescribe sea ice concentration (SIC) and sea surface temperatures (SST) identically for all simulations with forcing data from Hurrell et al. (2008). In order to provide SIC and SST associated with relatively wet years, I select the years from 1945 to 1974 to force the model cyclically.

TABLE 3.1: CO₂ concentrations (in ppm) and orbital parameters for simulated time slices at 8 ky, 6 ky, 4 ky, 2 ky, and 0 ky. For palaeo simulations, CO₂ concentrations are taken from Joos (2016) and orbital parameters are adjusted according to Berger (1978). The values for 0 ky conform to the standard preindustrial set up of MPI-ESM1.

time slice	CO ₂ [ppm]	eccentricity [-]	obliquity [-]	longitude of perihelion [°]
8 ky	259.9	0.019101	24.209	148.58
6 ky	264.6	0.01867	24.101	181.75
4 ky	273.2	0.018123	23.922	215.18
2 ky	277.6	0.017466	23.694	248.93
0 ky	284.725	0.016704	23.44	283.01

The model runs with three different types of simulations for each time slice: as a baseline serves the simulation *EXP_{ALL}* with all natural PFTs commonly used in JSBACH (Tropical Evergreen Tree (*TE*), Tropical Deciduous Tree (*TD*), Extratropical Evergreen Tree (*eTE*), Extratropical Deciduous Tree (*eTD*), Shrub Raingreen (*SRG*), Shrub Deciduous (*SD*), C3 Grass (*C3*), C4 Grass (*C4*)), see Tab. 2.1. The second type of simulation is a single-PFT experiment *EXP_{C4}* excluding all woody PFTs and their competition in the study domain. Third, I add again a single woody PFT to *C4* in the study domain for the experiments *EXP_{TE,C4}* and *EXP_{SRG,C4}*. In all simulations, the initial cover fractions are equally distributed over all included PFTs in the study domain. Due to limited computational resources, I waive a coupled high plant diversity experiment as presented in Chapter 2.

With the described set up, I do not expect simulations to match reconstructions (see Sec. 3.5 for the discussion of limitations). Rather I focus on qualitative differences between simulations to find mechanisms relevant in terms PFT diversity affecting climate-vegetation interaction.

3.3 Effects of PFT diversity on climate–vegetation interaction during the AHP

3.3.1 Results

PFT diversity and composition significantly affect climate–vegetation interaction during the AHP thereby altering land surface and atmospheric conditions, and eventually the extent of the “green” Sahara. In the following, I present simulated effects on land surface parameters, energy surface budget, hydrological cycle, atmospheric circulation patterns, and on the relationship between vegetation cover and precipitation for 8 ky equilibrium conditions. Fig. 3.2 exemplarily illustrates difference patterns between the performed simulations for precipitation P and vegetation cover fraction veg_{max} highlighting the two most affected regions: the transition zone between desert and savanna (Region 1, 18 to 22° N, 5 to 30° E) and the region southwest of the transition zone (Region 2, 12 to 18° N, -15 to 20° E).

For the quantitative analysis of PFT diversity effects on land surface parameters, I focus on the aforementioned two most affected regions. Tab. 3.2 summarizes 100-year spatial averages in the two regions for EXP_{ALL} as well as differences to the other simulations for the land surface parameters vegetation cover fraction veg_{max} , leaf area index LAI , albedo α , and surface roughness length z_0 .

In Region 1, EXP_{ALL} depicts a steppe-like vegetation cover (White, 1983) composed of $C4$ and SRG with an average veg_{max} of 0.4 and a leaf area index LAI of $1.33 \text{ m}^2 \text{ m}^{-2}$. Due to the sparse and low vegetation cover, $\alpha=0.28$ is relatively high – α of bare desert soil typically amounts to 0.38 whereas forests reach typically values of 0.18 – and $z_0=0.08 \text{ m}$ is small. The exclusion of woody PFTs in EXP_{C4} causes a strong “greening” compared to EXP_{ALL} . veg_{max} more than doubles while LAI increases by only 13%, thus the canopy enlarges mainly horizontally. The “greening” is accompanied by a significant reduction of α and z_0 . $EXP_{TE,C4}$ shows a response similar to EXP_{C4} in terms of “greening” but the magnitude is lower. veg_{max} expands by around 85% while changes in LAI are not significant. This indicates that the canopy enlarges horizontally but not vertically. Similar to EXP_{C4} , α significantly decreases, here by 21%, but other than in EXP_{C4} , z_0 strongly increases, here by 43%. In contrast, $EXP_{SRG,C4}$ exhibits a “browning” compared to EXP_{ALL} . The reduction of veg_{max} by 30% goes in conjunction

	EXP_{ALL}		ΔEXP_{C4}		$\Delta EXP_{TE,C4}$		$\Delta EXP_{SRG,C4}$	
	Region 1	Region 2	Region 1	Region 2	Region 1	Region 2	Region 1	Region 2
<i>Land surface parameters</i>								
Vegetation cover fraction [-]	0.40(0.22)	0.98(0.04)	0.44 (0.21)	0.02 (0.04)	0.34 (0.21)	0.01 (0.04)	-0.12 (0.13)	-0.40 (0.08)
Leaf area index [$\text{m}^2(\text{leaf}) \text{m}^{-2}(\text{canopy})$]	1.33(0.43)	3.00(0.7)	0.18 (0.33)	-0.43 (0.38)	0.03(0.32)	0.02(0.04)	-0.30 (0.17)	-1.11 (0.57)
Albedo [-]	0.28(0.07)	0.17(0.01)	-0.07 (0.06)	0.02 (0.01)	-0.06 (0.05)	-0.001 (0.001)	0.03 (0.04)	0.01 (0.02)
Roughness length [m]	0.08(0.07)	1.32(0.69)	-0.03 (0.07)	-1.24 (0.68)	0.03 (0.09)	0.07 (0.09)	-0.04 (0.06)	-1.19 (0.64)
<i>Surface energy budget</i>								
Solar net radiation [W m^{-2}]	275.26(14.03)	289.79(3.95)	12.33 (12.00)	-2.62 (1.46)	10.78 (10.37)	0.005(0.34)	-4.76 (7.24)	1.11 (4.24)
Sensible heat flux [W m^{-2}]	61.88(10.55)	47.18(17.15)	6.38 (11.00)	-1.36 (3.82)	7.17 (9.10)	-0.32(0.68)	-3.77 (6.26)	2.54 (5.23)
Latent heat flux [W m^{-2}]	20.07(7.88)	70.12(22.70)	5.21 (2.88)	-6.27 (4.75)	2.17 (2.29)	0.53(0.88)	-4.31 (2.74)	-7.63 (3.72)
2 m temperature [$^{\circ}\text{C}$]	24.95(1.54)	26.21(1.42)	0.46 (0.28)	0.47 (0.21)	0.50 (0.29)	0.04(0.07)	-0.07(0.11)	0.73 (0.28)
Cloud cover [-]	0.35(0.04)	0.53(0.06)	0.01(0.002)	-0.02 (0.01)	0.003(0.002)	-0.002(0.004)	-0.02 (0.003)	-0.03 (0.003)
<i>Hydrological cycle</i>								
Precipitation [mm yr^{-1}]	275.58(104.64)	1140.86(352.69)	84.87 (34.72)	-76.19 (83.79)	35.24 (28.97)	24.81(17.03)	-56.11 (33.16)	-110.25 (45.96)
Evapotranspiration [mm yr^{-1}]	253.31(99.45)	884.82(286.44)	65.76 (36.30)	-79.16 (59.91)	27.50 (28.84)	6.69(11.10)	-54.33 (34.55)	-96.23 (46.88)
Integrated water vapor [kg m^{-2}]	20.49(1.86)	32.62(3.52)	0.62 (0.09)	-0.40 (0.47)	0.09(0.08)	0.09(0.09)	-0.95 (0.24)	-1.40 (0.16)

TABLE 3.2: Effects of different PFT compositions on land surface parameters, surface energy budget, and hydrological cycle in coupled ECHAM6/JSBACH simulations in Region 1 (18 to 22° N, 5 to 30° E) and Region 2 (12 to 18° N, -15 to 20° E). The first two columns contain 100-year averages of the experiment with the standard PFT set EXP_{ALL} , the following show differences between EXP_{ALL} and simulations with modified PFT composition (Tropical Evergreen Tree TE , Raingreen Shrub SRG , C4 Grass $C4$). Bold values are significant ($\sigma = 0.05$) with regard to the time series of 100 years (yearly averages), values in brackets correspond to spatial standard deviations of difference fields.

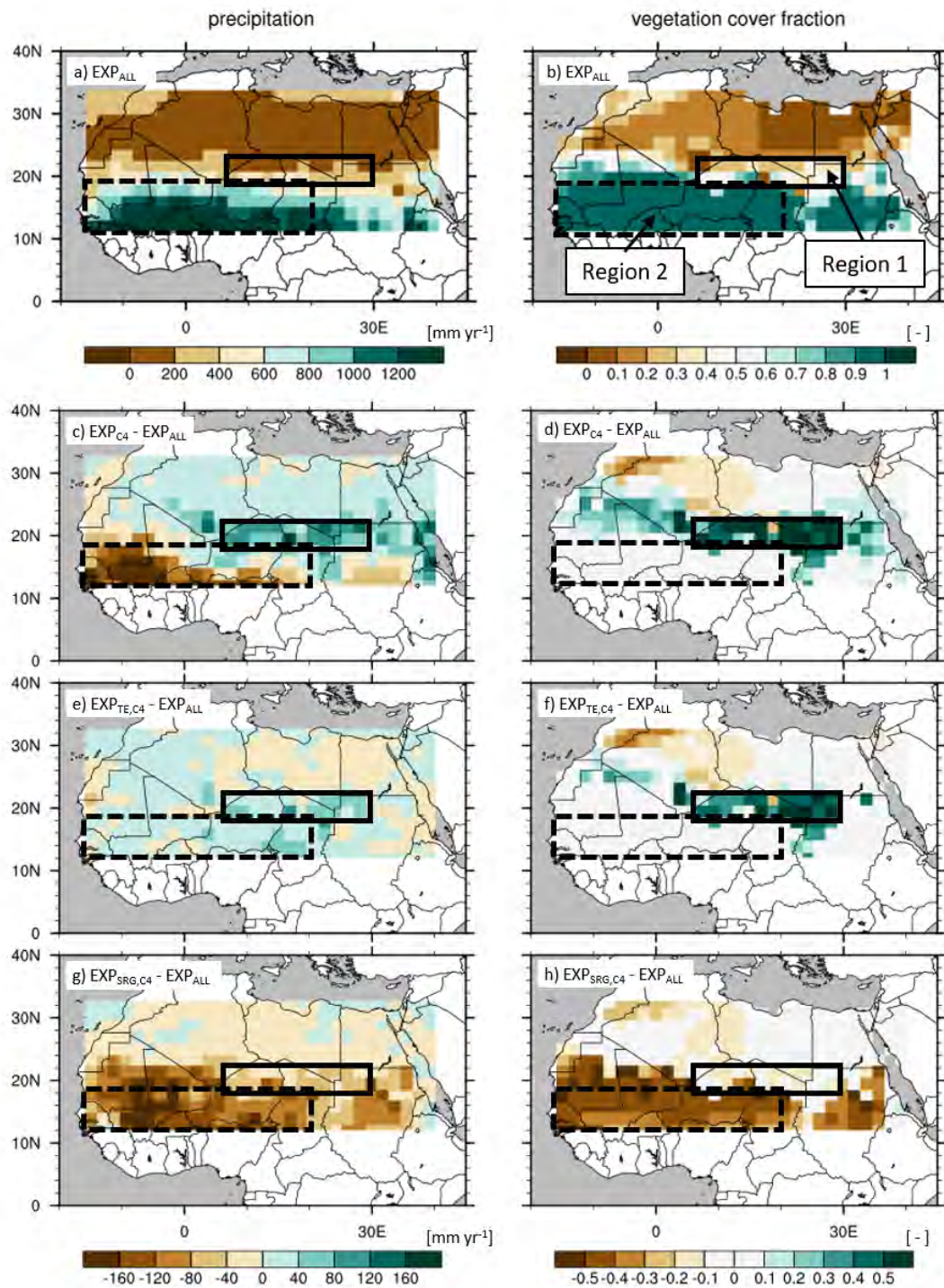


FIGURE 3.2: Effects of different PFT compositions on precipitation P (left column) and vegetation cover fraction veg_{max} (right column) at 8 ky in Region 1 (18 to 22° N, 5 to 30° E, solid box) and Region 2 (12 to 18° N, -15 to 20° E, dashed box). Panels (a, b) show 100-year averages for the experiment EXP_{ALL} with the standard PFT set up. The following panels illustrate differences in 100-year averages between EXP_{ALL} and EXP_{C4} (c, d), $EXP_{TE,C4}$ (e, f), and $EXP_{SRG,C4}$ (g, h).

with a reduction of LAI . The diminished vegetation, vertically and horizontally, is accompanied by a significant increase of α (12%) and a drastic reduction of z_0 by more than 60%.

In Region 2, EXP_{ALL} depicts a vegetation cover that can be categorized as open woodland/woodland (White, 1983). veg_{max} achieves almost 1.0 and is composed of 30 to 60% TE and 40 to 70% $C4$ respectively. Vegetation reaches on average a LAI of $3.0 \text{ m}^2 \text{ m}^{-2}$ accompanied by a lower α and a higher z_0 than in Region 1. In EXP_{C4} , veg_{max} is about 5% higher than in EXP_{ALL} , but the exclusion of woody PFTs translates into a reduction of LAI and α by more than 10% together with a radical decrease of z_0 by more than 90%. $EXP_{TE,C4}$ exhibits moderate differences to EXP_{ALL} . veg_{max} expands by 2%, leading to a slightly lower α and an increase of z_0 by around 5%. $EXP_{SRG,C4}$ shows similar to Region 1 a “browning” compared to EXP_{ALL} . The retreat of veg_{max} by 40% coincides with a decline of LAI indicating a vertical and horizontal canopy reduction. α slightly increases while z_0 drastically decreases by more than 90%.

As described in the introduction, changes in land surface parameters are expected to translate into changes in the energy surface budget. In order to detect these changes in the energy surface budget, I analyse 100-year spatial averages in the two aforementioned regions for EXP_{ALL} as well as differences to the other simulations for solar net radiation $S \downarrow_{net}$, sensible heat flux SH , latent heat flux LH , 2 m temperature T_{2m} , and integrated cloud cover CC , see Tab. 3.2.

In Region 1 in EXP_{ALL} , $S \downarrow_{net}$ amounts to 275 W m^{-2} and the Bowen ratio $\beta = SH/LH$ is 3.08 indicating that SH is around three times higher than LH . The cloud cover CC is low (0.35) and T_{2m} reaches on average $24.95 \text{ }^\circ\text{C}$. EXP_{C4} depicts an acceleration of energy cycling. $S \downarrow_{net}$ intensifies by 12.33 W m^{-2} and β slightly drops to 2.7 due to the relative decrease of SH accompanied by a warming of around 0.5 K. Changes in CC are not significant. In $EXP_{TE,C4}$, $S \downarrow_{net}$ intensifies by around 10.79 W m^{-2} while β remains very similar to EXP_{ALL} . T_{2m} is 0.5 K higher than in EXP_{ALL} and differences in CC are not significant. In contrast, energy cycling slows down in $EXP_{SRG,C4}$. $S \downarrow_{net}$ decreases by around 4.76 W m^{-2} and β rises to 3.69 which implies an increase of SH . Differences in T_{2m} are not significant, but CC declines significantly.

In Region 2, $S \downarrow_{net}$ amounts in EXP_{ALL} to almost 290 W m^{-2} and is therewith 25 W m^{-2} higher than in Region 1. β is much lower than in Region 1 with an average value of

0.67 because LH exceeds SH here. T_{2m} is more than 1 °C higher than in Region 1 reaching on average 26.21 °C. CC is around 50% higher than in Region 1. In EXP_{C4} , $S \downarrow_{net}$ slightly decreases while β rises due to the relative increase of SH accompanied by a warming of around 0.5 K and a significant CC reduction. $EXP_{TE,C4}$ exhibits no significant changes in Region 2. Just as in EXP_{C4} , $S \downarrow_{net}$ intensifies slightly in $EXP_{SRG,C4}$ and β slightly rises due to the relative increase of SH , here accompanied by a warming of around 0.7 K and a significant reduction of CC .

Land surface parameters and surface energy budget are closely linked to the hydrological cycle, and changes in vegetation cover are assumed to alter precipitation through feedbacks described in the introduction. Just as in the previous sections, I start the analysis of PFT diversity effects on the hydrological cycle considering 100-year spatial averages in the aforementioned two most affected regions. Tab. 3.2 summarizes values in the two regions for EXP_{ALL} and differences to the other simulations for precipitation P , evapotranspiration ET , and integrated water vapor IWV .

In Region 1 in EXP_{ALL} , P reaches on average around 280 mm yr⁻¹, evapotranspiration ET lies a similar range. The average integrated water vapor IWV amounts to 20.49 kg m². This rainfall regime is nowadays associated with the Sahelian/Sudanian type (Hély et al., 2014), thus simulated P is in agreement with the simulated steppe-like vegetation. The exclusion of woody PFTs in EXP_{C4} shows a significant intensification of water cycling compared to EXP_{ALL} . P and ET rise by around 30%, whereas IWV increases only slightly. In $EXP_{TE,C4}$, P and ET rise by around 10% with no significant changes in IWV . By contrast, P and ET diminish in $EXP_{SRG,C4}$ by around 20% and IWV drops significantly.

In Region 2, P amounts in EXP_{ALL} on average to around 1140 mm yr⁻¹ and exceeds ET by nearly 25%. This is accompanied by a moist atmosphere with IWV of 32.62 kg m². Nowadays, this rainfall regime is associated with the Sudanian/Guineo–Congolian type (Hély et al., 2014), thus simulated P is in agreement with the simulated woodland vegetation in this region. EXP_{C4} exhibits here effects different from Region 1: although veg_{max} is slightly higher than in EXP_{ALL} , P and ET significantly diminish reaching only 90% of EXP_{ALL} , and the atmosphere holds less water. $EXP_{TE,C4}$ exhibits in Region 2 no significant effects on water cycling compared to EXP_{ALL} which reflects the moderate differences in land surface parameters and surface energy budget. In

$EXP_{SRG,C4}$, water cycling slows down with P and ET dropping by more than 10% accompanied by a significant reduction of IWV .

A closer look into the 100-year average annual cycles of P in Fig. 3.3 illustrates that differences in P have different causes in the two regions. In Region 1, the difference can be attributed to different rainfall intensities, especially at the peak in August, while the timing of onset, peak and duration of the monsoon are almost identical in all simulations (Fig. 3.3a). In Region 2, not only the intensity of rainfall but also the duration of the monsoon peak are affected by alterations in PFT diversity. In EXP_{ALL} and $EXP_{TE,C4}$, the peak of the monsoon season lasts 2 months (August and September) while P starts to decline in EXP_{C4} and $EXP_{SRG,C4}$ already in September (Fig. 3.3b).

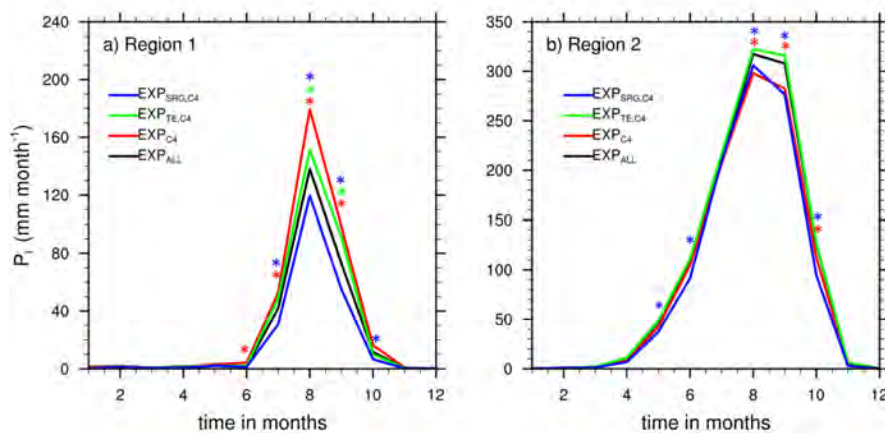


FIGURE 3.3: Mean annual cycle of precipitation P under 8 ky conditions in Region 1 (a; 18 to 22° N, 5 to 30° E) and Region 2 (b; 12 to 18° N, -15 to 20° E). Curves depict monthly averages of 100 simulated years for EXP_{ALL} (black), EXP_{C4} (red), $EXP_{TE,C4}$ (green), and $EXP_{SRG,C4}$ (blue). Stars in the respective colors indicate significant differences to EXP_{ALL} ($\sigma=0.05$).

It remains to study the effects of PFT diversity on the atmospheric circulation. The analysis focuses on the following tropical circulation features associated with the WAM: the low-level InnerTropical Convergence Zone (ITCZ, 925 hPa), the low-level westerlies connected with the southwest monsoon flow (LLW, 850 hPa), the mid-level African Easterly Jet (AEJ, 600 hPa), the upper-level Tropical Easterly Jet (TEJ, 150 hPa), and the Saharan Heat Low (SHL) (Nicholson, 2013).

The left column in Fig. 3.4 illustrates 100-year average horizontal low-level wind fields in the monsoon layer (925 hPa) and P fields during the monsoon season (JJAS) for EXP_{ALL} and differences to the other simulations. EXP_{ALL} nicely depicts the surface manifestation of the ITCZ, namely the convergence of northeasterly Harmattan winds

originating in the Sahara and the southwest monsoon flow emanating from Atlantic ocean between 18° N (in east Africa) and 20° N (in west Africa), as well as the SHL located around 22° N (Fig. 3.4a). This pattern indicates a northward shift of the system by around 2° compared to present day (Nicholson, 2013). In accordance with the current picture of the WAM, the core of the rain belt is located between the AEJ and the TEJ, around 8° equatorward of the ITCZ (Nicholson, 2013). EXP_{C4} shows compared to EXP_{ALL} an intensification of the southwest monsoon flow by more than 2 m s^{-1} south of 18° N, congruent with the region of reduced P (Fig. 3.4c). The southwest monsoon flow and the northeast winds converge around 2° further north than in EXP_{ALL} . The northward shift of the ITCZ goes in conjunction with higher P north of 18° N. Further, EXP_{C4} exhibits a deepening of the SHL and an intensification of northeasterly winds in the northwestern part of the study domain. $EXP_{TE,C4}$ depicts a rather moderate difference to EXP_{ALL} mainly characterized by a strengthening of the ITCZ between 5 and 30° E accompanied by higher P in this region (Fig. 3.4e). In the northwestern part of the study domain, northeasterly winds intensify by almost 2 m s^{-1} . $EXP_{SRG,C4}$ exhibits an intensification of the southwest monsoon flow by more than 2 m s^{-1} south of 16° N as well as an intensification of northeasterly winds between 16 and 22° N, congruent with the region of reduced P (Fig. 3.4g). This results in a strong deepening of the SHL. Other than in EXP_{C4} , the convergence zone is located around 4° further south than in EXP_{ALL} .

The right column in Fig. 3.4 shows vertical cross sections of zonal winds in the region -10 to 40° N, -10 to 40° E during the monsoon season (JJAS) and illustrates the strength and position of tropical circulation features at different pressure levels for EXP_{ALL} and differences to the other simulations. In EXP_{ALL} , the core of LLW lies around 12° N with wind speeds up to 6 m s^{-1} (Fig. 3.4b). The core of the AEJ is positioned at around 18° N reaching maximum wind speeds of almost 10 m s^{-1} . The core region of the TEJ is located around 10° N with maximum wind speeds of about 20 m s^{-1} . EXP_{C4} shows a significant ($\sigma=0.05$) strengthening and vertical expansion of LLW between 10 and 20° N as well as a considerable weakening of the AEJ, especially at the southern flank, which results in a northward shift of its core region (Fig. 3.4d). The TEJ is slightly stronger than in EXP_{ALL} . $EXP_{TE,C4}$ depicts rather moderate differences to EXP_{ALL} mainly characterized by a slight strengthening of near-surface westerlies and LLW around 15° N, a slight weakening of the AEJ, and a slight strengthening of the TEJ (Fig. 3.4f). $EXP_{SRG,C4}$

exhibits a significant strengthening of LLW very close to the surface between 10 and 20° N as well as a significant weakening of the AEJ and the TEJ (Fig. 3.4h). Other than in EXP_{C4} , the reduction of AEJ winds occurs especially at the northern flank which results in a southward shift of the core region.

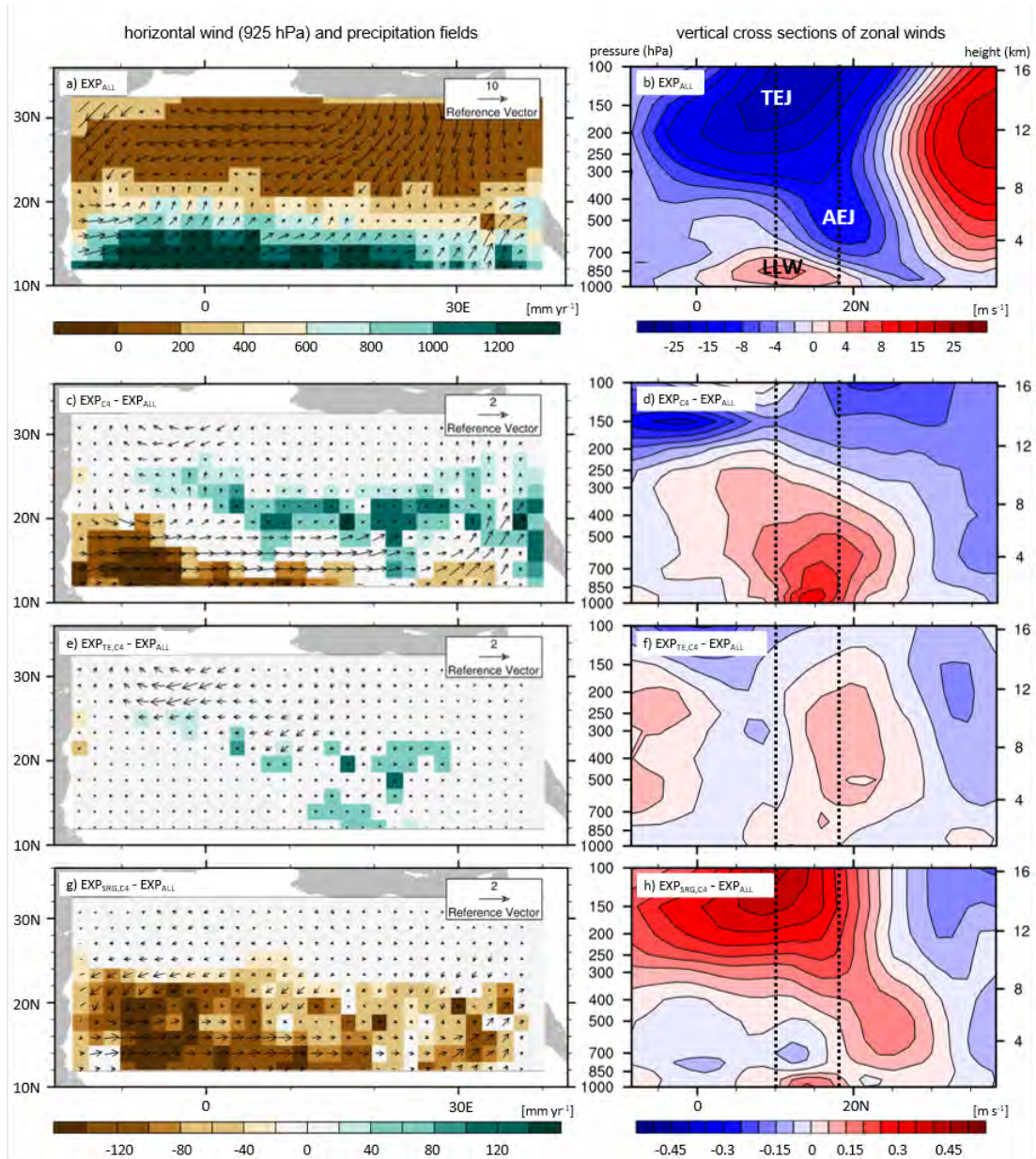


FIGURE 3.4: Left: Effects of different PFT compositions on precipitation and horizontal low-level wind fields in the monsoon layer at 8 ky. Right: Vertical cross sections of zonal winds illustrate the strength and position of tropical circulation features associated with the West African Monsoon at 8 ky: low-level equatorial westerlies (LLW, 850 hPa), mid-level African Easterly Jet (AEJ, 600 hPa), upper-level Tropical Easterly Jet (TEJ, 150 hPa). Dotted lines mark the core regions of AEJ and TEJ in EXP_{ALL} . Panels (a, b) show the 100-year average of the monsoon season (JJAS) for the experiment EXP_{ALL} with the standard PFT set up. The following panels illustrate differences between EXP_{ALL} and EXP_{C4} (c, d), $EXP_{TE,C4}$ (e, f), and $EXP_{SRG,C4}$ (g, h). Colored grid cells in panel (c), (e), (g) indicate significant differences to EXP_{ALL} ($\sigma=0.05$).

For a better understanding of the regional differences in P and veg_{max} it is worth looking at the relationship between the latter on grid cell level. The dots in the vegetation–precipitation diagrams (V–P diagrams) in Fig. 3.5 illustrate the relationships between P_i and $veg_{max,i}$ for all simulations i at 8 ky including all grid cells in the study domain (12 to 34° N, -15 to 40° E) to cover the full P spectrum. Note that the V–P diagrams represent the relationships in equilibrium.

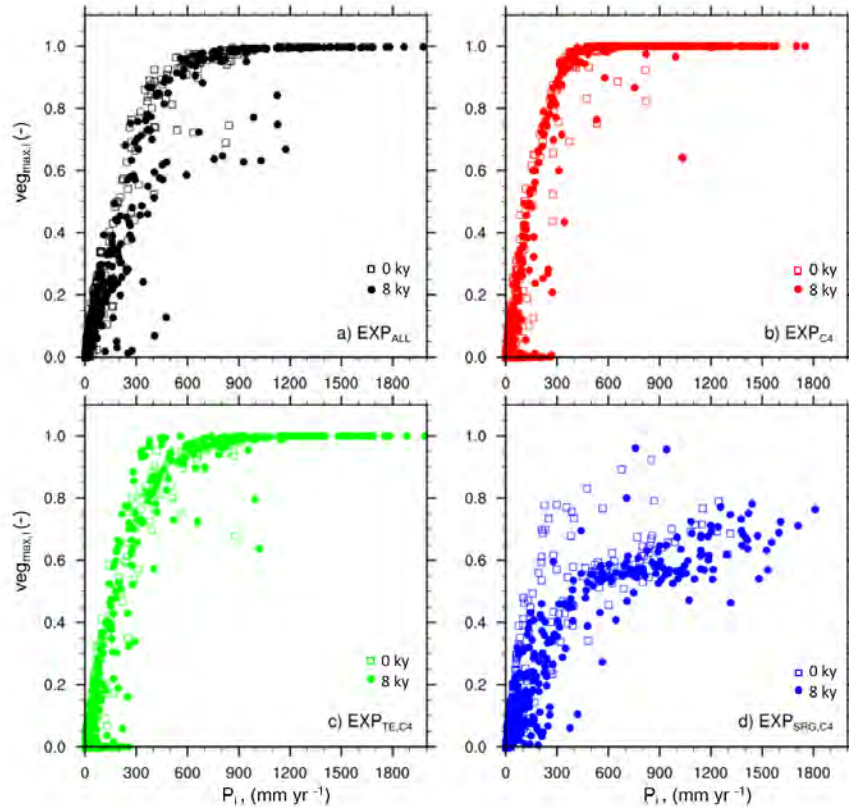


FIGURE 3.5: Vegetation–precipitation diagrams ($veg_{max,i}$, P_i) for simulations i with different PFT combinations including all grid cells in the study domain (12 to 34° N, -15 to 40° E). Values are derived from 100-year averages for EXP_{ALL} (a), EXP_{C4} (b), $EXP_{TE,C4}$ (c), and $EXP_{SRG,C4}$ (d). Dots depict relationships at 8 ky, squares represent relationships at 0 ky.

In all simulations multiple vegetation modes exist for the same P regime indicating factors other than P_i also determine $veg_{max,i}$. In EXP_{ALL} , the distribution is split in two “branches” (Fig. 3.5a, dots). The upper and dominant branch represents grid cells dominated by TE and $C4$ and reaches a veg_{max} of 1.0 at around 800 mm yr^{-1} . The lower more scattered branch has a shallower slope and converges to a threshold of approximately 0.7. The grid cells on this lower branch are located in mountainous regions and are covered with SRG and $C4$. The distribution in EXP_{C4} also shows two branches (Fig. 3.5b, dots). The upper dominant branch reaches a veg_{max} of 1.0

at around 450 mm yr⁻¹. The lower more scattered branch has a shallower slope and reaches a veg_{max} of 1.0 at around 800 mm yr⁻¹ representing grid cells in mountainous region. In $EXP_{TE,C4}$ the distribution is divided in three branches (Fig. 3.5c, dots). The upper branch reaches a veg_{max} of 1.0 at 450 mm yr⁻¹ representing grid cells that are exclusively covered with $C4$. The middle and dominant branch reaches a veg_{max} of 1.0 at around 700 mm yr⁻¹ and vegetation is composed of TE and $C4$. The lower more scattered branch has a shallower slope and converges to a threshold of 0.7 representing grid cells in mountainous region. The distribution in $EXP_{SRG,C4}$ is also divided in three branches (Fig. 3.5d, dots). The upper branch converges to a veg_{max} of 1.0 at around 800 mm yr⁻¹ representing grid cells dominated by $C4$. The second branch reaches its upper threshold of 0.6 at around 600 mm yr⁻¹. Here, SRG is the dominant PFT. The third branch lies over the second branch but shows a more scattered linear behaviour that tends towards higher cover fractions but doesn't reach a veg_{max} of 1.0 within the given P range. The grid cells on this branch are located south of 15° N.

3.3.2 Discussion

The presented results highlight that PFT diversity and composition significantly affect simulated climate–vegetation interaction during the AHP and thereby modify the extent of the “green” Sahara in ECHAM6/JSBACH simulations. veg_{max} is determined by the ratio of involved PFTs resulting from competition, their productivities and capabilities to suppress desert expansion. Remarkably, the introduction or removal of a single PFT drastically affects the vegetation extent. A surprisingly strong influence has the marginal PFT “Raingreen shrub” (SRG) which was previously expected to be of minor importance in PFT competition. SRG acts as desert promoter and its exclusion puts less competitive pressure on other PFTs which supports their growth and impedes desert expansion (see Sec. 2.3.3).

Changes in veg_{max} in turn cause significant differences in land surface parameters, hydrological cycle and surface energy budget indicating a substantial feedback between terrestrial biosphere and atmosphere during the AHP. The lower albedo due to higher veg_{max} in Region 1 in EXP_{C4} and $EXP_{TE,C4}$ compared to EXP_{ALL} enhances the absorption of solar energy available for evapotranspiration which accelerates energy and water cycling, and boosts moisture available in the atmosphere. Together with the

stronger turbulent fluxes this results in higher simulated P , supporting the hypothesis of a positive climate–vegetation feedback described in the introduction. On the other hand, a higher albedo and a decrease of surface roughness in Region 2 in EXP_{C4} and in both regions in $EXP_{SRG,C4}$ slows down water and surface energy fluxes and reduces turbulence which suppresses P , supporting the self-stabilizing mechanism of deserts suggested by Charney (1975). However, the presented simulations modify the hypothesis of a positive climate–vegetation feedback described in the introduction by showing that higher veg_{max} is not necessarily associated with higher P . Not only the covered fraction but also the properties of prevailing PFTs are crucial. In EXP_{C4} , veg_{max} is in Region 2 higher than in the other simulations while P is lower than in simulations that include woody PFTs. With an albedo of $C4$ higher than those of woody PFTs prevailing in other simulations, the absorption of solar energy decreases. Indeed, the reduced transpiration capacity on a comparatively small leaf area limits the transfer of interception and soil water to the atmosphere. The counteracting effect of clouds vanishes resulting in a net increase of insolation at the surface. The excess absorbed solar radiation cannot be translated in a strong enough latent heat flux to compensate the warming. The resulting increase in temperature rises the atmospheric demand for evapotranspiration and therewith water stress. The small surface roughness of $C4$ reduces turbulent fluxes and the likelihood of convection initiation. In $EXP_{SRG,C4}$, veg_{max} is lower than in the other simulations with the same P (see Fig. 3.5d). The explanation lies in the parametrization of SRG in JSBACH as explained in Chapter 2. Basically, due to its low specific leaf area, SRG requires a higher productivity to cover the same area as another PFT. SRG 's comparatively low productivity impedes reaching a NPP comparative to other PFTs. SRG thereby acts as desert promoter. Differences in the average annual cycle of P further support the hypothesis of positive climate–vegetation feedback, especially in Region 2. At the beginning of the monsoon peak in August, vegetation is leafless and P differences are relatively small. Later on in September when the canopy is developed, the feedback comes into play and the differences become more pronounced.

The analysis of atmospheric circulation features explains how changes in land surface parameters and surface energy balance translate into large scale alterations of the atmospheric circulation, and how these alterations affect P in the study domain. The lower roughness length in EXP_{C4} and $EXP_{SRG,C4}$ relative to EXP_{ALL} in the southern and in the northwestern part of the study domain accelerates near surface winds and thereby

intensifies the ITCZ and deepens the SHL. The positions of ITCZ, SHL, and AEJ are in all simulations determined by the extent of the meridional temperature gradient between the equator and the northern Tropics. In EXP_{C4} , the gradient reaches further north than in EXP_{ALL} due to the extensive veg_{max} in Region 1 that is accompanied by a moistening of the atmosphere and a surface warming because LH cannot compensate the excess absorbed solar energy due to lower albedo. As a result, the ITCZ, the AEJ, and consequently the core of the rain belt shift northward, leaving the southernmost part of the domain comparatively dry. In accordance with literature, a northward shift and weakening of the AEJ is associated with wetter conditions in the Sahel and a northward shift of the rain belt. The moderate effects on atmospheric features in $EXP_{TE,C4}$ reflect the relatively small changes in land surface properties. The slight northward shift of the ITCZ can be explained with the northward expansion of the meridional temperature and moisture gradient due to higher veg_{max} in Region 1, similar to EXP_{C4} . Complementary, the overall lower veg_{max} in $EXP_{SRG,C4}$ accompanied by a reduction in the meridional atmospheric moisture and temperature gradient causes a southward shift of the ITCZ, the AEJ and the core of the rain belt. In accordance with literature, a more equatorward position of the AEJ is associated with dry conditions over the Sahel. However, the weakening of the AEJ and the TEJ is usually linked to wetter conditions which is not the case in $EXP_{SRG,C4}$. This could be attributed to the low water recycling efficiency of vegetation compared to EXP_{ALL} , especially due to SRG , which implies less release of latent heat in the atmosphere which in turn decreases convection (Texier et al., 2000).

The different vegetation modes in the V–P diagrams indicate that factors other than P can affect veg_{max} in coupled simulations. Two important additional factors appear upon closer inspection of the non-dominant branches. First, the lower branches in all simulations represent grid cells in mountainous regions where shallow soils (in JSBACH) are not capable of holding water and therewith impede plant growth despite high P . In EXP_{ALL} , SRG and $C4$ establish and the branch resembles the main branch of $EXP_{SRG,C4}$. In EXP_{C4} and $EXP_{TE,C4}$, these grid cells are dominated by $C4$. Second, in regions where temperatures of the coldest month fall below the threshold of TE/TD (15.5°C), these tropical PFTs cannot establish thereby favoring the dominance of other PFTs, namely $C4$ in $EXP_{TE,C4}$ and SRG and $C4$ in EXP_{ALL} . This in turn alters veg_{max} according to their respective properties. Thus, alternative branches are alike the dominant branches of the simulations with the corresponding composition.

The differences in initial veg_{max} are qualitatively in accordance with the previous chapters. Just as in Chapter 1, the effective feedback between vegetation and precipitation emerges from the interacting properties of prevailing plant types. These properties are in the conceptual model condensed in the effective leaf area L_i and in JSBACH implemented as PFT land surface parameters and photosynthetic parameters. The stronger positive the feedback, the larger the enhancing effect on background P and the larger the resulting veg_{max} . In combined interaction with P , sensitive plant types benefit from additional water and a more life-sustaining environment, whereas resilient plant types suffer from competition. Regarding Chapter 2, the extent of vegetation depending on involved PFTs and their respective productivities is qualitatively comparable with the results presented in this chapter despite feedbacks with the atmosphere were not taken into account in offline simulations. This indicates that in equilibrium in a high P regime, the effect of plant composition is even more decisive for the extent of vegetation cover than the feedback with the atmosphere.

The V–P diagrams in Fig. 3.5 support the assumption underlying the analysis in Chapter 1 that P is a good measure for vegetation growth. Most grid cells are located on the dominant branches that represent the P -limited regime. As mentioned in Chapter 1, P is eventually not sufficient to determine veg_{max} because factors other than P – lacking in the conceptual model – might be of importance for the local vegetation response. These cases are represented by additional branches in the V–P diagrams in Fig. 3.5. The attempt to create V–P diagrams for offline simulations in Chapter 2 did not provide interpretable results. Due to the chosen set up that implies minimum $P \gg 0$ for the whole simulation period, it was not possible to derive continuous data series. Therefore, I forgo discussing the relationship between P and veg_{max} in transient offline simulations here.

In summary, PFT diversity and composition significantly affect land surface parameters, hydrological cycle, surface energy budget, and large scale atmospheric circulations patterns in coupled ECHAM6/JSBACH simulations, and consequently the extent of the “green” Sahara during the AHP. PFT composition is more decisive for the interaction with the atmosphere than veg_{max} and higher veg_{max} is not necessarily associated with higher P but determined by the properties of the prevailing PFTs. The V–P diagrams underline how competition affects the extent of veg_{max} during the AHP but also show that factors other than P can affect veg_{max} in coupled simulations.

3.4 Effects of PFT diversity on the transition from the “green” Sahara to the “desert” state

3.4.1 Results

For a first estimate of regional transition patterns from the “green” Sahara (8 ky) to the “desert” state (0 ky), I subtract 100-year averages of consecutive time slices for all simulations and compare the resulting transition maps of precipitation P and vegetation cover fraction veg_{max} in the study domain (12 to 34° N, -15 to 40° E). Note that this analysis does not represent the transient changes of vegetation extent and precipitation over the last 8000 years but provides an estimate of possible different states for a series of external forcings. As the time scales of the simulated vegetation dynamics and atmospheric processes are much shorter than the simulated periods, this approach is legitimate for this study.

Fig. 3.6 exemplarily shows transition maps of P and veg_{max} from EXP_{ALL} (see appendix for EXP_{C4} , $EXP_{TE,C4}$, $EXP_{SRG,C4}$). At the first glance, it is notable that the western part of the study domain experiences a stronger reduction of P than the eastern part in all periods in EXP_{ALL} (Fig. 3.6, left column). On closer inspection, the pattern of P decline shifts from northeast to southwest indicating a southward shift of the tropical rain belt by about 2° latitude per period. A slight P increase at the southwestern coast in the first two periods before P starts decreasing in concert with the rest of the domain supports this indication. The magnitude of P decline ranges from less than 50 mm (2 ky)⁻¹ in the northern part of the domain to more than 200 mm (2 ky)⁻¹ at the latitudes of maximum change between 12 and 20° N, with single cells in the western part reaching up to 250 mm (2 ky)⁻¹. veg_{max} follows the pattern of P decline with a latitudinal offset of around 2° to the north, reaching maximum rates of decrease from 0.1 to 0.2 (2 ky)⁻¹ in the transition zone between desert and savanna. This transition zone shifts southward from 18 to 22° N at 8 ky to around 14 to 20° N at 0 ky (Fig. 3.6, right column). The almost constant slopes of P and veg_{max} decline in the latitudes of maximum change in all periods indicate a gradual transition from the “green” Sahara to the “desert” state.

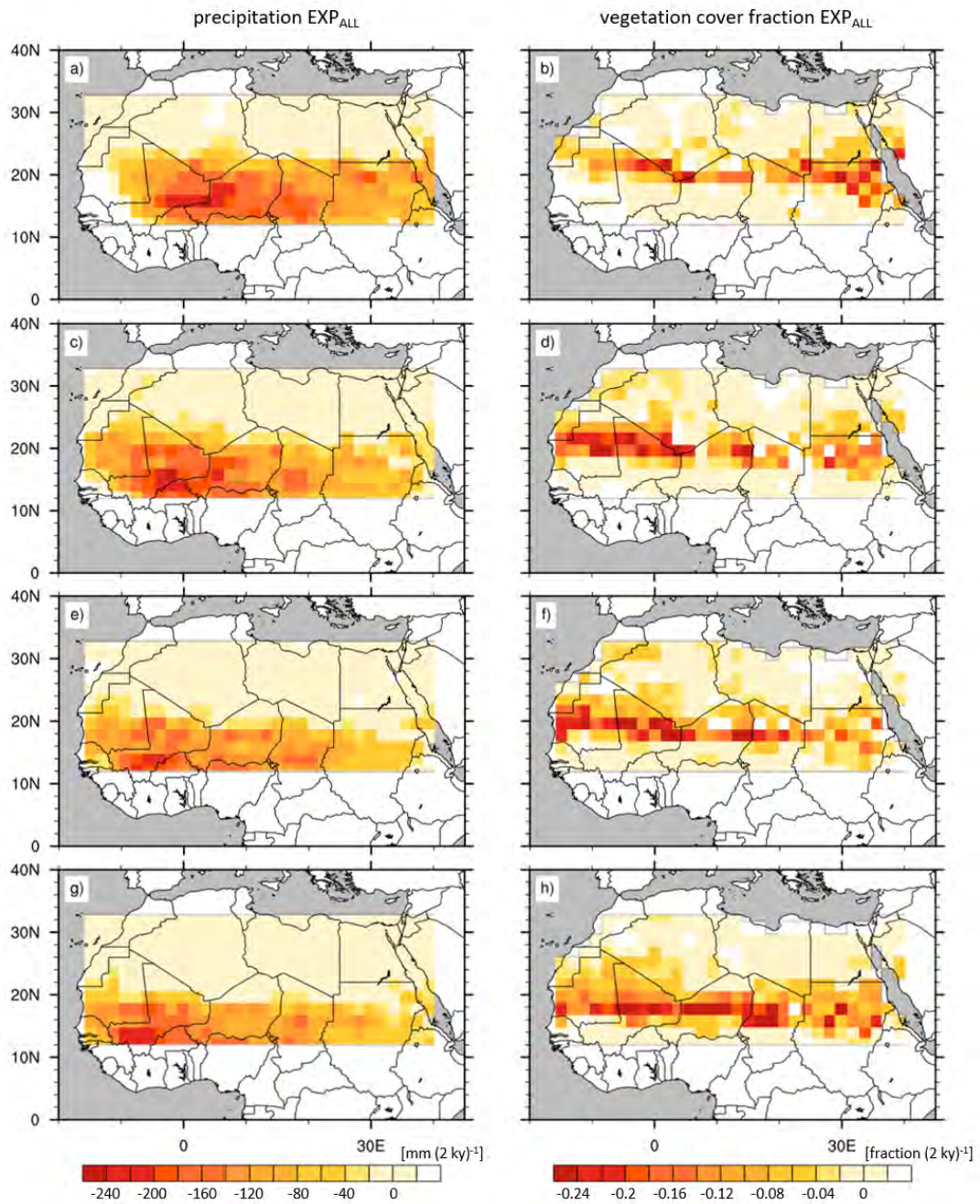


FIGURE 3.6: Rates of transition from the “green” Sahara to the “desert” state for precipitation P (left column) and vegetation cover fraction veg_{max} (right column) of a simulation with the standard PFT set up (EXP_{ALL}), including Tropical Evergreen Tree (TE), Tropical Deciduous Tree (TD), Extratropical Evergreen Tree (eTE), Extratropical Deciduous Tree (eTD), Shrub Raingreen (SRG), Shrub Deciduous (SD), C3 Grass ($C3$), C4 Grass ($C4$). Plots depict differences between consecutive time slices: 6 ky-8 ky (a, b), 4 ky-6 ky (c, d), 2 ky-4 ky (e, f), and 0 ky-2 ky (g, h).

The simulations with lower PFT diversity (EXP_{C4} , $EXP_{TE,C4}$, $EXP_{SRG,C4}$) show qualitatively similar patterns of P and veg_{max} decline in terms of northeast to southwest shift of the most changing region (see appendix). However, the timing and rate of transition substantially differ between simulations with different PFT compositions. For the quantitative comparison of all simulations, I condense the information of the transition maps by calculating zonal means of P and veg_{max} and subtract the values of consecutive time slices, in the following referred to as ΔP_i and $\Delta veg_{max,i}$ for all simulations i . Fig. 3.7 illustrates that the maximum as well as the time evolution of ΔP_i and $\Delta veg_{max,i}$ considerably differ between simulations.

Just as described above for the transition maps, the patterns of change shift in EXP_{ALL} gradually southward by 2° latitude per period (Fig. 3.7a). $\Delta veg_{max,ALL}$ follows the symmetric pattern of ΔP_{ALL} with a meridional offset of around 2° to the north, reaching maximum rates of decrease in the transition zone between desert and savanna between 4 and 0 ky (Fig. 3.7b). This indicates that vegetation does not respond directly to changes in P but declines when a threshold is reached at low P rates. The evolutions of ΔP_{C4} and $\Delta veg_{max,C4}$ indicate a delayed but sharpened transition in the simulation without woody PFTs compared to EXP_{ALL} (Fig. 3.7c, d). The decline of precipitation starts slowly between 8 and 6 ky with rates 50% lower than in EXP_{ALL} . Between 6 and 2 ky however, ΔP_{C4} sharply increases to up to $200 \text{ mm (2 ky)}^{-1}$, corresponding to an acceleration of more than 40%. Afterwards, ΔP_{C4} drops to values similar to, or even lower than in EXP_{ALL} . $\Delta veg_{max,C4}$ follows the southward retreat of ΔP_{C4} reaching its peak between 6 and 2 ky with maximum rates of up to 0.33 (2 ky)^{-1} , which is more than twice as fast as $\Delta veg_{max,ALL}$. Before and after this peak, the vegetation decline is of a similar magnitude as in EXP_{ALL} . $EXP_{TE,C4}$ depicts a response very similar to EXP_{C4} but considerably intensified (Fig. 3.7e, f). The major precipitation decline is limited to the period between 6 and 4 ky with $\Delta P_{TE,C4}$ reaching maximum values of up to $240 \text{ mm (2 ky)}^{-1}$, which is nearly twice as fast as ΔP_{ALL} . After 4 ky, the rate of precipitation decline drops to values similar to, or lower than in EXP_{ALL} . $\Delta veg_{max,TE,C4}$ follows the southward retreat of $\Delta P_{TE,C4}$ and correspondingly, the major vegetation decline occurs between 6 and 4 ky with $\Delta veg_{max,TE,C4}$ amounting to maximally 0.32 (2 ky)^{-1} , which is more than twice as fast as $\Delta veg_{max,ALL}$. Not only the temporal response is sharper, but also the band of major changes is latitudinally more confined than in EXP_{ALL} .

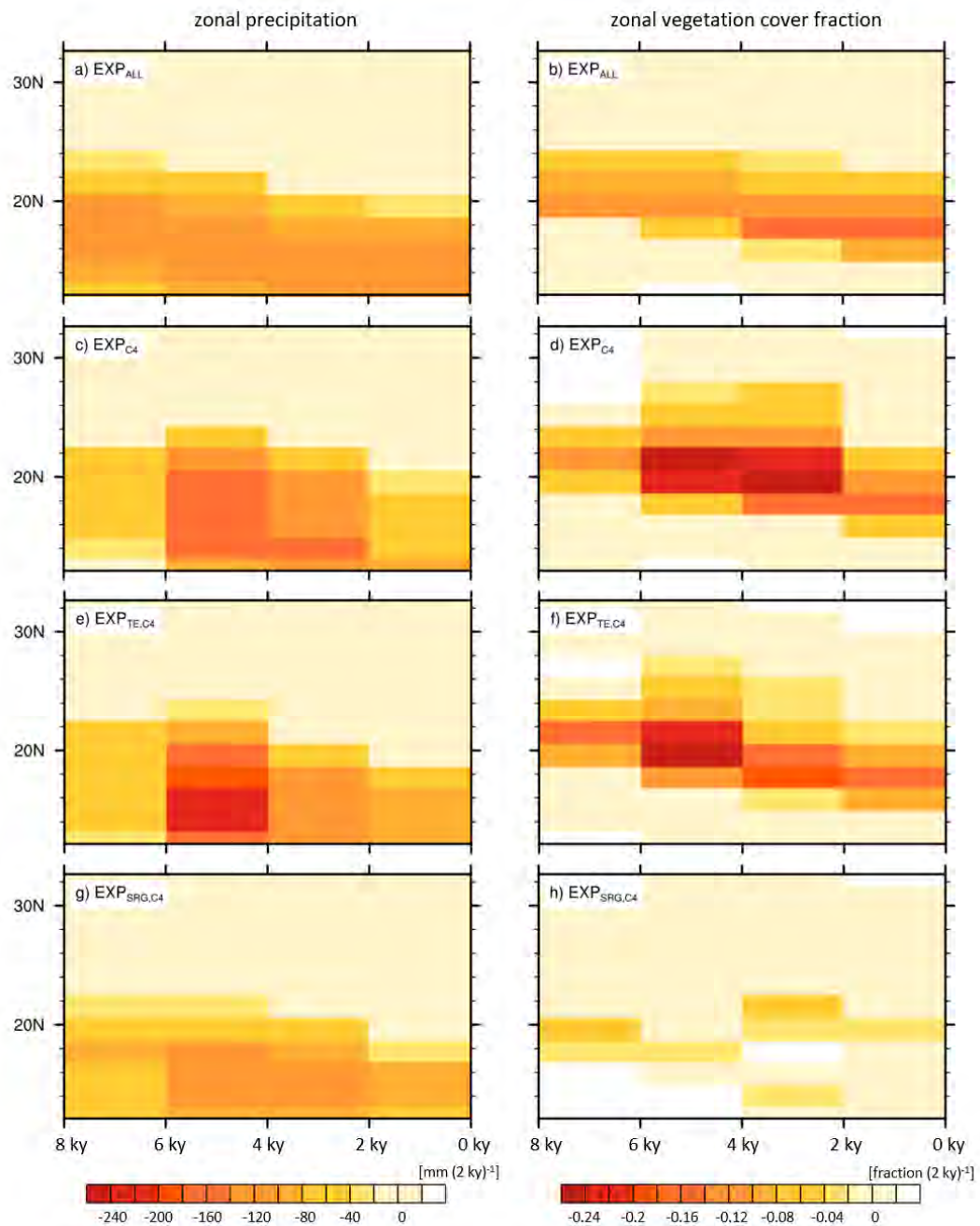


FIGURE 3.7: Zonally averaged rates of transition from the “green” Sahara to the “desert” state for precipitation ΔP_i (left column) and vegetation cover fraction $\Delta veg_{max,i}$ (right column) for simulations i : EXP_{ALL} (a, b) includes all standard PFTs (Tropical Evergreen Tree (TE), Tropical Deciduous Tree (TD), Extratropical Evergreen Tree (eTE), Extratropical Deciduous Tree (eTD), Shrub Raingreen (SRG), Shrub Deciduous (SD), C3 Grass ($C3$), C4 Grass ($C4$)), EXP_{C4} (c, d), $EXP_{TE,C4}$ (e, f), and $EXP_{SRG,C4}$ (g, h).

By contrast, $EXP_{SRG,C4}$ shows a delayed but smoothed transition from the already “brownier” initial state at 8 ky to the “desert” state at 0 ky compared to EXP_{ALL} (Fig. 3.7g, h). Between 6 and 4 ky, the rate of $\Delta P_{SRG,C4}$ lies in a similar range as ΔP_{ALL} ; before and after this period, the precipitation decline is even slower. $\Delta veg_{max,SRG,C4}$ shows an exceptional behavior with a slow but non-monotonous southward shift of the most changing latitudes.

It remains to explore if the relationships between precipitation and vegetation change over time. The squares in Fig. 3.5 depict the relationships between P_i and $veg_{max,i}$ at 0 ky including all grid cells in the study domain to cover the full P spectrum. The comparison to 8 ky (Fig. 3.5, dots) reveals that the relationships do not change qualitatively over time. Similar to the status at 8 ky, multiple vegetation modes, differentiated by the most limiting factor in the corresponding grid cells (precipitation, unfavourable soil conditions, bioclimatic limits; see Sec. 3.3.2), exist for the same P regimes in all simulations. However, the number of grid cells per branch alters in favour of the $C4$ dominated branches at 0 ky, and the boundaries of the branches become fuzzier.

3.4.2 Discussion

The transition from a wet “green” state to a dry “desert” state is in all simulations associated with a time-transgressive southward shift of the tropical rain belt from the mid-Holocene to present day. This trend is in accordance with hydrological reconstructions (Shanahan et al., 2015). The explanation for differences in timing and magnitude of vegetation and precipitation decline between simulations with different PFT compositions is twofold.

The first part of the explanation lies in dissimilar initial precipitation and vegetation cover fraction values. High initial values of P_i and $veg_{max,i}$ in EXP_{C4} and $EXP_{TE,C4}$ in the transition zone between desert and savanna imply a large gradient between “green” and “desert” state and therewith inherit a larger potential for high ΔP_i and $\Delta veg_{max,i}$ than EXP_{ALL} and $EXP_{SRG,C4}$ (see Sec. 3.4).

The second part of the explanation lies in the disparate relationships between precipitation and vegetation cover fraction depicted in the V–P diagrams, and in the associated different sensitivities to precipitation decline. The constant relationships between P_i

and $veg_{max,i}$ over time indicate that $veg_{max,i}$ “moves” left along the branches in the V–P diagrams when P_i declines. Within a certain precipitation range, $veg_{max,i}$ is not affected by a precipitation reduction until the threshold of maximum cover is reached. The position of this threshold is determined by the ratio of involved PFTs resulting from competition, their productivities and capabilities to suppress desert expansion (derived from Eq. 2.7, 2.8). Looking at the dominant branches, $C4$ with its high specific leaf area (see Tab. 2.1) and accordingly “cheap” leaves reaches a veg_{max} of 1.0 with the lowest P in single growth. $EXP_{SRG,C4}$ represents the other extreme never reaching a veg_{max} of 1.0 under the given P regime. SRG ’s comparatively low productivity to produce “expensive” leaves together with its dominance over $C4$ impedes extensive plant growth (see Sec. 2.3.3). Only in the southernmost latitudes of the study domain a veg_{max} close to 1.0 can be achieved. Non-dominant branches depict grid cells where the number of PFTs is altered due to limitations other than P such as unfavourable soil conditions or bioclimatic limits (see Sec. 3.3.2), and the thresholds are alike the main branches of the corresponding composition. When the threshold of maximum cover is reached, $veg_{max,i}$ starts to decrease according to the slope of the branch. If the threshold value is low, the slope of the branch is steep, and $veg_{max,i}$ drops abruptly with a small precipitation decline. If the threshold value is higher, the slope is shallower, and $veg_{max,i}$ retreats more gradually. With further precipitation decline below the threshold, not only the total vegetation cover decreases, but the PFT composition changes as well. PFTs with high moisture requirements cannot sustain growth and are consequently replaced by more drought resistant PFTs. The alteration in PFT composition implies that the relationship between P and veg_{max} changes in the respective grid cell, which can be observed in the V–P diagrams. When PFT composition changes, the grid cell value “jumps” to another branch and follows its trajectory with further P decrease. This jump happens most obviously in $EXP_{SRG,C4}$. When SRG disappears after 4 ky and thereby allows $C4$ to establish (see Fig. 3.7), affected grid cells shift to the upper branch in the diagram, which resembles the main branch of EXP_{C4} , and reach a higher veg_{max} with the same P . This shift also explains the non-monotonous vegetation retreat in Fig. 3.7h. Hence, the regional response is determined by the dominant branch, therewith sharp in EXP_{C4} and $EXP_{TE,C4}$, gradual in EXP_{ALL} , and very shallow in $EXP_{SRG,C4}$.

The presented results are qualitatively in accordance with Chapter 1 by confirming that the growth ranges of plant types in semi-arid regions are mainly constrained by P thresholds, and that the sensitivities of plant types are reflected in the slopes of the V– P diagrams. The buffering effect of higher plant diversity on veg_{max} and P described in Chapter 1 can be observed in EXP_{ALL} despite the underlying causes differ (see Sec. 2.2.4). Namely, EXP_{ALL} depicts a gradual decrease of both variables compared to the sharp decline in EXP_{C4} and $EXP_{TE,C4}$. At the same time, the smooth transition in $EXP_{SRG,C4}$ underlines once more that plant composition is more important than the absolute number of plant types, and that an increase in plant diversity does not necessarily stabilize the climate–vegetation system.

Regarding Chapter 2, coupled simulations show the same qualitative effect of PFT diversity on initial veg_{max} and transition rate, but the fast retreat of vegetation as a response to gradual P forcing cannot be observed. This can partly be attributed to the overall shallower P gradient between start and end in the coupled simulations. Moreover, this highlights the effect of coupling between a diverse terrestrial biosphere and atmosphere proposed by Claussen et al. (2013): by allowing combined interaction with the atmosphere, plant types “could give rise to a gradual decline and stability properties that are similar to a stable system” while “the specific composition of vegetation is the explanation for this weak feedback.”

In summary, all simulations show a transition from a wet “green” state to dry “desert” state depicting a time-transgressive southward shift of the tropical rain belt from the mid-Holocene to present day. The rate and timing of transition is determined by the ratio of involved PFTs resulting from competition, their productivities and capabilities to suppress desert expansion. PFT composition is more important than the total number of occurring PFTs and an increase in plant diversity does not necessarily increase the stability of a climate–vegetation system. Thus, the introduction or removal of a single PFT can bring about significant impacts on the simulated climate–vegetation system stability and the system response to changing external forcing.

3.5 Limitations

The main limitation for studying effects of PFT diversity on the transition from the “green” Sahara to the “desert” state is that the simulations were not performed transiently but as time slices run into equilibrium. This set up implies vegetation being permanently in equilibrium with climate. In reality, the delayed response of vegetation allows several potential transient conditions to exist before biodiversity slowly attains equilibrium (Vellend et al., 2006; Diamond, 1972; Brooks et al., 1999).

The prescription of constant SST and SIC does not give the full system response since the air/sea temperature gradient is the fundamental driver of the monsoon. Observational studies (e.g. Lamb, 1978; Hastenrath, 1984; Folland et al., 1986) as well as modelling approaches (e.g. Druryan, 1991; deMenocal & Rind, 1993; Kutzbach & Liu, 1997; Ganopolski et al., 1998; Braconnot et al., 1999; Rodriguez-Fonseca et al., 2011) demonstrated that P patterns of the WAM are very sensitive to SST changes in different ocean basins, especially in the adjunct north Atlantic. However, Ganopolski et al. (1998) proposed that major P changes in the subtropics arise from a strong positive feedback between vegetation and P , while the role of changes in oceanic temperature is ambiguous. Besides, the described set up ignores other forcings that might produce shorter period climatic changes (<100 years) such as volcanoes.

Another factor excluded in the presented study is the extend of palaeo lakes and wetlands reconstructed for the AHP (Hoelzmann et al., 1998; Kröpelin et al., 2008; Lézine et al., 2011). Previous modelling studies suggested that open-water surfaces in the present day Sahara and Sahel region could have strongly affected climate during the AHP (Coe & Bonan, 1997), “regionally more than doubling the simulated precipitation rate” (Krinner et al., 2012).

The modification of PFT diversity only in the study domain causes boundary effects that influence the larger scale dynamics, especially at the southern edge of the domain. Since the region most affected by changes in PFT composition, namely the transition zone between savanna and desert, lies further north, I assume that these boundary effects do not affect the quality of the results.

As already mentioned in Chapter 2, another shortcoming is that the soil map in JSBACH was initially not adjusted to AHP but reflected present day conditions. Due to lack of

paleosol data, I was obliged to assume that the soil characteristics have not changed during the considered period. Soils in the present day Sahara have a very low water holding capacity making growth difficult for PFTs with high moisture requirements even though provided precipitation is sufficient. Given a higher availability of paleosol data, the consideration of soil reconstructions to create model input could partly solve this problem, but points straight to a further limitation: the non-dynamic handling of physical land/soil characteristics. Various studies highlighted the impact of physical land characteristics on climate, including either land albedo (Bonfils et al., 2001; Levis et al., 2004; Schurgers et al., 2007; Vamborg et al., 2011), soil texture and maximum water-holding field capacity (Wang, 1999; Levis et al., 2004), or the combined effect (Stärz et al., 2016). Vamborg et al. (2011) proposed a dynamic background albedo scheme for JSBACH that models the background albedo as a slowly changing function of organic matter in the ground and of litter and standing dead biomass covering the ground. The disadvantage of this scheme is that soil carbon pools require a long spin up time to reach equilibrium, which could not be realized in the presented thesis due to computation and time limitations. Asynchronous coupling of a dynamic soil scheme to MPI-ESM showed that computed changes lead to significant amplification of positive feedbacks during the mid-Holocene (Stärz et al., 2016). The implementation of such a dynamic scheme could improve the representation of soil-climate feedbacks, and since soil properties are impacted by the present vegetation, this could reveal additional effects of variations in plant diversity. Additional interesting processes in this context are pedogenesis (see Minasny et al. (2008) for a review on quantitative models for pedogenesis) and soil degradation.

The distribution of initial vegetation cover fractions might have an impact on the resulting vegetation state. Previous studies showed that depending on initial vegetation cover, the climate–vegetation system might converge towards different stable states (Claussen, 1994; Claussen & Gayler, 1997; Claussen et al., 1998; Brovkin et al., 1998; Bathiany et al., 2012). This potential for multiple equilibria was not considered here, all simulations started with the same desert distribution.

Finally, as extensively discussed in Chapter 2, the PFT set in JSBACH – designed for global application – has only a limited applicability for detailed studies on the role of plant diversity in subtropical semi-arid regions.

3.6 Summary and conclusions

In this chapter, I have presented results from coupled ECHAM6/JSBACH simulations with different PFT compositions to show how precipitation could have been affected by plant diversity during the AHP and how the interaction between vegetation and atmosphere could have influenced the stability of the “green” Sahara and the transition to the “desert” state.

In simulations with AHP boundary conditions, PFT diversity and composition significantly affected the extent of vegetation which in turn impinged land surface parameters, water cycling and the surface energy budget. Remarkably, these changes had not only local consequences but significantly altered large scale atmospheric circulation patterns indicating a strong feedback between terrestrial biosphere and atmosphere.

However, at variance with the hypothesis of positive climate–vegetation feedback (Kleidon et al., 2000), higher veg_{max} was not necessarily associated with higher P ; properties of the predominant PFTs – especially albedo, surface roughness length and transpiration capacity – were more decisive for the interaction with the atmosphere than the extent of veg_{max} . The sign of change was strongly region dependent since the prevailing regional climate determined which PFTs could establish and thus how the alteration of PFTs changed climate–vegetation interaction. The positions of ITCZ, SHL, and AEJ were in all simulations determined by the extent of the meridional temperature gradient between the equator and the northern Tropics. In accordance with literature, a northward extent of $veg_{max,C4}$ was in conjunction with a northward shift of the ITCZ, the AEJ and the rain belt, whereas a southwards retreat of $veg_{max,SRG,C4}$ was linked to a southward shift of the ITCZ, the AEJ and the rain belt. Multiple branches in the V–P diagrams represented regions that experienced different limitations, the main branch representing the P -limited regime, the additional branches depicting grid cells where bioclimatic limits or unfavorable soil conditions limited plant growth.

Differences in initial veg_{max} were qualitatively in accordance with the previous chapters. Just as in Chapter 1, the stronger positive the climate–vegetation feedback emerging from plant properties, the larger the enhancing effect on background P and the more extensive the resulting vegetation fraction. In combined interaction with P , sensitive plant types benefited from additional water and a more life-sustaining environment,

whereas resilient plant types suffered from competition. Despite feedbacks with the atmosphere were not taken into account in Chapter 2, the differences in vegetation extent were qualitatively comparable with the results presented in this chapter. This indicates that in equilibrium in a high P regime, the effect of plant composition is even more decisive for the extent of vegetation cover than the feedback with the atmosphere.

The V–P diagrams supported the assumption implicit in the analysis presented in Chapter 1 that P is a good measure for vegetation growth in semi-arid regions. Most grid cells were located on the dominant branch that represented the P -limited regime. The additional branches captured factors other than P – lacking in the conceptual model – which were of importance for the local vegetation response. The attempt to create V–P diagrams for offline simulations in Chapter 2 did not provide interpretable results. Due to the chosen set up that implies minimum $P \gg 0$ for the whole simulation period, it was not possible to derive continuous data series.

Towards the end of the AHP, all simulations showed a transition from a wet “green” state to dry “desert” state depicting a time-transgressive southward shift of the tropical rain belt from the mid-Holocene to present day. Similar to the initial veg_{max} (8 ky), the rate and timing of transition were no universal properties of a certain region but determined by the ratio of involved PFTs resulting from competition, their productivities and capabilities to suppress desert expansion. PFT composition was more important than the total number of occurring PFTs and an increase in plant diversity did not necessarily increase the stability of a climate–vegetation system. The introduction or removal of only a single PFT drastically affected the simulated climate–vegetation system stability and the system response to changing external forcing.

The presented results were qualitatively in accordance with Chapter 1 by confirming that the growth ranges of plant types in semi-arid regions are mainly constrained by P thresholds, and that the sensitivities of plant types are reflected in the slopes of the V–P diagrams. The buffering effect of higher plant diversity on veg_{max} and P described in Chapter 1 could be observed in EXP_{ALL} despite the underlying causes differed (see Sec. 2.2.4). Namely, EXP_{ALL} depicted a gradual decrease of both variables compared to the sharp decline in EXP_{C4} and $EXP_{TE,C4}$. At the same time, the smooth transition in $EXP_{SRG,C4}$ underlined once more that plant composition is more important than

the absolute number of plant types, and that an increase in plant diversity does not necessarily stabilize the climate–vegetation system.

Regarding Chapter 2, coupled simulations showed the same qualitative effect of plant diversity on initial veg_{max} and transition rate, but the fast retreat of vegetation as a response to gradual P forcing could not be observed. This could partly be attributed to the overall shallower P gradient between start and end in the coupled simulations. Moreover, the qualitative similarity indicated that the effect of plant composition was even more decisive for the timing, magnitude, and rate of transition from the “green” Sahara to the “desert” state than the feedback with the atmosphere.

In summary, this chapter highlighted that the choice of PFTs as well as their representation in JSBACH can significantly affect simulated climate–vegetation interaction during the AHP, the extent of the “green” Sahara, and the timing and rate of transition to the “desert” state. PFT diversity should therefore be taken into account in future studies.

Final conclusions

Summary

The timing and abruptness of vegetation decline towards the end of the African Humid Period (AHP) has been studied and debated by various working groups using a wide range of models and palaeo-proxy reconstruction approaches. While some studies indicated an abrupt collapse of vegetation at the end of the AHP, others suggested a gradual decline. The potential effect of plant diversity on the strength of climate–vegetation feedback proposed by Claussen et al. (2013) has so far been omitted in modelling studies on climate–vegetation interaction towards the end of the AHP.

To close this gap, this thesis explored the role of plant diversity in simulated climate–vegetation interaction in models of different complexity, from the conceptual approach by Claussen et al. (2013) to the Dynamic Global Vegetation Model JSBACH, the land component of MPI-ESM1. Therewith, I aimed at contributing to the understanding of the role plant diversity plays in simulated climate–vegetation interaction and at shedding light into the discussion on the importance of climate–vegetation feedback towards the end of the AHP.

In the first chapter, I assessed the conceptual model by Claussen et al. (2013) from an ecological point of view, and provided an improved version that accounts for the diversity of AHP plant types as it was reconstructed from pollen by Hély et al. (2014). Therewith I addressed the first question:

Is the approach by Claussen et al. (2013) ecologically reasonable and do the conclusions hold if the model was adjusted to AHP vegetation reconstructed from pollen?

In the light of recently published pollen data and the current state of ecological literature, the conceptual model by Claussen et al. (2013) reproduces the main features of different plant types interacting together with climate, but it does not capture the reconstructed diversity of AHP vegetation. Especially tropical gallery forest taxa, indirectly linked to local precipitation, are not appropriately represented. With a new model version adjusted to AHP vegetation, I could simulate a diverse mosaic-like environment as reconstructed from pollen, and I observed the stabilizing effect of high functional diversity on vegetation cover and precipitation proposed by Claussen et al. (2013). Sensitivity studies with different combinations of plant types highlighted the importance of plant composition on system stability, and revealed the stabilizing or destabilizing potential a single plant type may inherit. The model's simplicity limits its application; however, it provides a useful tool to study the roles of real plant types in an ecosystem and their combined climate–vegetation feedback under changing precipitation regimes.

Since further complication of the conceptual model might have added relatively low gain of understanding, I stepped for further investigations in Chapter 2 towards the more sophisticated, comprehensive land surface model JSBACH and addressed the second question:

How is plant diversity represented in the comprehensive land surface model JSBACH and how do variations in plant diversity affect the vegetation response to a prescribed precipitation decline?

The assessment of plant diversity in JSBACH illustrated that the PFT set in JSBACH – designed for global application – is not capable to capture AHP plant types in terms of moisture requirements, species diversity or ratios between physiognomic types after White (1983). The model cannot depict mosaic-like environments and gallery forests as reconstructed from pollen. However, as a process-based model JSBACH offers the possibility to represent functional plant types accounting for a range of properties and simulate their competition. Offline simulations with different PFT compositions confirmed that high PFT diversity can smooth the vegetation response to a – here prescribed linear – precipitation decline. Eventually, the steepness of vegetation decline depended on the composition rather than on the number of PFTs. A very important player in this context was the PFT “Raingreen Shrub” which put high competitive pressure on other PFTs and acted as a desert promoter.

To complete the storyline, I presented in the third chapter coupled ECHAM6/JSBACH simulations with different degrees of PFT diversity to address the third question:

How does plant diversity in JSBACH in turn affect precipitation in coupled ECHAM6/JSBACH simulations and what consequences result for the stability of the “green” Sahara and the transition to the “desert” state?

In simulations with AHP boundary conditions, PFT diversity and composition significantly affected simulated climate–vegetation interaction and thereby modified the extent of the “green” Sahara. Remarkably, the introduction or removal of a single PFT drastically affected the vegetation extent. An unforeseen strong influence had the marginal PFT “Raingreen shrub” (*SRG*) which was previously expected to be of minor importance in PFT competition. Changes in vegetation cover in turn impinged land surface parameters, water cycling and the surface energy budget. These changes had not only local consequences but significantly altered large scale atmospheric circulation patterns indicating a strong feedback between terrestrial biosphere and atmosphere. However, at variance with the hypothesis of positive climate–vegetation feedback, higher precipitation was not necessarily associated with a higher vegetation cover fraction, but determined by the properties of prevailing PFTs, thus PFT composition.

Towards the end of the AHP, all simulations showed a transition from a wet “green” state to dry “desert” state depicting a time-transgressive southward shift of the tropical rain belt from the mid-Holocene to present day. Similar to the AHP vegetation extent, the rate and timing of transition were determined by the ratio of involved PFTs resulting from competition, their productivities and capabilities to suppress desert expansion. PFT composition was more important than the total number of occurring PFTs and an increase in plant diversity did not necessarily increase the stability of a climate–vegetation system. The introduction or removal of a single PFT drastically affected the simulated climate–vegetation system stability and the system response to changing external forcing. Therewith the presented results once more substantiated the conclusions from Claussen et al. (2013).

Future research perspectives

As mentioned above, the PFT set in JSBACH – designed for global application – has only a limited applicability for detailed studies on the role of plant diversity in subtropical semi-arid regions. In the following, I recapitulate the main shortcomings and suggest possible solutions for further studies.

The static set of discrete PFT parameters does not cover the range of taxa categorized as one PFT and disregards phenotypic plasticity. An elegant solution is the flexible handling of PFT traits. Verheijen et al. (2013, 2015) allowed several plant traits to vary within PFTs to investigate the impact of trait variability through observed trait-climate relationships on the performance of JSBACH. Simulations with variable traits reached a closer match with a natural vegetation map than default simulations, and showed that including ecologically based trait variation in PFTs reduces the projected land carbon sink. “The suggested approach, based on such data and concepts, reflects vegetation acclimation and adaptation to the environment, and will help enable more reliable modelling of vegetation behaviour under unknown climates” (Verheijen et al., 2013).

Some plant types relevant in north Africa are not covered with the PFT set in JSBACH, such as high perennial grasses and dry forest trees including gallery forest trees. Such PFTs could be designed and implemented based on observed vegetation. For perennial grasses, an adjustment of height and maximum leaf area index as well as the implementation of carbon storage pools would be necessary. Further, it has to be considered that tall grasses are more competitive for light but also more dependent on disturbances such as fire. The implementation of monsoon trees would imply an adjustment of the phenology, namely a decoupling of leaf formation from precipitation as well as an opportunistic leaf shedding. Dry forest trees exhibit three different strategies to optimize photosynthetic gain with a relatively short, wet growing season: First, leaf-exchanging species shed old leaves during the early dry season accompanied or immediately followed by bud break and expansion of new leaves. The timing varies considerably among conspecific individuals depending on soil water availability and inter-annual variation in the last major rain of rainy season (Rivera et al., 2002; Singh & Kushwaha, 2005; Elliott et al., 2006). This strategy is represented by riparian and upland evergreens, and semi-evergreens (De Bie et al., 1998). Second, deciduous species dehydrate strongly during

the early dry season, remain leafless for 3 to 5 months and rapidly rehydrate with the first wet season rainfalls of 20 to 30 mm. “The variability and patchiness of the rainfall causes large variation in the timing of leafing between years and among trees at different microsites in a landscape.” (Elliott et al., 2006). Third, spring-flushing species form leaves 1 to 2 months before the first monsoon rains induced by increasing day length (Rivera et al., 2002; Elliott et al., 2006). This strategy is highly synchronised among all conspecific trees in a landscape and varies minimally between years.

Sub-grid heterogeneity and plant diversity such as mosaic-like assemblages or gallery forests cannot be depicted in the JSBACH version used in the present study because most physical surface and soil processes, including the calculation of surface fluxes, surface temperature and soil moisture content, are modelled based on grid mean values. This problem could be addressed with a new approach that accounts for spatial sub-grid scale heterogeneity in ECHAM6/JSBACH. de Vrese (2015) presented the VERTEX scheme which provides a framework for relating atmospheric spatial sub-grid scale heterogeneity to the causative spatial sub-grid scale heterogeneity at the surface and the reference height above ground.

The definition of bioclimatic limits prevents tropical PFTs from establishment in areas where reconstructions indicate their presence during the AHP (Hély et al., 2014). Since it was cooler in parts of north Africa during the AHP, temperatures of the coldest month fall in these regions below 15.5°C , the bioclimatic limit for tropical PFTs (TE , TD), and thus prevent establishment. Although the definition of this limit is based on an empirical relationship between mean temperatures of the coldest month and absolute minimum temperature (frost occurrence) (Müller, 1982; Prentice et al., 1992), favorable microclimatic conditions could have allowed tropical taxa to establish. Another argument is that there might have been taxa that were partially frost tolerant and could survive short periods of freezing temperatures. A literature-based compilation of experimental cold tolerance thresholds for leaves (evergreens), buds and twigs or stem illustrates that “tropical evergreens show damage at -1°C or -2°C . Many of the broad-leaved evergreens can tolerate -10 to -15°C , with a few able to survive -20°C ” (Harrison et al., 2010). Test simulations indicate that lowering this bioclimatic limit to 10°C allows vegetation to expand further northward under 8 ky conditions than with the standard set up (see appendix). Consequently, tropical trees outcompete shrubs in the transition zone between desert and savanna which in turn favors the expansion of vegetation as described

earlier in Chapter 2 and Chapter 3. With the significant increase of vegetation cover fraction north of 20°N, the simulation reaches a closer match to reconstructions than previous studies. However, the final choice of this bioclimatic limits, for already existing PFTs or for additional new PFTs, requires further investigation.

Conclusions and implications

Remarkably, despite large differences in the underlying assumptions, all considered levels of model complexity led to the same conclusions: high plant diversity could stabilize a climate–vegetation system, but plant composition is the decisive factor for the system response to changes in orbital forcing. In the light of these findings, climate–vegetation feedback strength would not be a universal property of a certain region but depend on the vegetation composition. This highlights that the choice of plant types/PFTs and their representation in models significantly affect simulated climate–vegetation interaction during the AHP, the extent of the “green” Sahara, and the timing and rate of transition to the “desert” state. From this I conclude that accounting for plant diversity in future studies – not only on palaeo climates – could significantly improve the understanding of climate–vegetation interaction in semi-arid regions, the predictability of the vegetation response to changing climate, and respectively, of the resulting feedback on precipitation. A better predictability of rainfall is of particular importance in the Sahel as this region is extremely vulnerable to climate variability, ecologically as well as socio-economically. According to the Fifth Assessment Report of the Intergovernmental Panel of Climate Change (IPCC, 2014), the Sahel region experienced the strongest drying trend in the 20th century, and several studies highlighted the pronounced decadal variability of precipitation with anomalously strong rainfall in the 1950s and early 1960s, followed by a devastating dry period since the 1970s (see e.g. Folland et al., 1986; Nicholson, 2005). This climatic variability threatens the society living primarily from crops and livestock. Future projections of Sahelian climate for the 21st century in CMIP5 climate model simulations showed a large spread in temperature increase over the Sahara and North Atlantic and in the strengthening of low and mid-level winds, while rainfall projections even disagreed in sign of change (Monerie et al., 2017). Therefore it is all the more important that plant diversity, in the present thesis shown to have an influential impact on north African climate, is appropriately represented in future studies.

Appendix

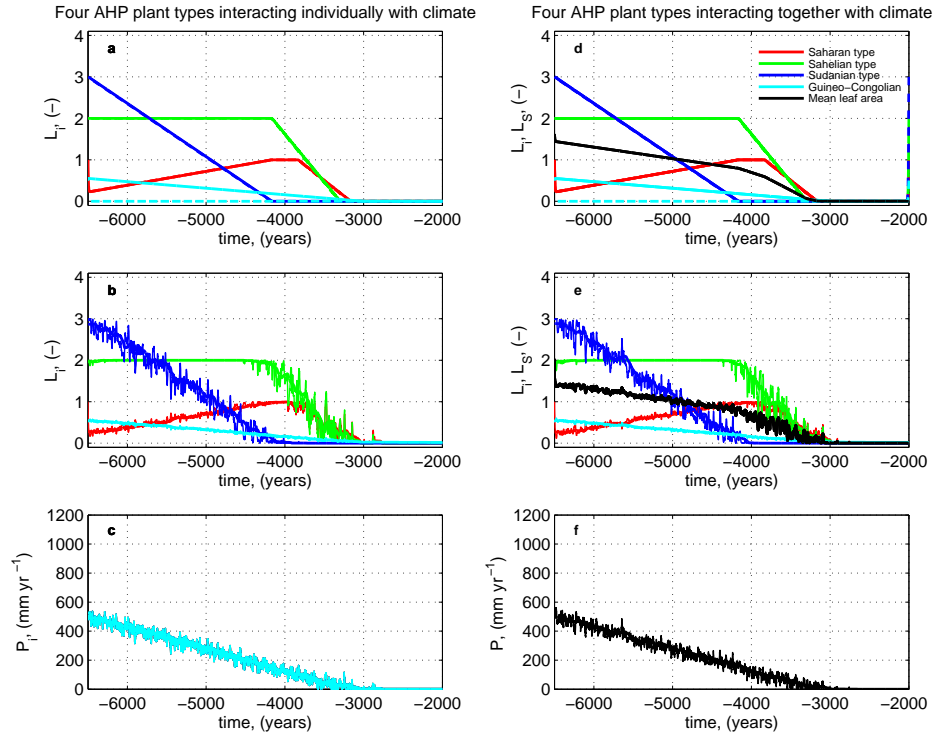


FIGURE A1: Transient dynamics of four African Humid Period (AHP) plant types interacting individually (a–c) and together (d–f) with climate for $D_B = 0 \text{ mm yr}^{-1}$. The effective leaf areas L_i and the corresponding precipitation amounts P_i are shown for the Saharan type (red), Sahelian type (green), Sudanian type (blue) and Guineo–Congolian type (light blue). Mean effective leaf area L_S and the corresponding precipitation P are calculated with the niche approach (black) (see Eq. 1.9). Simulations without background noise (a, e) include forward simulations (solid lines) and simulations backward in time (dashed lines). Simulations with background noise are depicted in (b, e) for L_i and L_S , and for precipitation P in (c, f). Thin lines show annual mean values and thick lines show a 100-year running mean.

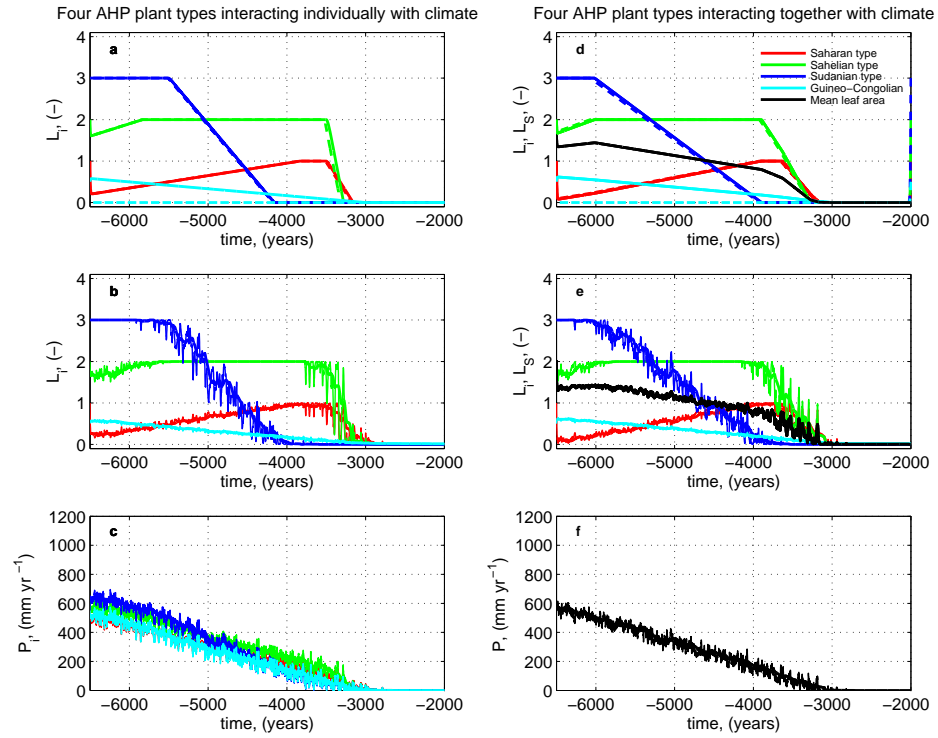


FIGURE A2: Transient dynamics of four African Humid Period (AHP) plant types interacting individually (a–c) and together (d–f) with climate for $D_B = 50 \text{ mm yr}^{-1}$. The effective leaf areas L_i and the corresponding precipitation amounts P_i are shown for the Saharan type (red), Sahelian type (green), Sudanian type (blue) and Guineo–Congolian type (light blue). Mean effective leaf area L_S and the corresponding precipitation P are calculated with the niche approach (black) (see Eq. 9). Simulations without background noise (a, e) include forward simulations (solid lines) and simulations backward in time (dashed lines). Simulations with background noise are depicted in (b, e) for L_i and L_S , and for precipitation P in (c, f). Thin lines show annual mean values and thick lines show a 100-year running mean.

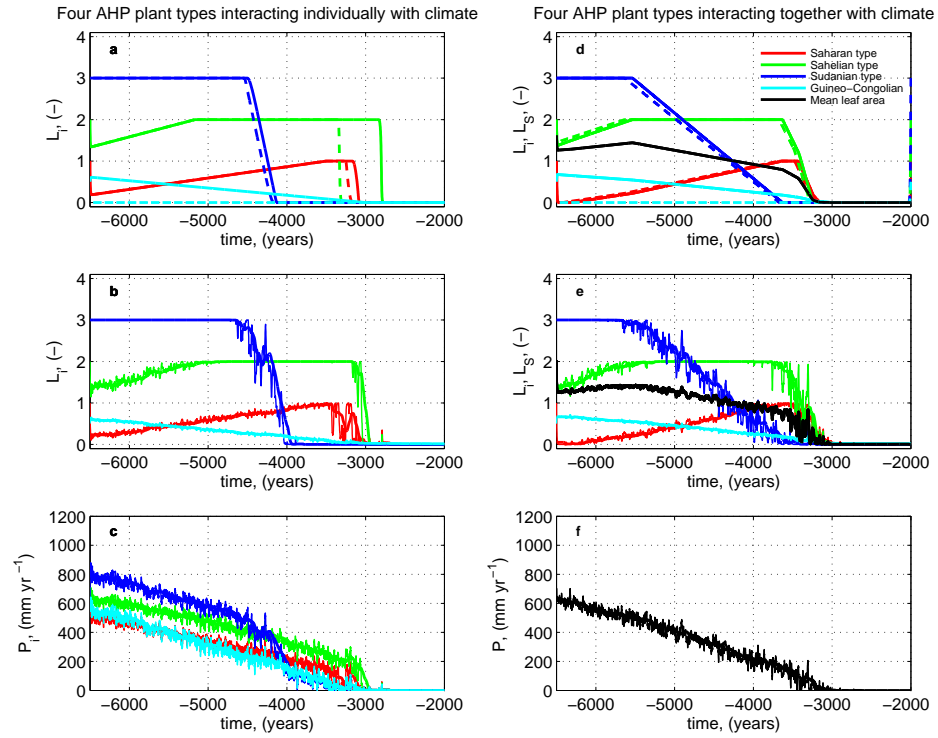


FIGURE A3: Transient dynamics of four African Humid Period (AHP) plant types interacting individually (a–c) and together (d–f) with climate for $D_B = 100 \text{ mm yr}^{-1}$. The effective leaf areas L_i and the corresponding precipitation amounts P_i are shown for the Saharan type (red), Sahelian type (green), Sudanian type (blue) and Guineo–Congolian type (light blue). Mean effective leaf area L_S and the corresponding precipitation P are calculated with the niche approach (black) (see Eq. 9). Simulations without background noise (a, e) include forward simulations (solid lines) and simulations backward in time (dashed lines). Simulations with background noise are depicted in (b, e) for L_i and L_S , and for precipitation P in (c, f). Thin lines show annual mean values and thick lines show a 100-year running mean.

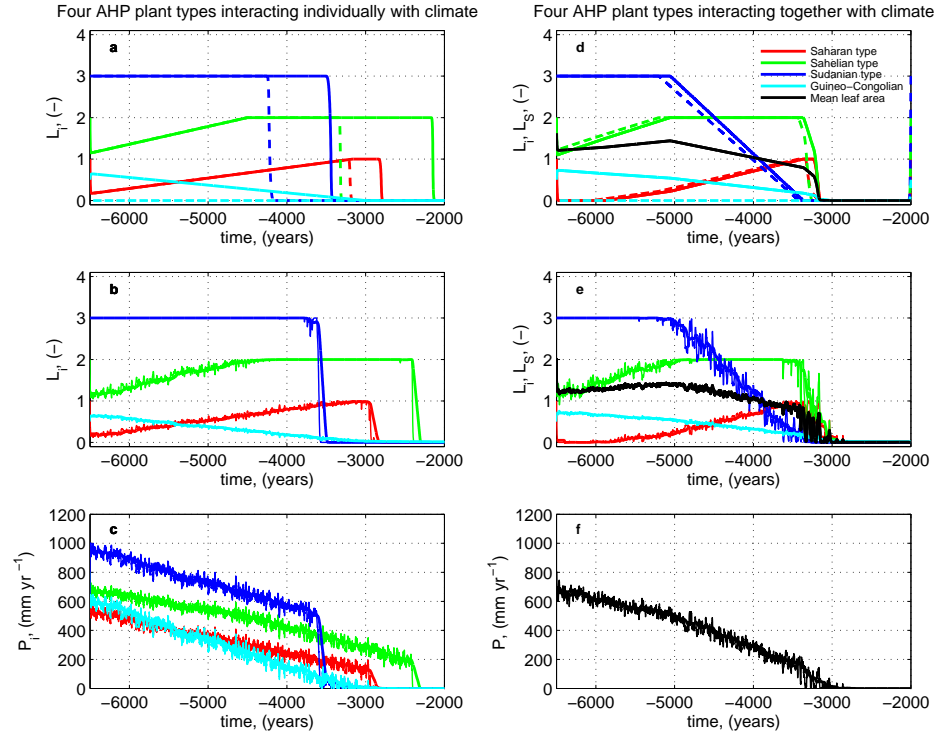


FIGURE A4: Transient dynamics of four African Humid Period (AHP) plant types interacting individually (a–c) and together (d–f) with climate for $D_B = 150 \text{ mm yr}^{-1}$. The effective leaf areas L_i and the corresponding precipitation amounts P_i are shown for the Saharan type (red), Sahelian type (green), Sudanian type (blue) and Guineo–Congolian type (light blue). Mean effective leaf area L_S and the corresponding precipitation P are calculated with the niche approach (black) (see Eq. 9). Simulations without background noise (a, e) include forward simulations (solid lines) and simulations backward in time (dashed lines). Simulations with background noise are depicted in (b, e) for L_i and L_S , and for precipitation P in (c, f). Thin lines show annual mean values and thick lines show a 100-year running mean.

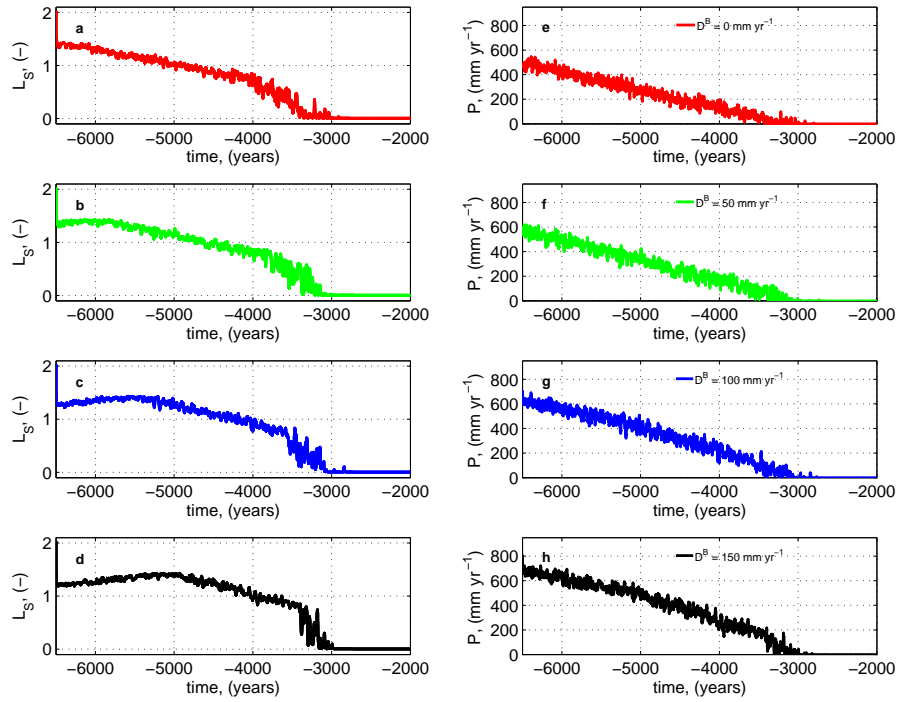


FIGURE A5: Transient dynamics of mean effective leaf area L_S of four African Humid Period (AHP) plant types interacting together with climate, and the corresponding precipitation P for different feedback sensitivity coefficients D^B . Simulations with background noise are depicted in (a–d) for L_S , and for mean annual precipitation P in (e–h) for $D^B = 0 \text{ mm yr}^{-1}$ (red), $D^B = 50 \text{ mm yr}^{-1}$ (green), $D^B = 100 \text{ mm yr}^{-1}$ (blue), and $D^B = 150 \text{ mm yr}^{-1}$ (black). Without feedback between vegetation and precipitation (a, e), L_S and corresponding P decrease almost linearly. Low feedback coefficients (b, f) result in a non-linear but gradual decline of L_S and corresponding P with small fluctuations. The higher D_B , the stronger the amplitude of fluctuations and the steeper the decline of L_S and corresponding P .

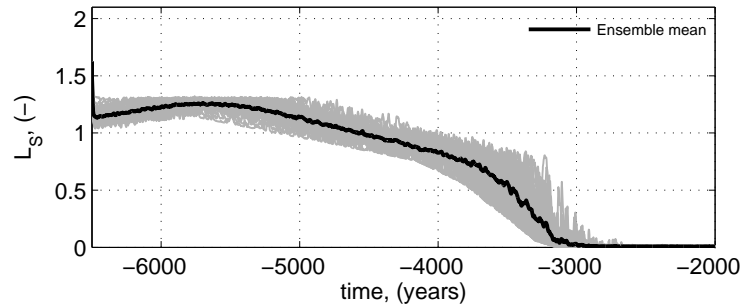


FIGURE A6: Mean effective leaf area L_S of four African Humid Period (AHP) plant types i interacting together with climate with different sets of specific climate feedback coefficients D_i^B . 30 simulations with different variations of D_i^B in the range from 0 to 150 mm yr^{-1} are shown in gray, the ensemble mean is shown in black.

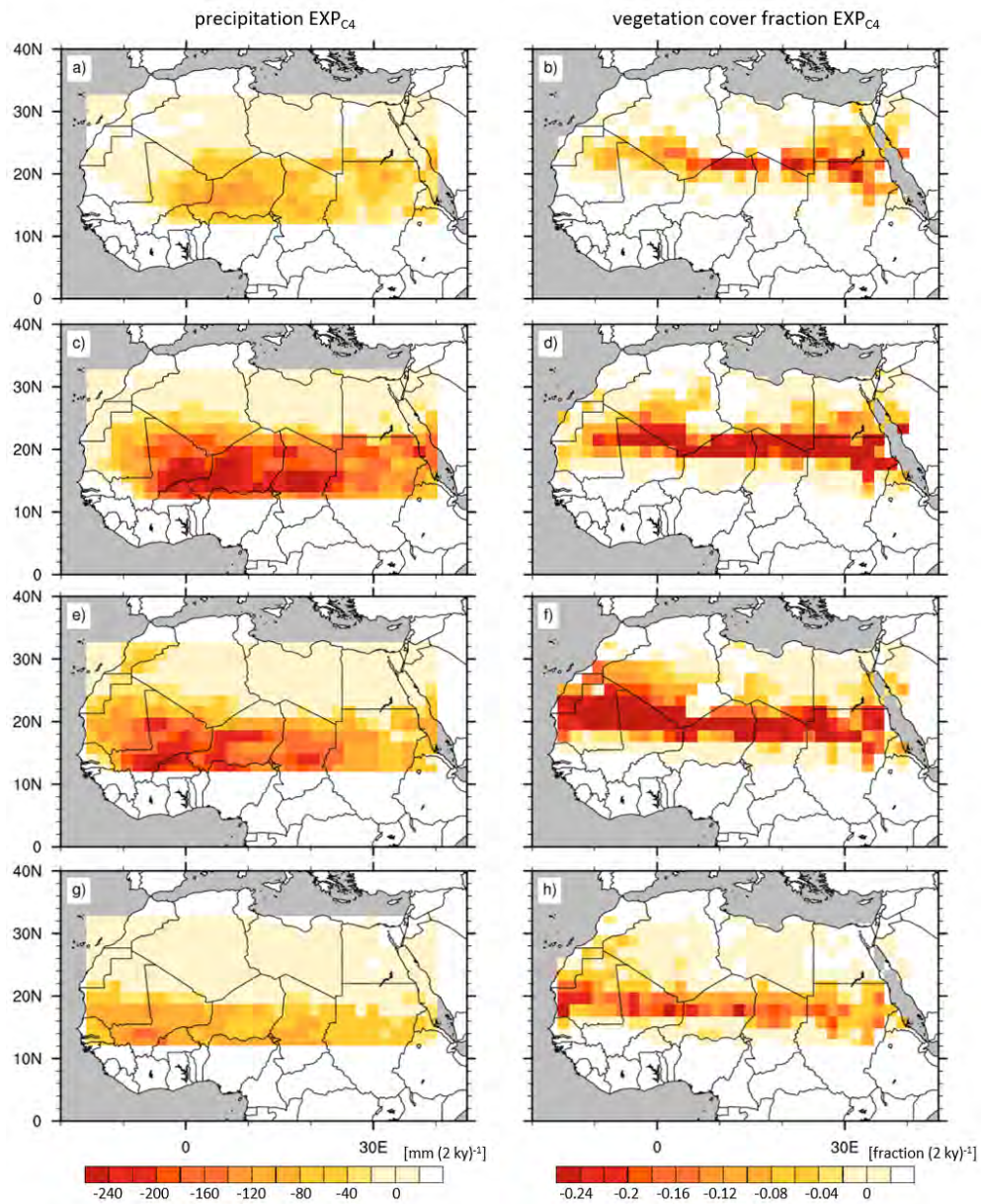


FIGURE A7: Rates of transition from the “green” Sahara to the “desert” state for precipitation P (left column) and vegetation cover fraction $veg_{max,i}$ (right column) of a simulation with $C4$ grass only (EXP_{C4}).

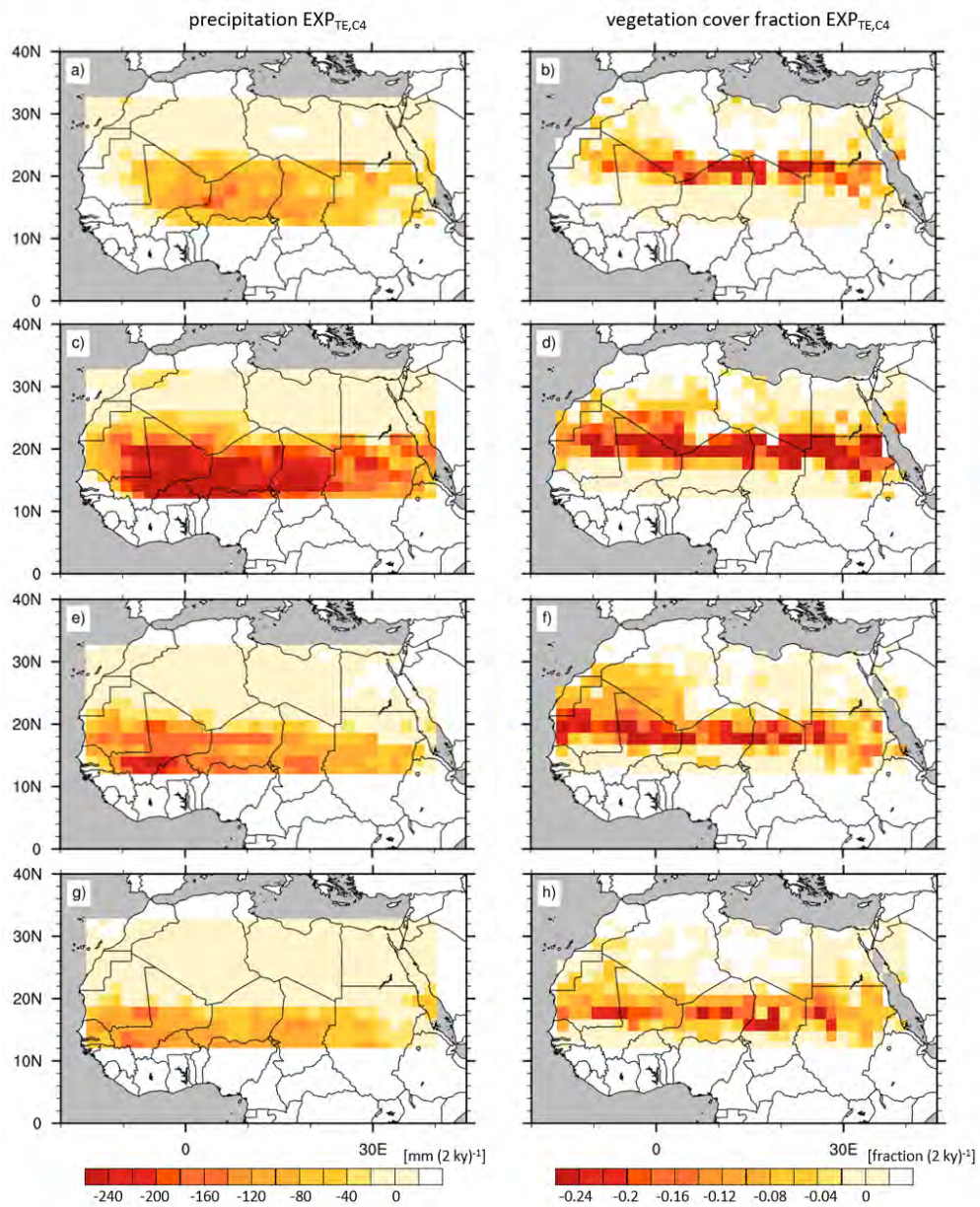


FIGURE A8: Rates of transition from the “green” Sahara to the “desert” state for precipitation P (left column) and vegetation cover fraction $veg_{max,i}$ (right column) of a simulation with tropical evergreen tree (TE) and $C4$ grass ($EXP_{TE,C4}$).

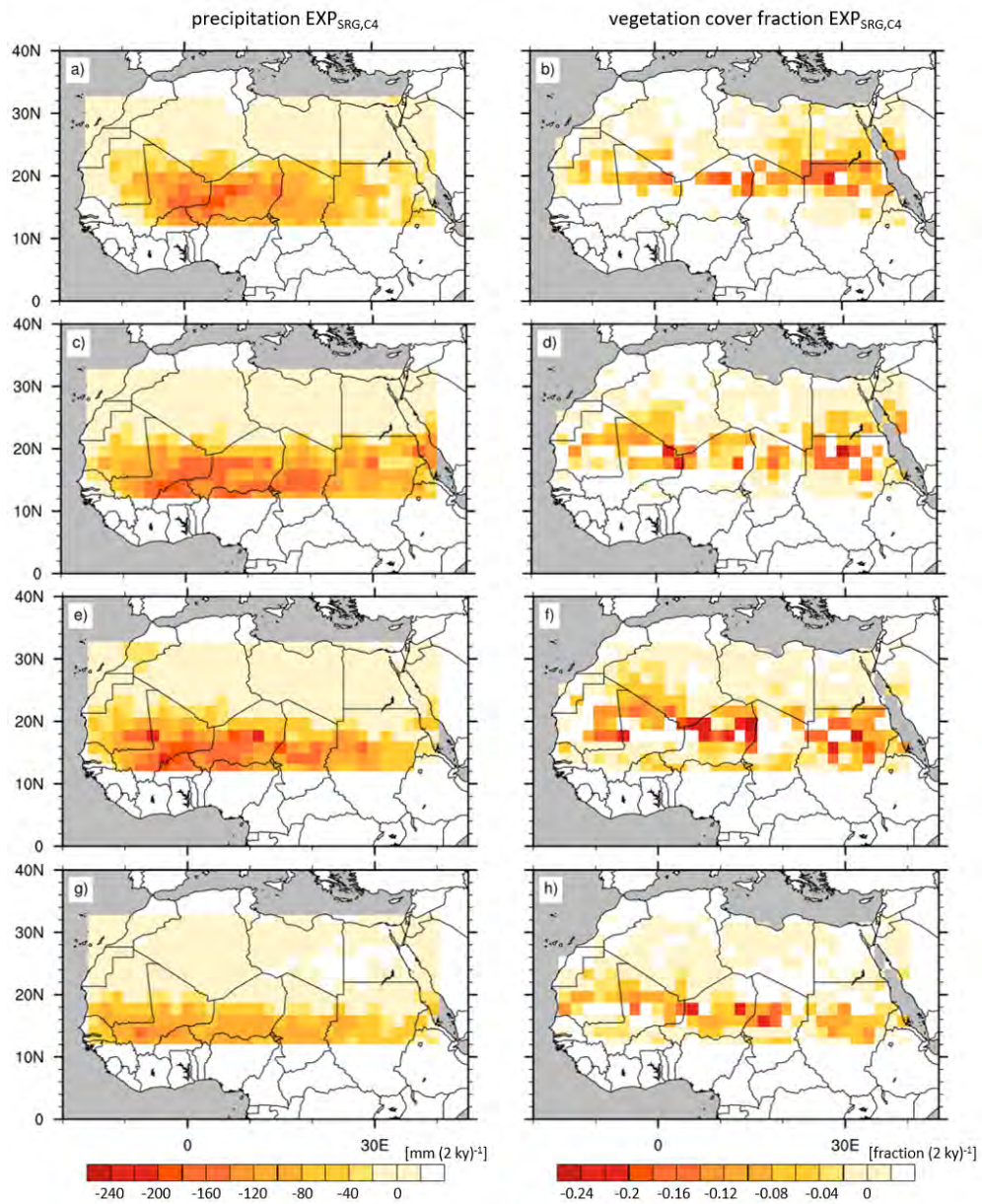


FIGURE A9: Rates of transition from the “green” Sahara to the “desert” state for precipitation P (left column) and vegetation cover fraction $veg_{max,i}$ (right column) of a simulation with Raingreen shrub (SRG) and $C4$ grass ($EXP_{SRG,C4}$).

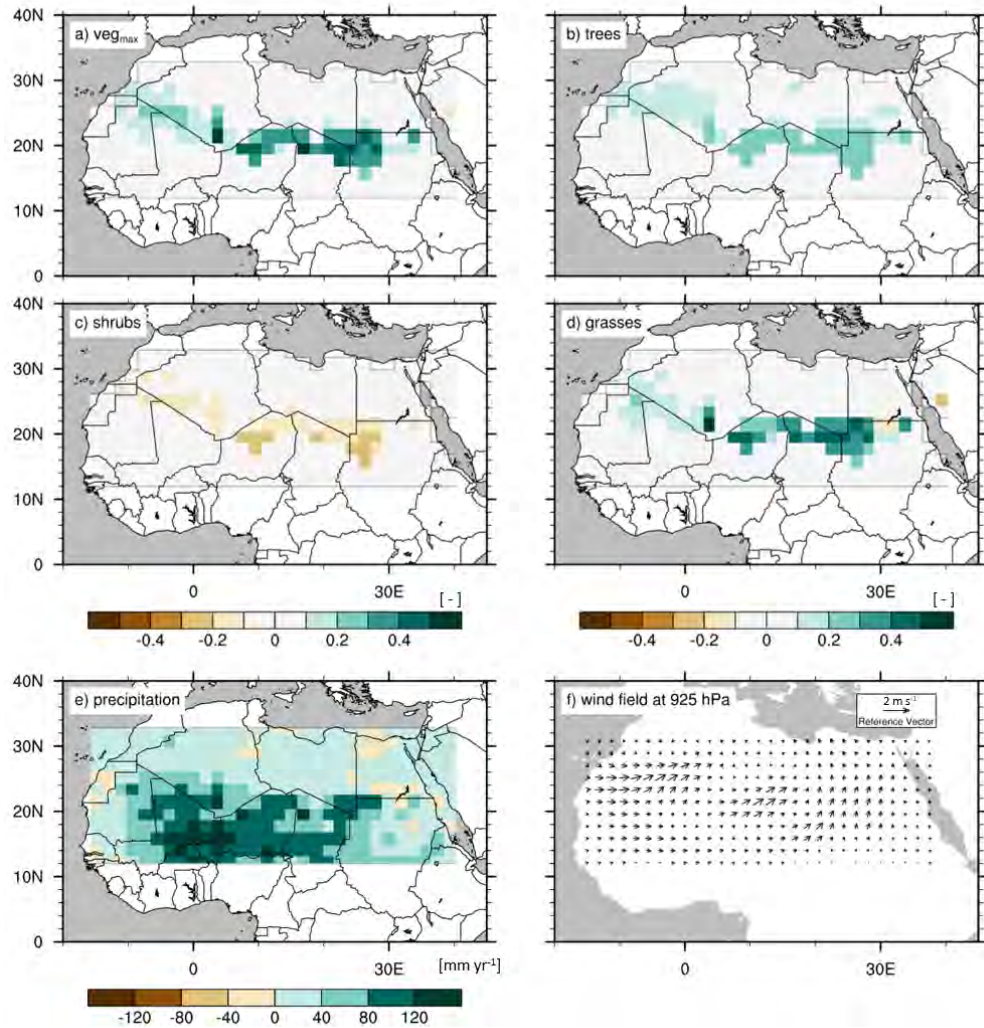


FIGURE A10: Effects of the implementation of a tropical tree with modified bioclimatic limits $EXP_{TD,cold}$ (minimum temperature of the coldest month reduced from 15.5 to 10°C) at 8 ky. Plots show the difference between $EXP_{TD,cold}$ and the experiment with the standard PFT set up (EXP_{ALL}) for vegetation cover fraction veg_{max} (a), tree cover fraction (b), shrub cover fraction (c), grass cover fraction (d), precipitation P (e), and horizontal wind fields in the monsoon layer (925 hPa, f). The comparison illustrates that TD_{cold} establishes in the transition zone between desert and savanna at the expense of SRG . As the bioclimatic limit can be overcome, the tropical PFT can establish and outcompete SRG due to its higher productivity. Consequently, $C4$ experiences less competitive pressure on short time scale which favors its expansion. The “greening” of the transition zone results in a northward shift of the ITCZ (f) and enhanced P in the whole study domain (e).

TABLE A1: Plant functional types in the high plant diversity set up of JSBACH, their woodiness type, associated time constants for establishment/mortality τ (in years) (Reick et al., 2013), maximum carboxylation capacities $V_{max,0}$ and electron transport capacities $J_{max,0}$ at 25 °C (in $\mu\text{mol}(\text{CO}_2)\text{ m}^{-2}\text{ s}^{-1}$) (Kattge et al., 2011). Photosynthesis parameter are not available for C4 grasses since their photosynthesis is calculated differently.

Plant Functional Type	ID	type	τ	$V_{max,0}$	$J_{max,0}$
Tropical evergreen tree 1	TE_1	woody	10	20	38
Tropical evergreen tree 2	TE_2	woody	20	20	38
Tropical evergreen tree 3	TE_3	woody	30	20	38
Tropical evergreen tree 4	TE_6	woody	10	30	57
Tropical evergreen tree 5	TE_7	woody	20	30	57
Tropical evergreen tree 6	TE_8	woody	30	30	57
Tropical evergreen tree 7	TE_{11}	woody	10	40	76
Tropical evergreen tree 8	TE_{12}	woody	20	40	76
Tropical evergreen tree 9	TE_{13}	woody	30	40	76
Tropical evergreen tree 10	TE_{16}	woody	10	50	95
Tropical evergreen tree 11	TE_{17}	woody	20	50	95
Tropical evergreen tree 12	TE_{18}	woody	30	50	95
Tropical evergreen tree 13	TE_{21}	woody	10	60	114
Tropical evergreen tree 14	TE_{22}	woody	20	60	114
Tropical evergreen tree 15	TE_{23}	woody	30	60	114
raingreen shrub 1	SRG_1	woody	5	30	57
raingreen shrub 2	SRG_2	woody	10	30	57
raingreen shrub 3	SRG_3	woody	15	30	57
raingreen shrub 4	SRG_6	woody	5	50	95
raingreen shrub 5	SRG_7	woody	10	50	95
raingreen shrub 6	SRG_8	woody	15	50	95
raingreen shrub 7	SRG_{11}	woody	5	70	133
raingreen shrub 8	SRG_{12}	woody	10	70	133
raingreen shrub 9	SRG_{13}	woody	15	70	133
raingreen shrub 10	SRG_{16}	woody	5	90	171
raingreen shrub 11	SRG_{17}	woody	10	90	171
raingreen shrub 12	SRG_{18}	woody	15	90	171
raingreen shrub 13	SRG_{21}	woody	5	110	209

raingreen shrub 14	<i>SRG₂₂</i>	woody	10	110	209
raingreen shrub 15	<i>SRG₂₃</i>	woody	15	110	209
C3 grass 1	<i>C₃₁</i>	non-woody	1	30	57
C3 grass 2	<i>C₃₂</i>	non-woody	1	40	76
C3 grass 3	<i>C₃₃</i>	non-woody	1	50	95
C3 grass 4	<i>C₃₄</i>	non-woody	1	60	114
C3 grass 5	<i>C₃₅</i>	non-woody	1	70	133
C3 grass 6	<i>C₃₆</i>	non-woody	1	80	152
C3 grass 7	<i>C₃₇</i>	non-woody	1	90	171
C3 grass 8	<i>C₃₈</i>	non-woody	1	100	190
C3 grass 9	<i>C₃₉</i>	non-woody	1	110	209
C3 grass 10	<i>C₃₁₀</i>	non-woody	1	120	228
C4 grass 1	<i>C₄₁</i>	non-woody	1	5	50
C4 grass 2	<i>C₄₂</i>	non-woody	1	10	100
C4 grass 3	<i>C₄₃</i>	non-woody	1	15	150
C4 grass 4	<i>C₄₄</i>	non-woody	1	20	200
C4 grass 5	<i>C₄₅</i>	non-woody	1	25	250
C4 grass 6	<i>C₄₆</i>	non-woody	1	30	300
C4 grass 7	<i>C₄₇</i>	non-woody	1	35	350
C4 grass 8	<i>C₄₈</i>	non-woody	1	40	400
C4 grass 9	<i>C₄₉</i>	non-woody	1	45	450
C4 grass 10	<i>C₄₁₀</i>	non-woody	1	50	500
Tropical evergreen tree	<i>TE</i>	woody	30	39	74.1
Tropical deciduous tree	<i>TD</i>	woody	30	31	59.8
extra-tropical evergreen tree	<i>eTE</i>	woody	60	44	83.6
extra-tropical deciduous tree	<i>eTD</i>	woody	60	66	125.4
raingreen shrub	<i>SRG</i>	woody	12	61.7	117.2
deciduous shrub	<i>SD</i>	woody	24	54	102.6
C3 grass	<i>C₃</i>	non-woody	1	78.2	148.6
C4 grass	<i>C₄</i>	non-woody	1	8	140

Bibliography

- biologie.uni-hamburg.de. <http://www1.biologie.uni-hamburg.de/b-online/afrika/tansania/serengeti/accac.htm>. Accessed: 2016-11-29.
- CRUNCEP data set. <http://dods.extra.cea.fr/data/p529viov/cruncep/readme.htm>. Accessed: 2016-04-06.
- eoearth.org. <http://editors.eol.org/eoearth/wiki/File:West-sudanian-savanna-burkina-faso.jpg>. Accessed: 2016-11-29.
- geographie.uni-stuttgart.de. http://www.geographie.uni-stuttgart.de/exkursionsseiten/Namibia_2007/landschaft_geologie_1.php. Accessed: 2016-11-29.
- greenpeace.org. <http://www.greenpeace.org/international/en/news/features/world-bank-cuts-olam-funding-121207/>. Accessed: 2016-11-29.
- Ackerly, D. & Cornwell, W. K. (2007). A trait-based approach to community assembly: partitioning of species trait values into within- and among-community components. *Ecol. Lett.*, 10(2), 135–145.
- Adler, B., Kalthoff, N., & Gantner, L. (2011). Initiation of deep convection caused by land-surface inhomogeneities in West Africa: a modelled case study. *Meteor. Atmos. Phys.*, 112(1), 15–27.
- Albert, L. (2010). Phenotypic Plasticity, Ecophysiology, and Climate Change. http://eebweb.arizona.edu/faculty/saleska/Ecol1596L/596L_Albert_Plasticity_2010.pdf. Accessed: 2014-03-18.
- Amarasekare, P. (2003). Competitive coexistence in spatially structured environments: a synthesis. *Ecol. Lett.*, 6(12), 1109–1122.
- Anjum, S. A., Xie, X.-Y., Wang, L.-C., Saleem, M. F., Man, C., et al. (2011). Morphological, physiological and biochemical responses of plants to drought stress. *Afr. J. Agric. Res.*, 6(9), 2026–2032.

- Aroca, R. (2012). *Plant Responses to Drought Stress: From Morphological to Molecular Features*. Springer Berlin Heidelberg.
- Arora, V. K., Boer, G. J., Friedlingstein, P., Eby, M., Jones, C. D., et al. (2013). Carbon-concentration and carbon-climate feedbacks in CMIP5 Earth system models. *J. Climate*, *26*, 5289–5314.
- Azihou, A. F., Kakaï, R. G., Bellefontaine, R., & Sinsin, B. (2013). Distribution of tree species along a gallery forest–savanna gradient: patterns, overlaps and ecological thresholds. *J. Trop. Ecol.*, *29*(1), 25–37.
- Bartlein, P. J., Harrison, S. P., Brewer, S., Connor, S., Davis, B. A. S., et al. (2011). Pollen-based continental climate reconstructions at 6 and 21 ka: a global synthesis. *Clim. Dyn.*, *37*(3), 775–802.
- Bathiany, S., Claussen, M., & Brovkin, V. (2014). CO₂-induced Sahel greening in three CMIP5 Earth system models. *J. Climate*, *27*(18), 7163–7184.
- Bathiany, S., Claussen, M., Brovkin, V., Raddatz, T., & Gayler, V. (2010). Combined biogeophysical and biogeochemical effects of large-scale forest cover changes in the MPI earth system model. *Biogeosciences*, *7*, 1383–1399.
- Bathiany, S., Claussen, M., & Fraedrich, K. (2012). Implications of climate variability for the detection of multiple equilibria and for rapid transitions in the atmosphere–vegetation system. *Clim. Dynam.*, *38*(9), 1775–1790.
- Bathiany, S., Dijkstra, H., Crucifix, M., Dakos, V., Brovkin, V., et al. (2016). Beyond bifurcation – using complex models to understand and predict abrupt climate change. *Dyn. Stat. Clim. Syst.*, *1*(1), 1–31.
- Baudena, M., Dekker, S. C., van Bodegom, P. M., Cuesta, B., Higgins, S. I., et al. (2015). Forests, savannas and grasslands: bridging the knowledge gap between ecology and Dynamic Global Vegetation Models. *Biogeosciences*, *12*, 1833–1848.
- Baumer, M., Food, Agriculture Organization of the United Nations, Programme, U. N. E., on the Ecological Management of Air, P., arid Rangelands in Africa, S., the Near, & of FAO, M. E. (1983). *Notes on Trees and Shrubs in Arid and Semi-arid Regions, Emashar Phase II, Food and Agriculture Organization of the United Nations*. Rome Italy.
- Baumhauer, R. & Runge, J. (2009). *Holocene Palaeoenvironmental History of the Central Sahara: Palaeoecology of Africa Vol. 29, An International Yearbook of Landscape Evolution and Palaeoenvironments*. Palaeoecology of Africa. CRC Press.

- Berger, A. L. (1978). Long-term variations of caloric insolation resulting from the earth's orbital elements. *Quat. Res.*, *9*(2), 139–167.
- Bertrand, R., Lenoir, J., Piedallu, C., Riofrio-Dillon, G., de Ruffray, P., et al. (2011). Changes in plant community composition lag behind climate warming in lowland forests. *Nature Letter*, *479*, 517–520.
- Bhark, E. W. & Small, E. E. (2003). Association between Plant Canopies and the Spatial Patterns of Infiltration in Shrubland and Grassland of the Chihuahuan Desert, New Mexico. *Ecosystems*, *6*(2), 185–196.
- Black, C. C., Chen, T. M., & Brown, R. H. (1969). Biochemical Basis for Plant Competition. *Weed Science*, *17*(3), 338–344.
- Bonan, G. B., Levis, S., Sitch, S., Vertenstein, M., & Oleson, K. W. (2003). A dynamic global vegetation model for use with climate models: concepts and description of simulated vegetation dynamics. *Glob. Change Biol.*, *9*(11), 1543–1566.
- Bonfils, C., de Noblet-Ducoudré, N., Braconnot, P., & Joussaume, S. (2001). Hot Desert Albedo and Climate Change: Mid-Holocene Monsoon in North Africa. *J. Clim.*, *14*(17), 3724–3737.
- Box, E. O. (1995). Factors determining distributions of tree species and plant functional types. *Vegetatio*, *121*(1-2), 101–116.
- Boysen, L., Brovkin, V., Arora, V. K., Cadule, P., de Noblet-Ducoudré, N., et al. (2014). Global and regional effects of land-use change on climate in 21st century simulations with interactive carbon cycle. *Earth Syst. Dynam.*, *5*, 309–319.
- Braconnot, P., Joussaume, S., Marti, O., & de Noblet, N. (1999). Synergistic feedbacks from ocean and vegetation on the African Monsoon response to Mid-Holocene insolation. *Geophys. Res. Lett.*, 2481–2484.
- Braconnot, P., Otto-Bliesner, B., Harrison, S., Joussaume, S., Peterchmitt, J.-Y., et al. (2007). Results of PMIP2 coupled simulations of the Mid-Holocene and Last Glacial Maximum – Part 1: experiments and large-scale features. *Clim. Past*, (3), 261–277.
- Bradshaw, A. D. (1965). Evolutionary significance of phenotypic plasticity in plants. *Adv. Gen.*, *13*, 115–155.
- Branch, O., Warrach-Sagi, K., Wulfmeyer, V., & Cohen, S. (2014). Simulation of semi-arid biomass plantations and irrigation using the WRF-NOAH model – a comparison with observations from Israel. *HESS*, *18*(5), 1761–1783.
- Brooker, R. W. (2006). Plant-plant interactions and environmental change. *New Phytol.*, (171), 271–284.

- Brooks, T. M., Pimm, S. L., & Oyugi, J. O. (1999). Time lag between deforestation and bird extinction in tropical forest fragments. *Conserv. Biol.*, *13*(5), 1140–1150.
- Brovkin, V. & Claussen, M. (2008). Comment on “Climate-driven ecosystem succession in the Sahara: the past 6000 years”. *Science*, (322), 1326.
- Brovkin, V., Claussen, M., Petoukhov, V., & Ganopolski, A. (1998). On the stability of the atmosphere–vegetation system in the Sahara/Sahel region. *J. Geophys. Res.-Atmos.*, *103*(D24), 31613–31624.
- Brovkin, V., Lorenz, S. J., Jungclaus, J., Raddatz, T., Timmreck, C., et al. (2010). Sensitivity of a coupled climate-carbon cycle model to large volcanic eruptions. *Tellus*, *62B*, 674–681.
- Brovkin, V., Raddatz, T., Reick, C. H., Claussen, M., & Gayler, V. (2009). Global biogeophysical interactions between forest and climate. *Geophys. Res. Lett.*, *36*, Seq. No.: L07405.
- Brown, J. H. (1995). *Macroecology*. Chicago: The University of Chicago Press.
- Bruecher, T., Brovkin, V., Kloster, S., Marlon, J., & Power, M. (2014). Comparing modelled fire dynamics with charcoal records for the Holocene. *Clim. Past*, *10*, 811–824.
- Budyko, M. I. (1969). The effect of solar radiation variations on the climate of the Earth. *Tellus*, *21*(5), 611–619.
- Bunting, J. & Middleton, R. (2005). Modelling pollen dispersal and deposition using HUMPOL software, including simulating windroses and irregular lakes. *Rev. Palaeobot. Palynol.*, *134*, 185–196.
- Charney, J. G. (1975). Dynamics of deserts and drought in the Sahel. *Q. J. Roy. Meteor. Soc.*, *101*(428), 193–202.
- Claussen, M. (1994). On coupling global biome models with climate models. *Clim. Res.*, *4*, 203–221.
- Claussen, M. (2009). Late Quaternary vegetation-climate feedbacks. *Clim. Past*, *5*, 203–216.
- Claussen, M., Bathiany, S., Brovkin, V., & Kleinen, T. (2013). Simulated climate–vegetation interaction in semi-arid regions affected by plant diversity. *Nat. Geosci.*, *6*, 954–958.
- Claussen, M., Brovkin, V., Ganopolski, A., Kubatzki, C., & Petoukhov, V. (1998). Modelling global terrestrial vegetation–climate interaction. *Philos. T. R. Soc. B*, *353*, 53–63.

- Claussen, M. & Gayler, V. (1997). The greening of the Sahara during the Mid-Holocene: results of an interactive atmosphere–biome model. *Global Ecol. Biogeogr.*, *6*(5), 369–377.
- Claussen, M., Kubatzki, C., Brovkin, V., Ganopolski, A., Hoelzmann, P., et al. (1999). Simulation of an abrupt change in Saharan vegetation in the Mid-Holocene. *Geophys. Res. Lett.*, *26*(14), 2037–2040.
- Coe, M. & Bonan, G. (1997). Feedbacks between climate and surface water in northern Africa during the middle Holocene. *J. Geophys. Res.*, *102*(D10), 11087–11101.
- Collatz, G. J., Ribas-Carbo, M., & Berry, J. A. (1992). Coupled photosynthesis-stomatal conductance model for leaves of C4 plants. *Aust. J. Plant Physiol.*, *19*(5), 519–538.
- Coughenour, M. B. & Ellis, J. E. (1993). Landscape and climatic control of woody vegetation in a dry tropical ecosystem: Turkana District, Kenya. *J. Biogeogr.*, *20*(4), 383–398.
- Cox, P. M. (2001). Description of the TRIFFID dynamic global vegetation model. Technical report. Technical report, Hadley Centre Tech. note 24, Bracknell, UK: Hadley Centre.
- Crimmins, S. M., Dobrowski, S. Z., Greenberg, J. A., Abatzoglou, J. T., & Mynsberge, A. R. (2011). Changes in Climatic Water Balance Drive Downhill Shifts in Plant Species' Optimum Elevations. *Science*, *331*(6015), 324–327.
- da Silva, E. C., de Albuquerque, M. B., de Azevedo Neto, A. D., & da Silva Junior, C. D. (2013). *Drought and Its Consequences to Plants – From Individual to Ecosystem, Responses of Organisms to Water Stress*. InTech.
- Dallmeyer, A., Claussen, M., & Otto, J. (2010). Contribution of oceanic and vegetation feedbacks to Holocene climate change in monsoonal Asia. *Clim. Past*, *6*, 195–218.
- De Bie, S., Ketner, P., Paasse, M., & Geerling, C. (1998). Woody plant phenology in the West Africa savanna. *J. Biogeogr.*, *25*(5), 883–900.
- De Kauwe, M. G., Zhou, S.-X., Medlyn, B. E., Pitman, A. J., Wang, Y.-P., et al. (2015). Do land surface models need to include differential plant species responses to drought? Examining model predictions across a mesic-xeric gradient in Europe. *Biogeosciences*, *12*(24), 7503–7518.
- de Noblet-Ducoudré, N., Claussen, M., & Prentice, C. (2000). Mid-Holocene greening of the Sahara: first results of the GAIM 6000 year BP Experiment with two asynchronously coupled atmosphere/biome models. *Clim. Dynam.*, *16*, 643–659.

- de Vrese, P. (2015). *Impact of surface heterogeneities on land surface water and energy fluxes*. PhD thesis, Universität Hamburg.
- deMenocal, P., Ortiz, J., Guilderson, T., Adkins, J., Sarnthein, M., et al. (2000). Abrupt onset and termination of the African Humid Period: rapid climate responses to gradual insolation forcing. *Quaternary Sci. Rev.*, *19*, 347–361.
- deMenocal, P. B. & Rind, D. (1993). Sensitivity of Asian and African climate to variations in seasonal insolation, glacial ice cover, sea surface temperature, and Asian orography. *J. Geophys. Res. Atmos.*, *98*(D4), 7265–7287.
- Diamond, J. M. (1972). Biogeographic kinetics: estimation of relaxation times for avifauna of southwest Pacific Islands. *Proc. Natl. Acad. Sci. U. S. A.*, *69*(11), 3199–3203.
- Díaz, S. & Cabido, M. (2001). Vive la difference: plant functional diversity matters to ecosystem processes. *Trends Ecol. Evol.*, *16*(11), 646–655.
- Díaz, S., Fargione, J., Chapin, F. S. I., & Tilman, D. (2006). Biodiversity loss threatens human well-being. *Plos Biology*, *4*(8), 1300–1305.
- D’Odorico, P., Caylor, K., Okin, G. S., & Scanlon, T. M. (2007). On soil moisture–vegetation feedbacks and their possible effects on the dynamics of dryland ecosystems. *J. Geophys. Res.: Biogeosc.*, *112*(G4).
- Doherty, R., Kutzbach, J., Foley, J., & Pollard, D. (2000). Fully coupled climate/dynamical vegetation model simulations over Northern Africa during the mid-Holocene. *Clim. Dynam.*, *16*(8), 561–573.
- Drake, N. A., Blench, R. M., Armitage, S. J., Bristow, C. S., & White, K. H. (2011). Ancient watercourses and biogeography of the Sahara explain the peopling of the desert. *P. Natl. Acad. Sci.*, *108*, 458–462.
- Druyan, L. M. (1991). The sensitivity of sub-Saharan precipitation to Atlantic SST. *Clim. Change*, *18*(1), 17–36.
- Duckworth, J. C., Kent, M., & Ramsay, P. M. (2000). Plant functional types: an alternative to taxonomic plant community description in biogeography? *Prog. Phys. Geogr.*, *24*(4), 515–542.
- Ehleringer, J. R., Sage, R. F., Flanagan, L. B., & Pearcy, R. W. (1991). Climate change and the evolution of C4 photosynthesis. *Trends Ecol. Evol.*, *6*(3), 95–99.
- Ekici, A., Beer, C., Hagemann, S., Boike, J., Langer, M., et al. (2014). Simulating high latitude permafrost regions by the JSBACH terrestrial ecosystem model. *Geosci. Model Dev.*, *7*, 631–647.

- Eldridge, D. J., Bowker, M. A., Maestre, F. T., Roger, E., Reynolds, J. F., et al. (2011). Impacts of shrub encroachment on ecosystem structure and functioning: towards a global synthesis. *Ecol. Let.*, *14*(7), 709–722.
- Eldridge, D. J., Whitford, W. G., & Duval, B. D. (2009). Animal disturbances promote shrub maintenance in a desertified grassland. *J. Ecol.*, *97*(6), 1302–1310.
- Ellenberg, H. (1975). Vegetationsstufen in perhumiden bis perariden Bereichen der tropischen Anden. *Phytocoenologia*, *2*(3-4), 368–387.
- Elliott, S., Baker, P. J., & Borchert, R. (2006). Leaf flushing during the dry season: the paradox of Asian monsoon forests. *Global Ecol. Biogeogr.*, *15*(3), 248–257.
- Elton, C. S. (1958). *Ecology of Invasions by Animals and Plants*. Chicago: Methuen & Co./Chapman & Hall, Kluwer Academic Publishers BV.
- Epstein, H. E., Chapin III, F. S., Walker, M. D., & Starfield, A. M. (2001). Analyzing the functional type concept in arctic plants using a dynamic vegetation model. *Oikos*, *95*(2), 239–252.
- FAO/UNESCO (1974). Soil map of the world 1:5,000,000, Vols. 1–10.
- Farquhar, G. C., Caemmerer, S., & Berry, J. A. (1980). A biochemical model of photosynthesis in leaves of C3 species. *Planta*, *149*, 78–90.
- Fisher, R., McDowell, N., Purves, D., Moorcroft, P., Sitch, S., et al. (2010). Assessing uncertainties in a second-generation dynamic vegetation model caused by ecological scale limitations. *New Phytol.*, *187*(3), 666–681.
- Folland, C., Parker, D., & Palmer, T. (1986). Sahel rainfall and worldwide sea temperatures, 1901-85. *Nature*, *320*, 602–607.
- Francus, P., von Suchodoletz, H., Dietze, M., Donner, R. V., Bouchard, F., et al. (2013). Varved sediments of Lake Yoa (Ounianga Kebir, Chad) reveal progressive drying of the Sahara during the last 6100 years. *Sedimentology*, *60*(4), 911–934.
- Friedlingstein, P., Cox, P., Betts, R., Bopp, L., Bloh, V., et al. (2006). Climate-Carbon Cycle Feedback Analysis: Results from the C4MIP Model Intercomparison. *J. Climate*, *19*, 3337–3353.
- Frost, P. G. H., Medina, E., Menaut, J. C., Solbrig, O., Swift, M., & Walker, B. H. (1986). Response of Savannas to Stress and Disturbance. In *Biology International Special Issue 10*. Paris: IUBS.
- Gaillard, M.-J., Sugita, S., Bunting, M. J., Middleton, R., Broström, A., et al. (2008). The use of modelling and simulation approach in reconstructing past landscapes from

- fossil pollen data: a review and results from the POLLANDCAL network. *Veg. Hist. Archaeobot.*, 17(5), 419–443.
- Ganopolski, A., Kubatzki, C., Claussen, M., Brovkin, V., & Petoukhov, V. (1998). The Influence of Vegetation-Atmosphere-Ocean Interaction on Climate During the Mid-Holocene. *Science*, 280(5371), 1916–1919.
- Ghil, M. (1976). Climate Stability for a Sellers-Type Model. *J. Atm. Sci.*, 33(1), 3–20.
- Giorgetta, M. A., Jungclaus, J., Reick, C. H., Legutke, S., Bader, et al. (2013). Climate and carbon cycle changes from 1850 to 2100 in MPI-ESM simulations for the Coupled Model Intercomparison Project phase 5. *Adv. Mod. Earth Sy.*, 5(3), 572–597.
- Griffiths, J. (1972). *World Survey of Climatology, Vol. 10, Climates of Africa*. Elsevier.
- Grist, J. P. & Nicholson, S. E. (2001). A Study of the Dynamic Factors Influencing the Rainfall Variability in the West African Sahel. *J. Clim.*, 14(7), 1337–1359.
- Groner, V. P. (2013). The impact of a large scale plantation of *Jatropha curcas* L. on convection initiation under monsoonal conditions in the coastal desert of Oman. Masterarbeit. Universität Hohenheim.
- Hales, K., Neelin, J. D., & Zeng, N. (2004). Sensitivity of Tropical Land Climate to Leaf Area Index: Role of Surface Conductance versus Albedo. *J. Clim.*, 17(7), 1459–1473.
- Hansen, M., DeFries, R., Townshend, J. R., Carroll, M., Dimiceli, C., et al. (2007). 2001 percent tree cover. In *Vegetation Continuous Fields MOD44B*. College Park, Maryland: University of Maryland.
- Harrison, S. P., Prentice, I. C., Barboni, D., Kohfeld, K. E., Ni, J., et al. (2010). Eco-physiological and bioclimatic foundations for a global plant functional classification. *J. Veg. Sci.*, 21, 300–317.
- Hastenrath, S. (1984). Interannual Variability and Annual Cycle: Mechanisms of Circulation and Climate in the Tropical Atlantic Sector. *Mon. Weather Rev.*, 112(6), 1097–1107.
- Hély, C., Braconnot, P., Watrin, J., & Zheng, W. (2009). Climate and vegetation: simulating the African humid period. *CR Geosci.*, 341(8-9), 671–688.
- Hély, C., Bremond, L., Alleaume, S., Smith, B., Sykes, M. T., et al. (2006). Sensitivity of African biomes to changes in the precipitation regime. *Global Ecol. Biogeogr.*, 15(3), 258–270.
- Hély, C., Lézine, A.-M., & APD contributors (2014). Holocene changes in African vegetation: tradeoff between climate and water availability. *Clim. Past*, 10, 681–686.

- Higgins, S. I., Bond, W. J., & Trollope, W. S. W. (2000). Fire, resprouting and variability: a recipe for grass–tree coexistence in savanna. *J. Ecol.*, *88*(2), 213–229.
- Hochberg, M. E., Menaut, J. C., & Gignoux, J. (1994). The influences of tree biology and fire in the spatial structure of West African savannah. *J. Ecol.*, *82*(2), 383–393.
- Hoelzmann, P., Jolly, D., Harrison, S. P., Laarif, F., Bonnefille, R., et al. (1998). Mid-Holocene land-surface conditions in northern Africa and the Arabian Peninsula: a data set for the analysis of biogeophysical feedbacks in the climate system. *Global Biogeochem. Cy.*, *12*(1), 35–51.
- Hooper, D. U., S., C. I. F., Ewel, J. J., Hector, A., Inchausti, P., et al. (2005). Effects of biodiversity on ecosystem functioning: a consensus of current knowledge. *Ecol. Monogr.*, *75*(1), 3–35.
- House, J. I., Archer, S., Breshears, D. D., Scholes, R. J., & NCEAS Tree–Grass Interactions Participants (2003). Conundrums in mixed woody–herbaceous plant systems. *J. Biogeogr.*, *30*(11), 1763–1777.
- Hulme, M. & Tosdevin, N. (1989). The Tropical easterly Jet and Sudan rainfall: A review. *Theor. Appl. Climatol.*, *39*(4), 179–187.
- Huntley, B., Bartlein, P. J., & Prentice, I. C. (1989). Climatic Control of the Distribution and Abundance of Beech (*fagus l.*) in Europe and North America. *J. Biogeogr.*, *16*(6), 551–560.
- Hurrell, J. W., Hack, J. J., Shea, D., Caron, J. M., & Rosinski, J. (2008). A New Sea Surface Temperature and Sea Ice Boundary Dataset for the Community Atmosphere Model. *J. Climate*, *21*(19), 5145–5153.
- Hutchinson, G. (1957). Concluding remarks. *Cold Spring Harbor Symposia on Quantitative Biology*, *22*, 415–427.
- IPCC (2014). *Index*, book section Index, (pp. pp. 688). Cambridge, United Kingdom and New York, NY, USA: Cambridge University Press.
- Ives, A. R. & Carpenter, S. R. (2007). Stability and Diversity of Ecosystems. *Science*, *317*(5834), 58–62.
- Jackson, S. T. & Overpeck, J. T. (2000). Responses of plant populations and communities to environmental changes of the Late Quaternary (suppl.). *Paleobiology*, *26*(4), 194–220.
- Jackson, S. T. & Sax, D. F. (2010). Balancing biodiversity in a changing environment: extinction debt, immigration credit and species turnover. *Trends Ecol. Evol.*, *25*(3), 153–160.

- Jeltsch, F., Milton, S., Dean, W., van Rooyen, N., & Moloney, K. (1998). Modelling the impact of small-scale heterogeneities on tree–grass coexistence in semi-arid savannas. *J. Ecol.*, *86*(5), 780–793.
- Jeltsch, F., Milton, S., Dean, W. R. J., & van Rooyen, N. (1996). Tree soacing and coexistence in semiarid savannas. *J. Ecol.*, *84*(4), 583–595.
- Jeltsch, F., Weber, G. E., & Grimm, V. (2000). Ecological buffering mechanisms in savannas: a unifying theory of long-term tree–grass coexistence. *Plant Ecol.*, *150*(1), 161–171.
- Jenkins, G. S., Gaye, A. T., & Sylla, B. (2005). Late 20th century attribution of drying trends in the Sahel from the Regional Climate Model (RegCM3). *Geophys. Res. Lett.*, *32*(22). L22705.
- Johnson, C. N. (1998). Species extinction and the relationship between distribution and abundance. *Nature*, *394*, 272–274.
- Jolly, D., Prentice, I. C., Bonnefille, R., Ballouche, A., Bengo, M., et al. (1998). Biome reconstruction from pollen and plant macrofossil data for Africa and the Arabian peninsula at 0 and 6000 years. *J. Biogeogr.*, *25*(6), 1007–1027.
- Joos, F. (2016). Evolution of atmospheric CO₂ over the last 23,000 years. Documentation of CO₂ compilation for PMIP, personal communication.
- Jungclaus, J. H., Fischer, N., Haak, H., Lohmann, K., Marotzke, J., et al. (2013). Characteristics of the ocean simulations in the Max Planck Institute Ocean Model (mpiom) the ocean component of the MPI-Earth system model. *Adv. Mod. Earth Sy.*, *5*(2), 422–446.
- Kattge, J., Díaz, S., Lavorel, S., Prentice, I. C., Leadley, P., et al. (2011). TRY – a global database of plant traits. *Glob. Change Biol.*, *17*(9), 2905–2935.
- Kleidon, A., Fraedrich, K., & Heimann, M. (2000). A Green Planet Versus a Desert World: Estimating the Maximum Effect of Vegetation on the Land Surface Climate. *Clim. Change*, *44*(4), 471–493.
- Knorr, W. (1998). Satellitengestützte Fernerkundung und Modellierung des globalen CO₂ Austauschs der Landvegetation, Examensarbeit Nr. 49, Max Planck Institute for Meteorology, Hamburg.
- Körner, C., Morgan, J., & Norby, R. (2007). *CO₂ Fertilization: When, Where, How Much?*, (pp. 9–21). Berlin, Heidelberg: Springer Berlin Heidelberg.

- Krinner, G., Lézine, A.-M., Braconnot, P., Sepulchre, P., Ramstein, G., et al. (2012). A reassessment of lake and wetland feedbacks on the North African Holocene climate. *Geophys. Res. Lett.*, *39*(7), L07701.
- Kröpelin, S., Verschuren, D., Lézine, A.-M., Eggermont, H., Cocquyt, C., et al. (2008). Climate-driven ecosystem succession in the Sahara: the past 6000 years. *Science*, *320*(5877), 765–768.
- Kutzbach, J. E. (1981). Monsoon climate of the Early Holocene: climate experiment with the Earth's orbital parameters for 9000 years ago. *Science*, *214*(4516), 59–61.
- Kutzbach, J. E. & Guetter, P. J. (1986). The influence of changing orbital parameters and surface boundary conditions on climate simulations for the past 18,000 years. *J. Atmos. Sci.*, *43*(10), 1726–1759.
- Kutzbach, J. E. & Liu, Z. (1997). Response of the African monsoon to orbital forcing and ocean feedbacks in the Middle Holocene. *Science*, *278*, 440–443.
- Lamb, P. J. (1978). Case Studies of Tropical Atlantic Surface Circulation Patterns During Recent Sub-Saharan Weather Anomalies: 1967 and 1968. *Mon. Weather Rev.*, *106*(4), 482–491.
- Lasslop, G., Brovkin, V., Reick, C. H., Bathiany, S., & Kloster, S. (2016). Multiple stable states of tree cover in a global land surface model due to a fire-vegetation feedback. *Geophys. Res. Lett.*, *43*(12), 6324–6331.
- Lasslop, G., Thonicke, K., & Kloster, S. (2014). SPITFIRE within the MPI Earth system model: Model development and evaluation. *Adv. Mod. Earth Sy.*, *6*(3), 740–755.
- Lavaysse, C., Flamant, C., Janicot, S., & Knippertz, P. (2010). Links between African easterly waves, midlatitude circulation and intraseasonal pulsations of the West African heat low. *Q. J. R. Meteorol. Soc.*, *136*(S1), 141–158.
- Lawesson, J. E. (1990). Sahelian woody vegetation in Sénégal. *Vegetatio*, *86*(2), 161–174.
- Le Houérou, H. N. (1980). Browse in Africa, the current state of knowledge. (pp. 83–100)., Addis Ababa, Ethiopia. ILCA.
- Levis, S., Bonan, G. B., & Bonfils, C. (2004). Soil feedback drives the mid-Holocene North African monsoon northward in fully coupled CCSM2 simulations with a dynamic vegetation model. *Clim. Dyn.*, *23*(7), 791–802.
- Lézine, A.-M. (2009). Timing of vegetation changes at the end of the Holocene humid period in desert areas at the northern edge of the Atlantic and Indian monsoon systems. *Comptes Rendus Geoscience*, *341*(8-9), 750–759.

- Lézine, A.-M., Hély, C., Grenier, C., Braconnot, P., & Krinner, G. (2011). Sahara and Sahel vulnerability to climate changes, lessons from Holocene hydrological data. *Quat. Sc. Rev.*, *30*(21–22), 3001–3012.
- Lézine, A.-M., Zheng, W., Braconnot, P., & Krinner, G. (2011). Late Holocene plant and climate evolution at Lake Yoa, northern Chad: pollen data and climate simulations. *Clim. Past*, *7*, 1351–1362.
- Li, P.-X., Wang, N., He, W.-M., Krüsi, B., Gao, S.-Q., et al. (2008). Fertile islands under *Artemisia ordosica* in inland dunes of northern China: effects of habitats and plant developmental stages. *J. Arid Environ.*, *72*, 953–963.
- Li, Z.-X., Ide, K., Le Treut, H., & Ghil, M. (1997). Atmospheric radiative equilibria in a simple column model. *Clim. Dyn.*, *13*(6), 429–440.
- Liu, Z., Notaro, M., Kutzbach, J., & Liu, N. (2006). Assessing global vegetation-climate feedbacks from observations. *J. Climate*, *19*(5), 787–814.
- Liu, Z., Wang, Y., Gallimore, R., Gasse, F., Johnson, T., et al. (2007). Simulating the transient evolution and abrupt change of Northern Africa atmosphere-ocean-terrestrial ecosystem in the Holocene. *Quaternary Sci. Rev.*, *26*(13–14), 1818–1837.
- Liu, Z., Wang, Y., Gallimore, R., Notaro, M., & Prentice, I. C. (2006). On the cause of abrupt vegetation collapse in North Africa during the Holocene: climate variability vs. vegetation feedback. *Geophys. Res. Lett.*, *33*, L22709.
- MacArthur, R. H. (1955). Fluctuations of animal populations and a measure of community stability. *Ecology*, *36*(3), 533–536.
- Mason, N. W. H. & de Bello, F. (2013). Functional diversity: a tool for answering challenging ecological questions. *J. Veg. Sci.*, *24*(5), 777–780.
- May, R. M. (1973). *Stability and complexity in model ecosystems*. Princeton Univ. Press.
- McCann, K. S. (2000). The diversity–stability debate. *Nature*, *405*, 228–233.
- McIntyre, S., Lavorel, S., Landsberg, J., & Forbes, T. D. A. (1999). Disturbance response in vegetation – towards a global perspective on functional traits. *J. Veg. Sci.*, *10*(5), 621–630.
- Meinzer, F. C. (2003). Functional convergence in plant responses to the environment. *Oecologia*, *134*, 1–11.
- Menaut, J., Gignoux, J., Prado, C., & Clobert, J. (1990). Tree community dynamics in a humid savanna of the Côte-d’Ivoire: modelling the effects of fire and competition with grass and neighbours. *J. Biogeogr.*, *17*(4–5), 471–481.

- Midgley, G., Hughes, G., Thuiller, W., Drew, G., & Foden, W. (2005). Assessment of potential climate change impacts on Namibia's floristic diversity, ecosystem structure and function. Climate Change Research Group, South African National Biodiversity Institute, Kirstenbosch Botanical Garden, Rhodes Drive Cape Town. For: Namibian National Biodiversity Programme, Directorate of Environmental Affairs, Private Bag 13306, Windhoek, Namibia.
- Minasny, B., McBratney, A. B., & Salvador-Blanes, S. (2008). Quantitative models for pedogenesis – A review. *Geoderma*, 144(1–2), 140–157. Antarctic Soils and Soil Forming Processes in a Changing Environment.
- Moncrieff, W. J., Scheiter, G. R., Bond, S., & Higgins, S. I. (2013). Increasing atmospheric CO₂ overrides the historical legacy of multiple stable biome states in Africa. *New Phytol.*, 201(3), 908–915.
- Monerie, P.-A., Sanchez-Gomez, E., & Boé, J. (2017). On the range of future Sahel precipitation projections and the selection of a sub-sample of CMIP5 models for impact studies. *Clim. Dyn.*, 48(7), 2751–2770.
- Müller, J. M. (1982). *Selected climatic data for a global set of standard stations for vegetation science*. The Hague: Junk.
- New, M. H. M. & Jones, P. D. (1999). Representing twentieth century space-time climate variability. Part 1: development of a 1961–90 mean monthly terrestrial climatology. *J. Climate*, 12(3), 829–856.
- Nicholson, S. (2005). On the question of the “recovery” of the rains in the West African Sahel. *J. Arid Environ.*, 63(3), 615–641. Special Issue on The “Greening” of the Sahel.
- Nicholson, S. E. (2008). The intensity, location and structure of the tropical rainbelt over west Africa as factors in interannual variability. *Int. J. Climatol.*, 28(13), 1775–1785.
- Nicholson, S. E. (2009). A revised picture of the structure of the “monsoon” and land ITCZ over West Africa. *Clim. Dyn.*, 32(7), 1155–1171.
- Nicholson, S. E. (2013). The West African Sahel: A Review of Recent Studies on the Rainfall Regime and Its Interannual Variability. *ISRN Meteorology*, 2013, 1–32.
- Nicholson, S. E. & Grist, J. P. (2003). The Seasonal Evolution of the Atmospheric Circulation over West Africa and Equatorial Africa. *J. Clim.*, 16(7), 1013–1030.
- North, G. R., Cahalan, P. F., & Coakley, J. A. J. (1981). Energy balance climate models. *Rev. Geophys.*, 19, 91–121.

- Notaro, M., Wang, Y., Liu, Z., Gallimore, R., & Levis, S. (2008). Combined statistical and dynamical assessment of simulated vegetation–rainfall interactions in North Africa during the mid-Holocene. *Glob. Change Biol.*, *14*, 347–368.
- of the Convention on Biological Diversity, S. (1992). Convention on biological diversity. Montreal, Canada.
- Otto, J., Raddatz, T., Claussen, M., Brovkin, V., & Gayler, V. (2009). Separation of atmosphere-ocean-vegetation feedbacks and synergies for mid-Holocene climate. *Geophys. Res. Lett.*, *36*, Seq. No.: L09701.
- Pan, Y., McGuire, A. D., Melillo, J. M., Kicklighter, D. W., Sitch, S., et al. (2002). A Biogeochemistry-Based Dynamic Vegetation Model and Its Application along a Moisture Gradient in the Continental United States. *J. Veg. Sci.*, *13*, 369–382.
- Parker, D. J., Burton, R. R., Diongue-Niang, A., Ellis, R. J., Felton, M., et al. (2005). The diurnal cycle of the West African monsoon circulation. *Q. J. R. Meteorol. Soc.*, *131*(611), 2839–2860.
- Pavlick, R. (2012). *Development and evaluation of a diverse dynamic global vegetation model based on plant functional tradeoffs*. PhD thesis, Universität Hamburg.
- Pearman, P. B., Guisan, A., Broennimann, O., & Randin, C. F. (2008). Niche dynamics in space and time. *Trends Ecol. Evol.*, *23*(3), 149–158.
- Peter Chesson, N. H. (1997). The Roles of Harsh and Fluctuating Conditions in the Dynamics of Ecological Communities. *Am. Nat.*, *150*(5), 519–553.
- Peterson, A. T. (2011). Ecological niche conservatism: a time-structured review of evidence. *J. Biogeogr.*, *38*, 817–827.
- Peterson, A. T., Soberon, J., & Sanchez-Cordero, V. (1999). Conservatism of ecological niches in evolutionary time. *Science*, *285*, 1265–1267.
- Pfadenhauer, J. S. & Klötzli, F. A. (2015). *Vegetation der Erde: Grundlagen, Ökologie, Verbreitung*. Springer Berlin Heidelberg.
- Pimm, S. L. (1984). The complexity and stability of ecosystems. *Nature*, *307*, 321–326.
- Pimm, S. L. & Lawton, J. H. (1978). On feeding on more than one trophic level. *Nature*, *275*, 542–544.
- Pongratz, J., Reick, C., Raddatz, T., & Claussen, M. (2008). A reconstruction of global agricultural areas and land cover for the last millennium. *Global Biogeochem. Cycles*, *22*(3), GB3018.

- Prentice, I., Cramer, W., Harrison, S., Leemans, R., Monserud, R., et al. (1992). Special Paper: A Global Biome Model Based on Plant Physiology and Dominance, Soil Properties and Climate. *J. Biogeogr.*, *19*(2), 117–134.
- Prentice, I. C. & Jolly, D. (2000). Mid-Holocene and glacial-maximum vegetation geography of the northern continents and Africa. *J. Biogeogr.*, *27*, 507–519.
- Rachmayani, R., Prange, M., & Schulz, M. (2015). North African vegetation-precipitation feedback in early and mid-Holocene climate simulations with CCSM3-DGVM. *Clim. Past*, *11*, 175–185.
- Raddatz, T. J., Reick, C. J., Knorr, W., Kattge, J., Roeckner, E., et al. (2007). Will the tropical land biosphere dominate the climate - carbon cycle feedback during the twenty-first century? *Clim. Dynam.*, *29*(6), 565–574.
- Reich, P. B., Wright, I. J., & Lusk, C. H. (2007). Predicting leaf physiology from simple plant and climate attributes: a global GLOPNET analysis. *Ecol. Appl.*, *17*(7), 1982–1988.
- Reick, C. H., Gayler, V., Raddatz, T., Schnur, R., & Wilkenskjeld, S. (2014). JSBACH – the new land component of ECHAM. Documentation.
- Reick, C. H., Raddatz, T., Brovkin, V., & Gayler, V. (2013). Representation of natural and anthropogenic land cover change in MPI-ESM. *Adv. Model. Earth Sy.*, *5*(3), 459–482.
- Reitalu, T., Kuneš, P., & Giesecke, T. (2014). Closing the gap between plant ecology and Quaternary palaeoecology. *J. Veg. Sci.*, *25*(5), 1188–1194.
- Renssen, H., Brovkin, V., Fichefet, T., & Goosse, H. (2003). Holocene climate instability during the termination of the African humid period. *Geophys. Res. Lett.*, *30*(4), 1184.
- Renssen, H., Brovkin, V., Fichefet, T., & Goosse, H. (2006). Simulation of the Holocene climate evolution in Northern Africa: The termination of the African Humid Period. *Quat. Int.*, *150*(1), 95–102.
- Ritchie, J. & Haynes, C. (1987). Holocene vegetation zonation in the eastern Sahara. *Nature*, *330*, 645–647.
- Rivera, G., Elliott, S., Caldas, L. S., Nicolossi, G., Coradin, V. T., et al. (2002). Increasing day-length induces spring flushing of tropical dry forest trees in the absence of rain. *Trees*, *16*(7), 445–456.
- Rodriguez-Fonseca, B., Janicot, S., Mohino, E., Losada, T., Bader, J., et al. (2011). Interannual and decadal SST-forced responses of the West African monsoon. *Atmos. Sci. Lett.*, *12*(1), 67–74.

- Sankaran, M., Hanan, N. P., Scholes, R. J., Ratnam, J., Augustine, D. J., et al. (2005). Determinants of woody cover in African savannas. *Nature*, *438*, 846–849.
- Sankaran, M. & McNaughton, S. J. (1999). Determinants of biodiversity regulate compositional stability of communities. *Nature*, *401*, 691–693.
- Sankaran, M., Ratnam, J., & Hanan, N. P. (2004). Tree–grass coexistence in savannas revisited – insights from an examination of assumptions and mechanisms invoked in existing models. *Ecol. Lett.*, *7*(6), 480–490.
- Sarmiento, G. (1984). *The Ecology of Neotropical Savannas*. Cambridge: Harvard University Press.
- Scheffer, M., Bascompte, J., Brock, W. A., Brovkin, V., Carpenter, S. R., et al. (2009). Early–warning signals for critical transitions. *Nature*, *461*, 53–59.
- Scheffer, M., Carpenter, S., Foley, J. A., Folke, C., & Walker, B. (2001). Catastrophic shifts in ecosystems. *Nature*, *413*, 591–596.
- Scheiter, S. & Higgins, S. I. (2009). Impacts of climate change on the vegetation of Africa: an adaptive dynamic vegetation modelling approach. *Glob. Change Biol.*, *15*(9), 2224–2246.
- Scheiter, S., Langan, L., & Higgins, S. I. (2013). Next-generation dynamic global vegetation models: learning from community ecology. *New Phytol.*, *198*(3), 957–969.
- Scherer-Lorenzen, M. (2005). Biodiversity and ecosystem functioning: basic principles. In W. Barthlott, K. E. Linsenmair, & S. Porembski (Eds.), *Biodiversity: Structure and Function*. In *Encyclopedia of Life Support Systems (EOLSS) vol Developed under the Auspices of the UNESCO*. Oxford: EOLSS Publisher.
- Schlesinger, W., Reynolds, J., Cunningham, G., Huenneke, L., Jarrell, W., et al. (1990). Biological feedbacks in global desertification. *Science*, *247*, 1043–1048.
- Schlesinger, W. H., Raikes, J. A., Hartley, A. E., & Cross, A. F. (1996). On the Spatial Pattern of Soil Nutrients in Desert Ecosystems. *Ecology*, *77*(2), 364–374.
- Scholes, R. J. & Archer, S. R. (1997). Tree–grass interactions in Savannas. *Annu. Rev. Ecol. Syst.*, *28*(1), 517–544.
- Schuldt, R. J., Brovkin, V., Kleinen, T., & Winderlich, J. (2013). Modelling Holocene carbon accumulation and methane emissions of boreal wetlands – an Earth system model approach. *Biogeosciences*, *10*, 1659–1674.
- Schurgers, G., Mikolajewicz, U., Gröger, M., Maier-Reimer, E., Vizcaïno, M., et al. (2007). The effect of land surface changes on Eemian climate. *Clim. Dyn.*, *29*(4), 357–373.

- Segschneider, J., Beitsch, A., Timmreck, C., Brovkin, V., Ilyina, T., et al. (2013). Impact of an extremely large magnitude volcanic eruption on the global climate and carbon cycle estimated from ensemble Earth System Model simulations. *Biogeosciences*, *10*, 669–687.
- Sellers, W. D. (1969). A Global Climatic Model Based on the Energy Balance of the Earth-Atmosphere System. *J. Appl. Meteorol.*, *8*(3), 392–400.
- Shanahan, T. M., McKay, N. P., Hughen, K. A., Overpeck, J. T., Otto-Bliesner, B., et al. (2015). The time-transgressive termination of the African humid period. *Nat. Geosci.*, *8*, 140–144.
- Shelford, V. E. (1913). *Animal communities in a temperate America*. Chicago: University of Chicago Press.
- Silva, L. C. R., Sternberg, L., Haridasan, M., Hoffmann, W. A., Miralles-Wilhelm, F., et al. (2008). Expansion of gallery forests into central Brazilian savannas. *Glob. Change Biol.*, *14*(9), 2108–2118.
- Singh, K. P. & Kushwaha, C. P. (2005). Paradox of leaf phenology: *Shorea robusta* is a semi-evergreen species in tropical dry deciduous forests in India. *Curr. Sci.*, *88*, 1820–1824.
- Sitch, S., Prentice, I., Smith, B., Cramer, W., Kaplan, J., et al. (2000). LPJ – a coupled model of vegetation dynamics and the terrestrial carbon cycle. *Lund University, Sweden*.
- Smith, B., Prentice, I. C., & Sykes, M. T. (2001). Representation of vegetation dynamics in the modelling of terrestrial ecosystems: comparing two contrasting approaches within European climate space. *Glob. Ecol. Biogeogr.*, *10*, 621–637.
- Snell, R. S., Huth, A., Nabel, J. E. M. S., Bocedi, G., Travis, J. M. J., et al. (2014). Using dynamic vegetation models to simulate plant range shifts. *Ecography*, *37*(12), 1184–1197.
- Solbrig, O. T. (1996). *Biodiversity and Savanna Ecosystem Processes. A Global Perspective*, volume 121 of *Ecological Studies*. Berlin Heidelberg: Springer-Verlag.
- Stärz, M., Lohmann, G., & Knorr, G. (2016). The effect of a dynamic soil scheme on the climate of the mid-Holocene and the Last Glacial Maximum. *Clim. Past*, *12*(1), 151–170.
- Staver, A. C., Archibald, S., & Levin, S. A. (2011). The Global Extent and Determinants of Savanna and Forest as Alternative Biome States. *Science*, *334*, 230–232.

- Stevens, B., Giorgetta, M., Esch, M., Mauritsen, T., Crueger, T., et al. (2013). Atmospheric component of the MPI-M Earth System Model: ECHAM6. *Adv. Mod. Earth Sys.*, 5(2), 146–172.
- Stigall, A. L. (2012). Using ecological niche modelling to evaluate niche stability in deep time. *J. Biogeogr.*, 39(4), 772–781.
- Sugita, S. (1994). Pollen Representation of Vegetation in Quaternary Sediments: Theory and Method in Patchy Vegetation. *J. Ecol.*, 82(4), 881–897.
- Susiluoto, S. & Berninger, F. (2007). Interactions between morphological and physiological drought responses in *Eucalyptus microtheca*. *Silva Fennica*, 41(2), 221–233.
- Swihart, R. K., Gehring, T. M., Kolozsvary, M. B., & Nupp, T. E. (2003). Responses of resistant vertebrates to habitat loss and fragmentation: the importance of niche breadth and range boundaries. *Div. and Dist.*, 9(1), 1–18.
- Texier, D., de Noblet, N., & Braconnot, P. (2000). Sensitivity of the African and Asian Monsoons to Mid-Holocene Insolation and Data-Inferred Surface Changes. *J. Clim.*, 13(1), 164–181.
- Texier, D., de Noblet, N., Harrison, S. P., Haxeltine, A., Jolly, D., et al. (1997). Quantifying the role of biosphere-atmosphere feedbacks in climate change: coupled model simulations for 6000 years BP and comparison with palaeodata for northern Eurasia and northern Africa. *Clim. Dynam.*, 13(12), 865–882.
- Thonicke, K., Spessa, A., Prentice, I. C., Harrison, S. P., Dong, L., & Carmona-Moreno, C. (2010). The influence of vegetation, fire spread and fire behaviour on biomass burning and trace gas emissions: results from a process-based model. *Biogeosciences*, 7(6), 1991–2011.
- Thorncroft, C. D., Nguyen, H., Zhang, C., & Peyrillé, P. (2011). Annual cycle of the West African monsoon: regional circulations and associated water vapour transport. *Q. J. R. Meteorol. Soc.*, 137(654), 129–147.
- Thuiller, W., Lavorel, S., & Araújo, M. B. (2005). Niche properties and geographical extent as predictors of species sensitivity to climate change. *Glob. Ecol. Biogeogr.*, 14(4), 347–357.
- Tilman, D. (1996). Biodiversity: population versus ecosystem stability. *Ecology*, 77(2), 350–363.
- Tilman, D., Knops, J., Wedin, D., Reich, P., Ritchie, M., et al. (1997). The influence of functional diversity and composition on ecosystem processes. *Science*, 277(5330), 1300–1302.

- Vamborg, F. S. E., Brovkin, V., & Claussen, M. (2011). The effect of a dynamic background albedo scheme on Sahel/Sahara precipitation during the mid-Holocene. *Clim. Past*, 7(1), 117–131.
- van Wijk, M. T. & Rodriguez-Iturbe, I. (2002). Tree-grass competition in space and time: Insights from a simple cellular automata model based on ecohydrological dynamics. *Water Resour. Res.*, 38(9), 18–1–18–15.
- Vellend, M., Verheyen, K., Jacquemyn, H., Kolb, A., Van Calster, H., et al. (2006). Extinction debt of forest plants persists for more than a century following habitat fragmentation. *Ecology*, 87(3), 542–548.
- Verheijen, L., Aerts, R., Brovkin, V., Cavender-Bares, J., Cornelissen, J., et al. (2015). Inclusion of ecologically based trait variation in plant functional types reduces the projected land carbon sink in an earth system model. *Glob. Change Biol.*, 21, 3074–3086.
- Verheijen, L. M., Brovkin, V., Aerts, R., Bnisch, G., Cornelissen, J. H. C., et al. (2013). Impacts of trait variation through observed trait–climate relationships on performance of an earth system model: a conceptual analysis. *Biogeosciences*, 10, 5497–5515.
- Walter, H. (1971). *Ecology of Tropical and Sub-tropical Vegetation*. Oliver & Boyd.
- Wang, G. & Eltahir, E. A. B. (2000). Ecosystem dynamics and the Sahel Drought. *Geophys. Res. Lett.*, 27(6), 795–798.
- Wang, H.-J. (1999). Role of vegetation and soil in the Holocene megathermal climate over China. *J. Geophys. Res. Atmos.*, 104(D8), 9361–9367.
- Warner, T. (2004). *Desert Meteorology*. New York: Cambridge University Press.
- Watrin, J., Lézine, A.-M., Hély, C., Cour, P., Ballouche, D., et al. (2009). Plant migration and plant communities at the time of the “Green Sahara”, histoire climatique des déserts d’Afrique et d’Arabie Climatic history of the African and Arabian deserts. *CR Geosci.*, 341(8-9), 656–670.
- Westoby, M., Falster, D., Moles, A., Vesk, P., & Wright, I. J. (2002). Plant ecological strategies: Some leading dimensions of variation between species. *Annu. Rev. Ecol. Syst.*, 33, 125–159.
- White, F. (1983). The vegetation of Africa, a descriptive memoir to accompany the UNESCO/AETFAT/UNSO vegetation map of Africa. *Nat. Resources Res.*, 20, 1–356.
- Whitford, W. G. (2002). *Ecology of desert systems*. Academic Press.

- Whitley, R., Beringer, J., Hutley, L. B., Abramowitz, G., De Kauwe, M. G., et al. (2016). Challenges and opportunities in modelling savanna ecosystems. *Biogeoscience Discuss.*, 2016, 1–44.
- Whittaker, R. H. (1972). Evolution and Measurement of Species Diversity. *Taxon*, 21(2/3), 213–251.
- Wickens, G. E. (1998). *Ecophysiology of Economic Plants in Arid and Semi-Arid Lands, Adaptations of Desert Organisms*. Berlin, Heidelberg, New York: Springer.
- Wilkenskjeld, S., Kloster, S., Pongratz, J., Raddatz, T., , & Reick, C. H. (2014). Comparing the influence of net and gross anthropogenic land-use and land-cover changes on the carbon cycle in the MPI-ESM. *Biogeosciences*, 11, 4817–4828.
- Williams, J. W., Blois, J. L., & Shuman, B. N. (2011). Extrinsic and intrinsic forcing of abrupt ecological change: case studies from the late Quaternary. *J. Ecol.*, 99(3), 664–677.
- Williams, J. W., Shuman, B. N., Webb III, T., Bartlein, P. J., & Leduc, P. L. (2004). Late-quaternary vegetation dynamics in North America: scaling from taxa to biomes. *Ecol. Monogr.*, 74(2), 309–334.
- Wilson, E. O. (1988). *Biodiversity*. National Academy Press.
- Wilson, J. B. (1999). Guilds, functional types and ecological groups. *Oikos*, 86(3), 507–522.
- Wittig, K., Schmidt, R., Zizka, M., Thiombiano, G., Sinsin, A., et al. (2010). *Atlas de la Biodiversité de l'Afrique de l'Ouest. Tome II: Burkina Faso / Biodiversity Atlas of West Africa, Volume II: Burkina Faso*. Ouagadougou & Frankfurt/Main: BIOTA.
- Wright, I. J., Reich, P. B., Cornelissen, J. H. C., Falster, D. S., Garnier, E., et al. (2005). Assessing the generality of global leaf trait relationships. *New Phytol.*, 166, 485–496.
- Wu, H., Guiot, J., Brewer, S., & Guo, Z. (2007). Climatic changes in Eurasia and Africa at the last glacial maximum and mid-Holocene: reconstruction from pollen data using inverse vegetation modelling. *Clim. Dynam.*, 29(2), 211–229.
- Wulfmeyer, V., Branch, O., Warrach-Sagi, K., Bauer, H.-B., Schwitalla, T., et al. (2014). The Impact of Plantations on Weather and Climate in Coastal Desert Regions. *J. Appl. Meteor. Climatol.*, 53(5), 1143–1169.
- Xiao, X. Y., Shen, J., Wang, S., Xiao, H., & Tong, B. G. (2008). The plant diversity and its relationship with paleoenvironment since 2.78 Ma revealed by pollen records in the Heqing deep drilling core. *Sci. Bull.*, 53(23), 3686–3698.

-
- Yu, G. & Harrison, S. P. (1996). An evaluation of the simulated water balance of Eurasia and northern Africa at 6000 yr B.P. using lake status data. *Clim. Dyn.*, 12(11), 723–735.
- Zhu, K., Woodall, C. W., & Clark, J. S. (2012). Failure to migrate: lack of tree range expansion in response to climate change. *Glob. Change Biol.*, 18(3), 1042–1052.
- Zink, K. (2014). *Einfluss der Konvektionsparametrisierung auf die Dynamik der Wechselwirkung Atmosphäre-Vegetation in Nordafrika*. Masterarbeit, Universität Hamburg.

